Aus dem

Helmholtz Zentrum München
Comprehensive Pneumology Center (CPC),
Institute of Lung Health and Immunity (LHI),
Vorstand: Ali Önder Yildirim

Dissertation
zum Erwerb des Doctor of Philosophy (Ph.D.)
an der Medizinischen Fakultät der
Ludwig-Maximilians-Universität zu München

Real time in vivo investigation of nanoparticle dynamics and immune response during ventilator-assisted nanoparticle inhalation

vorgelegt von:

Qiongliang Liu
.....

aus:

Nanchang, China
.....

Jahr:

2023

_____

Mit Genehmigung der Medizinischen Fakultät der
Ludwig-Maximilians-Universität zu München

First evaluator (1. TAC member): Prof. Dr. rer. nat. Markus Rehberg
Second evaluator (2. TAC member): Prof. Dr. med. Markus Sperandio
Third evaluator: Priv. Doz. Dr. Kathrin Kahnert
Fourth evaluator: apl. Prof. Dr. Dr. Nikolaus Kneidinger

Dean: **Prof. Dr. med. Thomas Gudermann**

date of the defense:

05.04.2023

Affidavit

Liu, Qiongliang

Surname, first name

Address

I hereby declare, that the submitted thesis entitled

Real time in vivo investigation of nanoparticle dynamics and immune response during ventilator-assisted nanoparticle inhalation

is my own work. I have only used the sources indicated and have not made unauthorised use of services of a third party. Where the work of others has been quoted or reproduced, the source is always given.

I further declare that the dissertation presented here has not been submitted in the same or similar form to any other institution for the purpose of obtaining an academic degree.

Munich, 10.04.2023

Place, Date

Qiongliang Liu

Signature doctoral candidate

Confimation of congruency between printed and electronic version of the doctoral thesis

Doctoral Candidate: Qiongliang Liu

Address:

I hereby declare that the electronic version of the submitted thesis, entitled

Real time in vivo investigation of nanoparticle dynamics and immune response during ventilator-assisted nanoparticle inhalation

is congruent with the printed version both in content and format.

Munich, 10.04.2023

Place, Date

Qiongliang Liu

Signature doctoral candidate

Table of contents

Abstract

Many lung diseases have been associated with exposure to various factors of air pollution including (nano)particles. In the past, research investigating cell-particle interactions was mainly based on cultured cells or ex-vivo tissues. Such experimental methods cannot reproduce in full, the complex reactions of the immune system, which might be triggered by nanoparticles (NPs) in vivo. To visualize and measure in real-time the cellular pulmonary innate immune response elicited by different inhaled NPs, we apply state of the art intravital microscopy on the peripheral alveolar region of the murine lung, in combination with ventilator-assisted inhalation of nebulized Quantum-Dot and carbon black NP aerosols.

Fluorescent Quantum-Dot NPs (with carboxyl-, amine-PEG- or PEG-surface modifications) became visible within seconds after the onset of inhalation and accumulated as distinct fluorescent spots at the alveolar walls.

As early as 60 min after inhalation, a deposited dose of 16 cm^2/g (NP surface area /mass lung) elicited an increase in neutrophil numbers only for cQDs, but neither for aPEG-QDs nor PEG-QDs. Neutrophils preferentially arrested in microvessels in close proximity to the site of cQD deposition, where they exhibited probing and crawling behavior, followed by rapid translocation into the alveolar space, where neutrophils ingested cQDs. This early immune response was not specific to cQDs as a comparable increase in neutrophil numbers was

also observed upon inhalation of an equivalent dose of carbon black NPs (CNP), a typical component of urban air pollution.

The neutrophil response was accompanied by resident alveolar macrophages (AMs) increasingly internalizing cQDs up to the maximum observation time of 90 min, and again only little uptake was detected for aPEG-QDs. Similar results were observed in in vitro experiments using the AM-like M-HS cell line.

Analysis of neutrophil numbers in a 30 µm radius (which roughly corresponds to one alveolar diameter) around cQD-positive AMs clearly showed increased neutrophil amounts, whereas no local increase in neutrophil numbers was detected neither around cQD-negative AMs, nor close to cell-free cQD, thus indicating a central role of AMs in the initiation of a spatially restricted innate-immune response.

Intriguingly, cQDs as well as CNPs increased the migration velocity of AMs in the alveoli of exposed mice, whereas aPEG-QDs exposure decreased AM crawling velocity, as compared to sham controls.

In order to decipher the chain of effects leading to NP-induced neutrophil recruitment, we applied specific blocking antibodies and inhibitors in order (1) to weaken AM-epithelial bonds to inhibit AM migration and affect NP uptake (anti-ICAM1 and anti-LFA1 mAbs), (2) to inhibit NP uptake and AM stimulation via Complement 5a receptor 1 (anti-CD88 mAbs) and Fcγ receptor (anti-CD64 mAbs), (4) to block NP-induced ROS formation via N-acetyl cysteine (NAC) application, (5) to prevent NP induced cellular degranulation (cromolyn), (6) and

to assess if fast acting inflammatory mediator release (TNF-α) contributes to the NP induced immune cell recruitment.

These mechanistic studies suggest that the induction of NP-elicited neutrophil recruitment depends on several key events:

1. NP-induced neutrophil recruitment is initiated by AMs and related to NP internalization/uptake by AMs.
2. The particle uptake efficacy depends on three factors: (1) NP surface modification; (2) the speed of macrophage patrolling movement in the alveoli; (3) AMs phagocytic/internalizing capability.

(1) PEGylation of QDs which are deposited in alveoli renders the NPs invisible to AMs via avoiding protein corona formation and impairs subsequent NP-induced neutrophil recruitment.

(2) Alveolar AM patrolling mainly involves ICAM-1 and LFA-1 interactions and can be blocked by respective antibodies applied to the airway side but not to the vascular side. Blocking ICAM-1 and LFA-1 also effectively impaired particle-triggered neutrophil recruitment.

(3) The macrophage receptors C5aR1 and FcγRI mediate particle internalization by AMs. Blocking C5aR1 or FcγRI also completely blocks Neutrophile recruitment.

3. NP-triggered neutrophil recruitment requires cellular degranulation and can be inhibited by cromolyn treatment.
4. Recruitment of neutrophils further requires TNFα as an anti-TNFα

application into the airways to reduce the neutrophilic inflammatory response.

5. Scavenging ROS via NAC also decreased cQDs-induced neutrophil recruitment to some extent but was less effective than ICAM-1/LFA-1 blocking.

Overall, our data indicate a close relation between AM activity (phagocytosis, migration) and the rapid and site-specific recruitment of neutrophils during the early phase (1h and 24h) of particle inhalation, demonstrating a specific role of AMs in triggering the immune response by different NPs.

1. Introduction

1.1 Nanotoxicology

In general, nanomaterials are considered to be particles with a size from 1nm to 100nm at least in one dimension (International Organization for Standardization, 2008). Nanomaterials can be divided into carbon nanomaterials, inorganic nanomaterials, organic nanomaterials, and composite nanomaterials according to the source of the material. In addition, nanomaterials also can be divided into two types: natural and man-made (Jeevanandam et al., 2018). NPs have distinct physicochemical characteristics as well, such as nanoscale size, large specific surface area, strong surface reactivity, good photocatalytic activity, and superior thermal conductivity(Sukhanova et al., 2018). As a consequence of these special properties, nanomaterials are widely used in daily life, for instance, in cosmetics, electronic devices, pharmaceuticals, and other industries, throughout the time, these tiny particles are likewise being developed and put into several new applications (Yang et al., 2021). Nanomaterials-based nanotechnology has been developed as a diagnostic and therapeutic method, which is being extensively applied in clinical medicine (Gupta et al., 2014; Yohan & Chithrani, 2014), for example, quantum dots (QDs) are being utilized for tumor diagnosis or medical imaging (Volkov, 2015). Gold (Au) NPs are applied in adjuvants for vaccines to reduce side effects, enhance immune effects and increase vaccine

stability (Dykman & Khlebtsov, 2012; Dykman & Khlebtsov, 2011). QDs are widely used as nano-fluorescent materials by virtue of their special optical properties (Ren et al., 2021). Furthermore, there are four main areas of application in the respiratory system: imaging of the respiratory system (Saitoh et al., 2012), targeted delivery vehicles for lung tumors (Duman et al., 2019; Matysiak-Brynda et al., 2018), diagnosis of thoracic tumors (Boeck et al., 2013; Li et al., 2020; Ma et al., 2016), and treatment of lung diseases (Gunaydin et al., 2021; Lai et al., 2014; Zhao et al., 2019). Conversely, the potential risk of NPs, such as the threshold of harmful doses, and the active response (neutrophil recruitment, phagocytic clearance) in vivo, which is not entirely clear yet ("Current Strategies for Engineering Controls in Nanomaterial Production and Downstream Handling Processes," 2013).

Vehicle emissions and exhaust are supposed to be a prime source of micro and nano-sized particles in the atmosphere (Kagawa, 2002). NPs from diesel engine combustion (20-130 nm) (Morawska et al., 1998) were slightly larger than those from gasoline engine combustion (20-60 nm) (Ristovski et al., 1998). Moreover, most carbon NPs (CNPs) (>90%) in atmosphere are produced by the combustion of diesel fuel (Kittelson, 2001).

Nevertheless, maternal exhaust gas exposed in the air could result in cardiopulmonary mortality (Vermylen et al., 2005), and childhood cancer during or after pregnancy (Knox, 2005). Coronary heart disease (Bigert et al., 2003), and pro-inflammatory, pro-thrombotic, and hemolytic effects (Riediker et al.,

2004) are several health threats that occurred in humans due to high exposure with vehicle exhaust and emissions.

Earlier studies in our laboratory indicated that exposure of healthy mice to high concentrations of CNP could induce a localized acute inflammatory response in the lungs (André et al., 2006). CNP exposure can induce ROS production, leading to TNFα released from rat AM via activation of NF-Kappa B and AP1 driven by intracellular calcium-related signaling pathways (Brown et al., 2004). It has been presented in a previous study by our group showed that CXCL1, CXCL5 and TNFα levels in Bal peaked 12 h after CNP intratracheal instillation (Chen et al., 2016). In addition to that, it has been revealed as well that CNP inhalation was triggering endothelial dysfunction in secondary organs, which induced thrombosis and further cardiovascular damage (Khandoga et al., 2010). Inhalation of ultrafine carbon particles in asthma subjects can alter peripheral blood leukocyte distribution and expression of adhesion molecules: descending percentages of CD4+ T cells, basophils, and eosinophils, as well as decreased expression of CD11b on monocytes and eosinophils and CD54 on granulocytes (Frampton et al., 2006).

The toxicity of NPs could be affected by several factors:

a. Size: Inhaling NPs is more harmful than inhaling larger particles at the same mass and in the same chemical composition (Ge et al., 2014). This is mainly due to the fact that nanomaterials have a very high surface-to-mass ratio, and they are more likely to deposit in the alveolar regions where clearance

efficiency is low. In consequence, NPs are able to be removed from the lung more slowly than larger particles, resulting in prolonged nanoparticle presence in the alveolar region. Therefore, NPs with larger surface area and longer residence time in the lung, are more likely to cause acute inflammation (Hadrup et al., 2020).

b. Functional groups: Nanomaterials can be combined with proteins/biomolecules on their surface to form a NP specific corona. Therefore, surface coating, which prevents or influences biomolecule adsorption, is an essential factor that can affect the toxicity of nanomaterials (Zhao & Liu, 2012). However, shells are generally used to improve the solubilization and reduce the toxicity of NPs such as QDs, for the reason that the metal cores of QDs are hydrophobic, and composed of toxic heavy metals like cadmium, tellurium, and mercury. The shell prevents desalination and oxidative or photolytic degradation thereby reducing QDs toxicity (Guo et al., 2007; Hardman, 2006; Huang et al., 2013; Peng et al., 2013). These shells can be made up of organic and inorganic compounds such as polyethylene glycol (PEG), polyglycolic acid, lipids, low molecular weight compounds, silicon, and others (Sibi & Dhruv, 2020). The shell on the surface of engineered NPs improves the biocompatibility and solubility of NPs to reduce their aggregation ability and increase the NP stability (Sukhanova et al., 2018). Additionally, toxic effects crucially depend on the oxidative stress response (Nguyen et al., 2015; Xia et al., 2009;

Zhang et al., 2015). ZnS shell and Polyethylene glycol coating significantly extenuate or revoke toxicological effects of CdSe/ZnS QDs (Peng et al., 2013).

c. Shape: Aspect ratios can be used to distinguish the shapes of NPs, with high and low aspect ratios for nanospheres and nano-cubes. NPs with high aspect ratio are more cytotoxic than those with low aspect ratios (Madani et al., 2013). Melanoma cell lines were exposed to mesoporous silica NPs (MSNs) with similar physicochemical properties but different longitudinal ratios (AR=1, 2, and 4). NPs with high aspect ratios were more likely to be internalized and bring about cytoskeleton disruption and apoptosis (Huang et al., 2010).

The Global Burden of Disease Study ("Global, regional, and national comparative risk assessment of 79 behavioural, environmental and occupational, and metabolic risks or clusters of risks, 1990-2015: a systematic analysis for the Global Burden of Disease Study 2015," 2016) has reported that 4,200,000 people died of environmental particulate matter (PM) exposition; 2,900,000 died of household air pollution; 400,000 people died of occupational PM exposure, and 200,000 people died of asbestos during 2015. Environmental nanoparticle exposure is particularly relevant for the development of lung diseases, such as asthma (Khreis et al., 2017; Liu, Jørgensen, et al., 2021) and COPD (Liu, Lim, et al., 2021). It was further demonstrated that PM2.5 was significantly associated with death from all

causes in a meta-analysis of 107 published studies (stroke, COPD, lung cancer, etc.) (Chen & Hoek, 2020).

Inhalation exposure holds one of the most common forms of exposure. The factors that can affect nanoparticle deposition in the airway are the shape and size of the NPs or their agglomerates. Compared with larger particles, NPs are more likely to deposit in the terminal bronchus, and the alveoli. If the NPs are deposited in the lungs, a fraction will enter the blood circulation through the lung epithelial cell barrier and be transported to secondary organs, such as the brain, kidney, and liver (Figure 1) (Kreyling et al., 2010). For instance, Semmler-Behnke et al. have exposed rats with two sizes of gold NPs by instillation into the lungs. After 24 hours, the 18-nm NPs were essentially retained in the lung (99.8% of the injected dose (ID)), while 8.5% of 1.4-nm NPs were found in secondary organs (blood, liver, skin, and carcass) (Semmler-Behnke et al., 2008). Non-cationic inorganic/organic hybrid NPs (< 34 nm) cannot bind to serum proteins and can be observed in regional lymph nodes within 0.5 hours. On the contrary, larger NPs (>34 nm) can be retained in the lungs for an extended period of time (Kreyling et al., 2010). About half of the zwitterionic NPs (< 6nm) could quickly enter the bloodstream from the alveoli and be eliminated from the body in the urine (Choi et al., 2010).

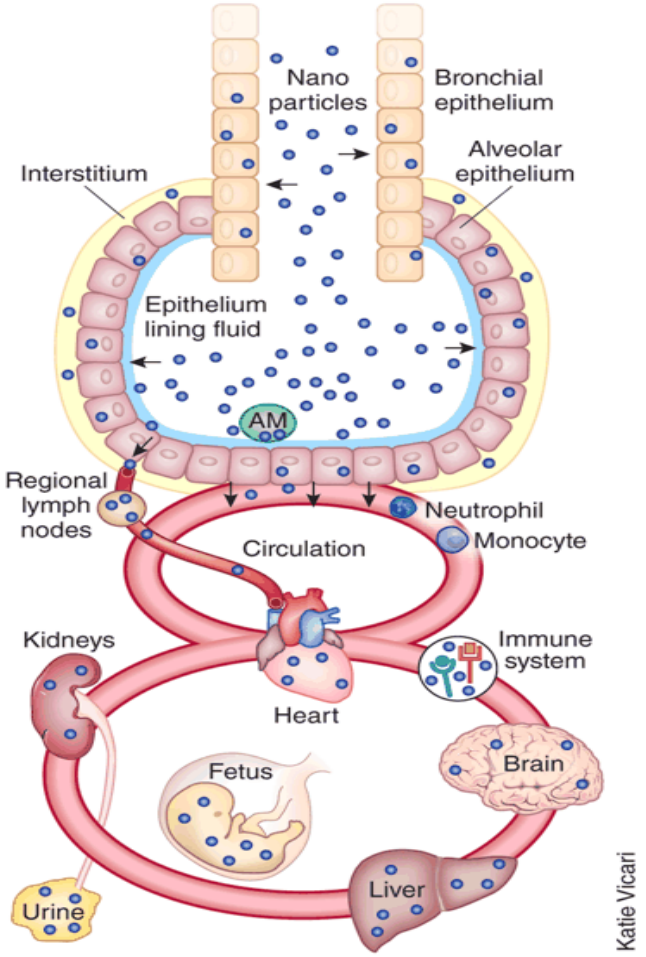

Figure 1 Aggregation of NPs in various organs or tissues of the body. Adapted from (Wolfgang G Kreyling, et al. Nature Biotechnology, Dec. 2010)

O. Schmid et al. retrospectively analyzed 9 studies using particles in vivo-induced acute pulmonary toxicity in mice or rats and found that the deposited nanoparticle surface area was the most relevant dose indicator for acute nanoparticle pulmonary toxicity. Transition metal oxides (Co, Ni, Zn) are about 12 times more toxic than low-solubility, low-toxicity (LSLT) materials (including carbonaceous materials) (Schmid & Stoeger, 2016). Neutrophils reach prominent culmination within 12 to 24 hours after carbonaceous NPs are instilled, showing an acute inflammatory response in the lung (Chen et al., 2016). Accordingly, our group found a positive correlation between the

inflammatory response in the lungs of mice and the BET surface area after intratracheal instillation of six combustion-derived nanoparticles (CDNPs) (Stoeger et al., 2006; Stoeger et al., 2009).

Asbestos deposition in the lungs can cause mesothelial damage and inflammation, resulting in continuous oxidative stress, and ultimately induce lung cancer and chest wall mesothelioma (Donaldson et al., 2010). Long-term exposure to nano-silicon in the lung is closely related to the occurrence of silicosis, and the silicic acid released from the surface of the quartz is a toxic component. In summary, a series of acute and chronic adverse health effects and diseases are related to human exposure to NPs, especially through the respiratory system.

1.2 Fluorescent nanomaterials for biomedical applications as research tools

In the recent ten years, nanotechnology has achieved unprecedented developments, and a variety of nano-fluorescent materials have been invented and applied in various fields. Due to their cytotoxicity and poor biocompatibility, traditional organic dyes have been limited in biomedical usage (Jamalipour Soufi & Iravani, 2020). However, compared to traditional organic dyes, the emergence of fluorescent nanomaterials exhibits superior prospects. Common fluorescent nanomaterials are Quantum Dots, Carbon Dots, Carbon Nanotubes, Graphene-Based Nanomaterials, Metal Nanomaterials, Phosphors, Organic

Frameworks, and various other nanomaterials (Liu et al., 2020). The application of fluorescent nanomaterials has covered various fields of biomedicine, including bioimaging, bio-detection, and bio-therapy methods (Xiao et al., 2021). With the development of microscopy and nano-drug modification techniques, fluorescent NPs have been valued for their traceability in nano-toxicology or nano-drug delivery research (Riehemann et al., 2009). Fluorescent “model” NPs can be used to study basic aspects of NP bio-distribution, bio-interactions, and possible adverse effects. In order to compare the distributions of infrared wavelength melamine particles in the lung after inhalation and instillation administration, Lin Yang et al., who are working in our institute, established a 3D co-recording image of lung structure and NPs maximum intensity projection (MIP) based on the application of Light-sheet Fluorescence Microscopy after 3DISCO lung tissue clearance. Unlike instillation, inhalation delivery resulted in a uniform nanoparticle distribution pattern, with central and peripheral acini receiving similar NP doses (Yang et al., 2019). In addition to their excellent optical properties (high brightness, less photobleaching, and narrow emission wavelength) (Volkov, 2015), commercial QDs offer various commonly used surface modifications, such as PEG-, carboxyl-, amine-PEG-complexed modified surfaces, which are excellently suited to study the different biological effects of different NP surface modifications in vivo. To investigate whether the surface modification of fluorescent nanomaterial QDs could mediate the targeting of specific parts of the body, Praetner et al. injected carboxyl-, amine-

and PEG-QDs into the blood vessels of mice. The distributions of different QDs in cremaster blood vessels, myocardial and skeletal muscle was traced by fluorescence microscopy. After exposure in the circulatory system, carboxyl-QDs (cQDs) had a short residence time in the blood, and their content was high in various organs, especially organs rich in capillary networks, such as the liver and spleen (Praetner et al., 2010).

1.3 Lung Intravital microscopy

Intravital Microscopy is a unique imaging method which allows real-time observation of cellular functions and interactions without the need to extract tissue from the body and allows the recording of immune cell dynamics at a cellular level resolution in the physiological or pathophysiological context (Alizadeh-Tabrizi et al., 2020; Wells et al., 2019). Until now, in vivo imaging technology has been mainly applied to uncover time-sequential immune cell activity in many organs, such as the liver, kidney, brain, and others (Khandoga et al., 2005; Kramer et al., 2000; Kuhnle et al., 1993; Ochi et al., 2019; Tabuchi et al., 2008). Using intravital microscopy on mouse cremasteric vessels, Rehberg et al. investigated the effect of quantum dot surface chemistry (carboxyl-, amine- and PEG- modification) on leukocyte recruitment in the circulatory system. After the intravenous (i.v.) application of cQDs, the rolling velocity of leukocytes was significantly reduced, while the number of adherent leukocytes in postcapillary venules and recruited leukocytes into the

surrounding tissue increased. However, upon injection of amine-PEG-Quantum dots (aPEG-QDs) or PEG-QDs, these parameters were almost identical to those of the control group (Rehberg et al., 2010). Bryan Ronain Smith et al. found that after administration of fluorescently labeled single-walled carbon nanotubes (SWNTs), most nanotubes were internalized by Ly-6C(hi) monocytes and delivered to tumors in mice. About 25% of SWNTs delivered into tumors are mediated by monocytes (Smith et al., 2014).

Due to the closed negative pressure environment in the chest and continuous breathing movement, the lung intravital microscope is the most difficult to achieve in-vivo imaging technology.

Prior to imaging, the mice underwent a minimally invasive procedure to open a window in the thoracic cavity, through which a portion of the lung tissue can be viewed directly under the microscope. The biggest obstacle to lung intravital microscopy is the continuous breathing motion of the lung, which greatly affects the imaging quality, especially at the cellular resolution level.

In 1939, Terry invented a vacuum-based stabilization technique to achieve cat in vivo imaging (Terry, 1939). Recently, vacuum-based stabilization of the murine lung using a miniaturized easy insertable vacuum window, established by Headley et al in 2016 (Headley et al., 2016), has become the gold standard for lung intravital microscopy, judged by the number of recent publications. Bryan G. Yipp applied the lung intravital microscopy platform to reveal that the pulmonary microvasculature is a vital host neutrophilic defense niche for the

lung (Yipp et al., 2017). By the negative pressure vacuum environment, the observed local lung tissue is stabilized, which minimizes surgical trauma and lung tissue exposure, and provides stable, high-resolution images of lung cells (Figure 2). In this approach, continuous negative pressure suction has the risk of causing local inflammation, but short-term (<2h) imaging did not lead to obvious neutrophilic pneumonia (Looney et al., 2011). Skilled microsurgeons can build models within 30 minutes, and multiple experiments can be performed in the same day.

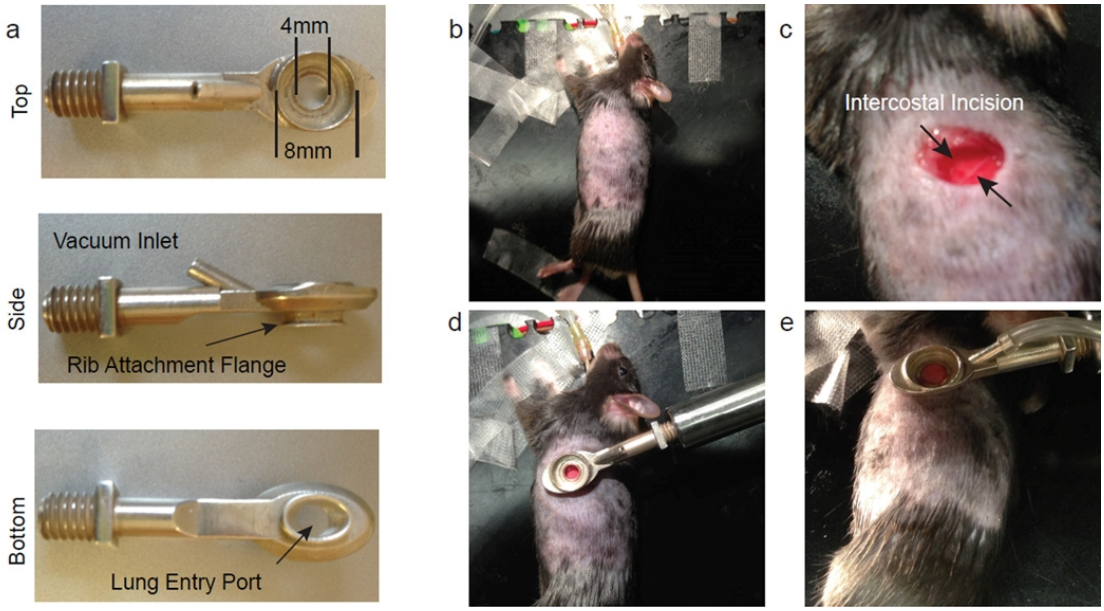

Figure 2 Observation window of L-IVM. a, Top, side, and bottom views of the observation window. b–e. detailed surgical procedure images with viewing windows installed. Adapted from (Mark B. Headley, et al. Nature. 2016)

Despite decades of intensive research, our knowledge about the process of lung-deposited NPs causing acute pulmonary disease remains incompletely understood. The lack of a clear comprehension of nanoparticle toxicological mechanisms is the main reason why valid therapies for particle-induced lung disease do not exist (Rehberg et al., 2016). The leukocyte total number and the ratio of different subtypes were applied as criteria to determine the occurrence

of inflammation. However, the applicability of this method is very limited for some specific patients or treatment stages. Children with Omenn syndrome, an autoimmune disease, have a marked decrease in lymphatic B cells and an increase in lymphatic T cells (Aleman et al., 2001). Myelosuppression occurs in patients with cancer during chemotherapy (Geissler et al., 2018). Abnormal leukocyte ratios occur in non-infectious patients, such as stroke patients with markedly increased neutrophils and lymphocyte counts (Hermann & Gunzer, 2019). These numbers are usually obtained by analyzing blood smears with automated blood cell counters based on the principles of flow cytometry or by manual inspection using a microscope (Brunck et al., 2014; Lim et al., 2020). What both methods have in common is that they do not look at the active immune cell state, but simply enumerate their numbers from fixed/inactivated samples. Although we have known the mechanisms of neutrophil migration for more than a century (Kienle et al., 2021). Researchers have also begun to study other immune cell immune dynamic responses with intravital microscopy (AS., 2021; Melnicoff et al., 1988). Lung intravital microscopy (LIVM) has been widely used to visualize and measure in real-time the cellular pulmonary innate immune response in the lungs. Using IVM to evaluate the immune response and the behavior of resident immune cells under various conditions helps us explain some very complex lung biology problems.

1.4 Ventilator-assisted aerosol inhalation

To study the pulmonary toxicology of NPs or the pulmonary delivery for applications in nanomedicine, the establishment of a dose-controlled lung nanoparticle exposure/pulmonary nanoparticle delivery system is a very important step. Many genera have been used to build this model. This includes large animals such as non-human primates, dogs, pig, and small animals such as guinea pigs, mice, and rats (Cryan et al., 2007). Mice are the most commonly used animals because of their small size (easy to raise and low cost), high reproduction rate (high number of fetuses and short generation time), and high genetic similarity to humans (99% of the genes in mice can be found in homologous genes in the human genome (Zhu et al., 2019)).

Different delivery methods can affect pharmacological or toxicological results in vivo. Pulmonary delivery in preclinical studies is achieved via nasal aspiration, oropharyngeal aspiration, intra-tracheal spray/dry powder insufflator, nose only and whole-body aerosol exposure chamber as well as ventilator-assisted aerosol inhalation (Ehrmann et al., 2020).

Ventilator-assisted aerosol inhalation is a direct route of administration. The entire system consists of tracheal intubation, mechanical ventilation, and liquid nebulization (Robichaud et al., 2015). This method is performed with a cannula inserted into the trachea of an anesthetized animal. The cannula is connected to a mechanical ventilator equipped with a nebulizer, where the aerosol droplets are generated, then the droplets are delivered to the mouse airway through the

cannula (Yang et al., 2019).

1.5 Lung immune system

Even when the body is in a steady state, the lung is an active organ with continuous respiration. The abundant capillaries in the vasculature minimize the direct distance between blood and air, thereby greatly increasing oxygen exchange efficiency (Knudsen & Ochs, 2018). However, this direct exposure increases the possibility of alveolar localized pathogenic microorganisms invading the human body from the respiratory system. Therefore, there is also a complex network of immune cells in the lungs. This network can monitor the conditions in the lungs in real time and quickly generate immune responses and it contains different kinds of immune cells such as neutrophils, monocytes, T cells, B cells, NK cells, alveolar macrophages, interstitial macrophages and dendritic cells (Looney & Headley, 2020). Under healthy conditions, most cells are maintained at relatively low levels to ensure the homeostasis of the immune environment in the lungs. However, in disease states (infection, allergies, cancer, etc.), the types and numbers of immune cells will change dramatically to eliminate pathogens and restore the immune environment in the lungs to a steady state as soon as possible (Looney & Headley, 2020).

1.5.1 Alveolar macrophages (AMs)

AMs are the main phagocytes located in the alveolar sac. They are derived from the liver of the fetus (Yona et al., 2013) and have the ability to self-renew. In

acute lung injury, the lost AMs are replaced by monocyte recruitment (Misharin et al., 2017; Mould et al., 2021; van de Laar et al., 2016; Yona et al., 2013).

Like most tissues residing macrophages, which constitute the first line of defense against pathogens at the interface with the surrounding environment, AMs provide a sentinel function against inhaled pathogens (Islam et al., 2012). At the same time, AMs also perform a key homeostasis function, constantly removing endogenous debris (dead cells and ineffective surfactants) in the lungs (Guilliams et al., 2013; Kopf et al., 2015; Trapnell & Whitsett, 2002). It has been described that in the lung of mice during acute lung injury, AMs rapidly release micro vesicles (MVs) into the alveoli after LPS treatment, and these MVs carry large amounts of tumor necrosis factor (TNF) inducing an increase in the acute influx of neutrophils into the alveoli (Soni et al., 2016).

AMs play an important role in many respiratory diseases, such as infectious diseases (viral, bacterial and fungal infections), and lung inflammation related to genetic or environmental exposure (Hussell & Bell, 2014). These diseases have a huge impact on global health. Lower respiratory tract infections and chronic obstructive pulmonary disease (COPD) are the 4th and 6th leading causes of death. In addition, 8 million people die every year from environmental pollution exposure (Gordon et al., 2014; Shaddick et al., 2018).

Air pollution, especially PM2.5, is one of the top 5 major risk factors for death worldwide (Organization, 2016). When fine particles are inhaled into the lungs, they are mainly deposited in the respiratory bronchioles, and tracheal

macrophages are the main immune cells that phagocytose particles in the trachea (Alexis et al., 2006; Geiser, 2002; Pinkerton et al., 2000). AMs are vital in removing air-pollution-induced airway debris, but other studies have shown that AMs may also aggravate lung inflammation caused by air pollution, and the mechanism is unknown (Miyata & van Eeden, 2011; Pinkerton et al., 2000).

Silicosis is an inflammatory fibrotic disease, mainly caused by occupational exposure and inhalation of silica crystals produced by mining or glass manufacturing. AMs are crucial to the formation of silicosis (Rimal et al., 2005). AMs phagocytose silica particles and the cells die and lyse subsequently, releasing the particles and passing them to other cells, producing a chain reaction. Local inflammation occurs during this process, including the secretion of pro-inflammatory cytokines (IL-1β and TNF-α), the activation of inflammasomes, and the release of reactive oxygen species (ROS) (Dostert et al., 2008; Rimal et al., 2005; Srivastava et al., 2002).

Carbonaceous nanoparticles (CNPs) are one of the main components of urban particulate air pollution. High-dose CNP exposure can trigger a proinflammatory response in the lung with CXCL1, -2, -5, and TNFα highest levels 12 h after NP (Chen et al., 2016). As early as 3 hours after CNPs instillation, half of AMs showed nanoparticle loading. However, AMs acquired from the lungs for 3-12 hours upon CNPs exposure didn’t exhibit proinflammatory features (Chen et al., 2016). Furong Tian et al. revealed that particles were found in AMs 1, 3, and 7 days after DWCNT instillation exposure. Upon exposure on day 3, the

contribution of macrophages and related cytokines such as CCL2, CCL3, IL6, and CSF3 became more pronounced (Tian et al., 2013). Similarly, 24 h after CNP and DWCNT exposure, the number of polymorphonuclear neutrophils (PMNs) in the alveoli peaked and then gradually decreased (Chen et al., 2016; Tian et al., 2013).

1.5.2 Lung epithelial cells

Lung epithelium is directly connected to the external environment and responsible for coordinating the innate immune response and repair after inflammatory damage. The lung epithelium is a complex and adjustable system required for efficient breathing. It has different physiological effects depending on the position in the respiratory tract. There are a variety of epithelial cell types in the respiratory tract, and various cells have complex cellular interaction networks and regulatory mechanisms, which are necessary for maintaining homeostasis and repair after injury (Crystal et al., 2008). Alveolar epithelial cells (AEC), which form the alveolar structure are the most common in the respiratory tract, and they include two subtypes, type I and type II pneumocytes (Davis & Wypych, 2021). Type I pneumocytes occupy about 90-95% of the alveolar surface and are the main place for gas exchange (Wang et al., 2018) , while type II pneumocytes secrete alveolar surfactant to reduce alveolar surface tension and prevent alveolar collapse (Olajuyin et al., 2019). Epithelial cells are the first firewall against the external environment and have many properties or functions to maintain homeostasis in the lungs, such as tight junctions between

epithelial cells and secretion of antimicrobial active molecules (Adivitiya et al., 2021; Leiva-Juárez et al., 2018; Marchiando et al., 2010; Tam et al., 2011; Whitsett & Alenghat, 2015). Lung epithelial cell death, a hallmark of acute lung injury (ALI), contributes to ALI by causing damage to the air barrier and structural integrity (Deshpande & Zou, 2020). Apoptosis and ferroptosis were also observed in NiONPs-exposed human lung epithelial cells, accompanied by increased numbers of inflammatory cells and secretion of inflammatory factors (Liu et al., 2022). Early exposure to TiO2 NPs produced cytotoxic, genotoxic, and inflammatory responses in human alveolar and bronchial epithelial cells (Ursini et al., 2014), but long-term exposure did not affect epithelial cell viability, but caused oxidative damage to DNA (Armand et al., 2016).

1.5.3 Neutrophils

Neutrophils are the main effector cells of inflammation and mainly found in the peripheral organs, like the lung (Burn et al., 2021; Rosales, 2018). Interestingly, although it is a terminally differentiated immune cell, it has a very short life span, with a half-life of 1.5-8 hours after leaving the bone marrow into the blood circulation (Pillay et al., 2010). The main functions of neutrophils are to generate ROS, release pro-inflammatory mediators, release neutrophil extracellular traps (NETs) for kill, and limit the spread of pathogenic microorganisms (Gazendam et al., 2016). In addition to these weapons, they also swallow and remove cell debris or pathogens (Gazendam et al., 2016; Segal, 2005).

Ultimately, neutrophils undergo an orderly programmed breakdown (apoptosis), and are eliminated (Nauseef & Borregaard, 2014). Meanwhile, the neutrophils promote the resolution of inflammation via neutrophil exosomes release to modulate the activity of other phagocytes (macrophages and dendritic cells (DCs)) for vascular homeostasis (Angelillo-Scherrer, 2012; Eken et al., 2013). During the differentiation and maturation of neutrophils, they express a variety of receptors, such as pathogen recognition receptors, chemokine receptors, innate immune receptors (like Toll-like receptors and C-type lectins), Fc receptors, and cell adhesion molecules (Futosi et al., 2013). When inflammation occurs, neutrophils adhere to endothelial cells close to the tissue injury site, cross the endothelial cell barrier, and finally transfer to the site of inflammation. In skeletal muscle, neutrophils migrate to inflamed tissues through the postcapillary venules (Marki et al., 2015), for which they first roll along and later arrest on the surface of endothelial cells in the lumen of these microvessels. During inflammation, glycocalyx degradation induced by metalloproteinases and heparinases released by injured endothelial cells occurs, and cytokines, proteases, histamines, and heparinases are secreted by activated mast cells (Tarbell & Cancel, 2016). The cytokine-evoked degradation of glycocalyx exposes adhesion molecules, like intercellular adhesion molecules (ICAMs) on the surface of endothelial cells. Cytokines also promote the expression of selectins and integrins, which are required for neutrophil recruitment on these cells (Hu et al., 2021). Subsequently, neutrophils cross the

endothelial barrier towards the inflammation site (Kolaczkowska & Kubes, 2013).

The vascular system of the lung consists of a continuous layer of endothelial cells (Marki et al., 2015). Neutrophils have two routes to enter the lungs: 1. The post-capillary venules of the systemic circulation, 2. The alveolar capillaries of the pulmonary circulation (Figure 3). The average size of the capillaries (6 μm) of the respiratory tract is smaller than the size of neutrophils (8-10 μm) (Doerschuk et al., 1993; Tasaka et al., 2003), which greatly slows down the transit time of neutrophils in the respiratory capillaries. In addition, neutrophils must deform to pass through the respiration capillary cavity. In this process, neutrophils and endothelial cells are tightly attached (Kim & Luster, 2015; Kolaczkowska & Kubes, 2013). Therefore, the rolling of neutrophils mediated by CD62L in the pulmonary capillaries hardly occurs (Hogg & Doerschuk, 1995). Neutrophils entering the pulmonary circulation can react quickly and on a large scale to pathogens entering the alveoli.

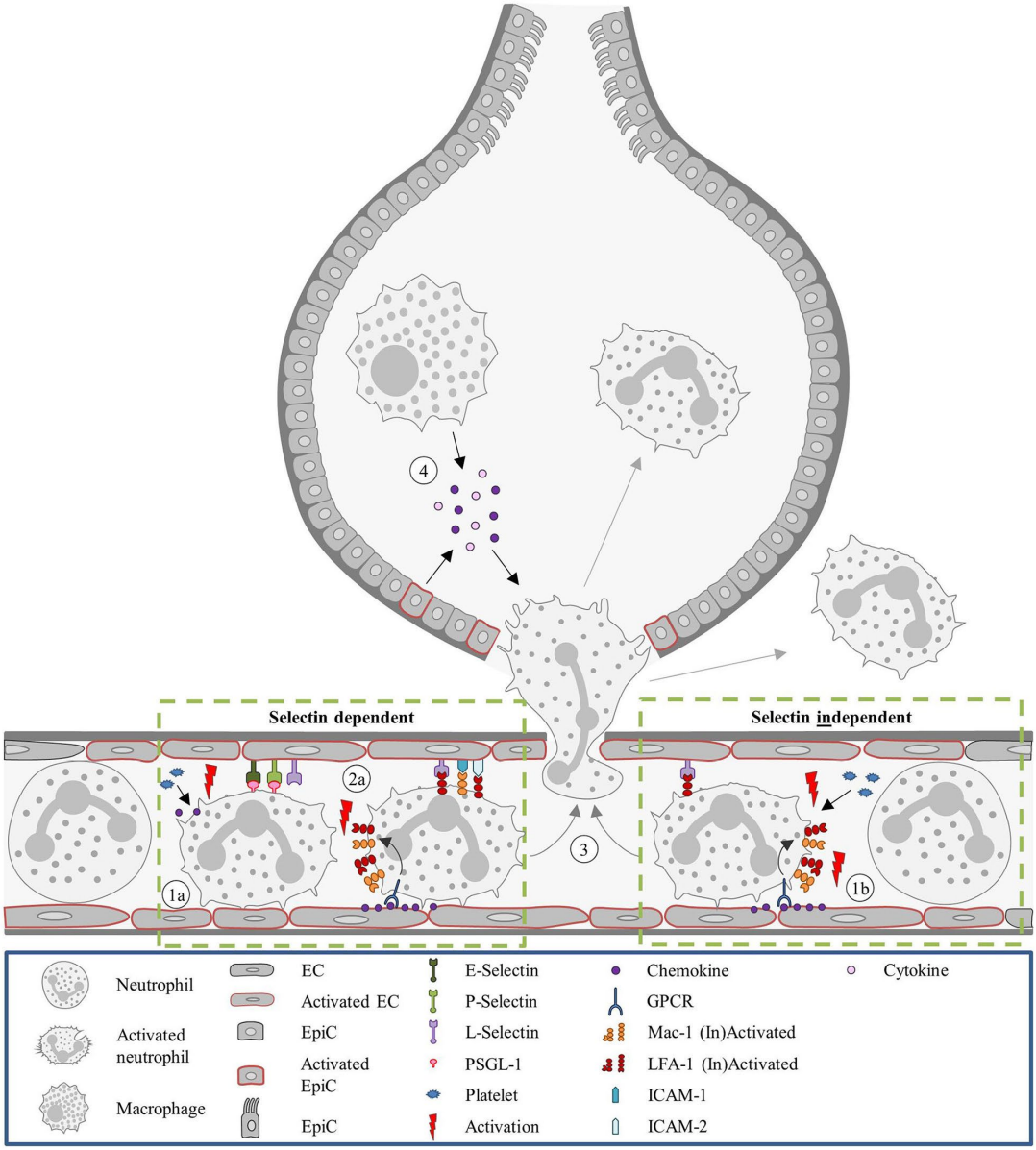

Figure 3 The trafficking of neutrophils in the lung. Adapted from (Sanne L. Maas, et al. Frontiers in Immunology. 2018)

1.5.3.1 Microbial infection

a) Bacterial infection

The rapid response to bacterial infection is the most obvious and main function of neutrophils in innate immunity. In order to achieve this rapid immune response, neutrophils use non-specific antibacterial activities, such as NADPH

oxidase-mediated ROS production, which attack pathogenic cells and host cells indiscriminately (Gazendam et al., 2016; Khan et al., 2017; Naumenko et al., 2018; Segal, 2005; Subramaniam et al., 2014). In addition to the production of reactive oxygen species, neutrophils produce a large amount of reactive nitrogen, such as nitric oxide (NO) in the airway (Ichinose et al., 2000), which also plays a very important role in destroying bacteria (Wright et al., 1989). Another antibacterial mechanism involves the release of neutrophil extracellular traps (NET) composed of a branched network of extracellular DNA filaments (Schimmel et al., 2013), and cytoskeletal proteins and proteases are mostly related to host defense during infection by pathogenic microorganisms (Papayannopoulos, 2018).

b) Viral infection

Although previous studies have investigated the function of granulocytes in bacterial infections, more and more studies have demonstrated its importance in dealing with viral infections. Early in viral infection, neutrophils are rapidly recruited from the blood to inflammation sites. At the same time, the bone marrow is rapidly mobilized and differentiated into mature neutrophils in the periphery. In lung virus-induced infections, such as influenza, respiratory syncytial virus (RSV), and Middle East respiratory syndrome-related coronavirus (MERS), numerous infiltrated neutrophils had been found in the alveolar space (Baseler et al., 2016; Geerdink et al., 2015; Narasaraju et al., 2011).

c) Fungi infection

In fungal infections, neutrophils also produce a strong immune response. The most common fungal infection is Aspergillus fumigatus, which also induces the recruitment of a large number of neutrophils (Morán et al., 2018). This process is related to the proteolytic regulation of VWF by ADAMTS-13 or ADAMTS-13 by itself. In addition to the direct removal of hyphae and spores, neutrophils play a key role in regulating the adaptive immunity caused by Aspergillus fumigatus infection (Alflen et al., 2017).

1.5.3.2 Nano-particle exposure

After exposure to NPs, neutrophils produce an immune response to infiltrate into the alveoli, secrete chemokines, and activate downstream pathways (Cronin et al., 2020). In an earlier study of our group, bronchoalveolar lavage (BAL) analysis showed that CNP instillation elicited an acute inflammatory response, where numerous neutrophils accumulated in the alveoli after 1 day after nanoparticle exposure and neutrophil chemokines CXCL1, -2 and -5 reached peak levels upon 12 hours after CNP application (Chen et al., 2016). Our group further compared the immune responses elicited by CNP inhalation versus intra-artery injection of a CNP dose with equivalent surface area. Increased retention of activated leukocytes, secondary thrombocytosis, and pro-inflammatory responses in secondary organs were detected only 4 and 24 hours after CNP inhalation exposure (Ganguly et al., 2017). Various

physicochemical properties like the size, charge, surface area, reactivity, surface coating, synthesis method, and impurities of NPs are the main factors affecting the innate immune response (Getts et al., 2015; Moyano et al., 2016; Petrarca et al., 2015; Vivier & Malissen, 2005; Warheit, 2008). According to the review of O. Schmid et al., the surface area of NPs is the most biologically relevant dose indicator for spherical NPs when infiltrated PMNs amounts were chosen as the toxicological endpoint, explaining approximately 80% of the observed variation in acute lung toxicity (Schmid & Stoeger, 2016). Frédéric Cosnier and colleagues compared data on benchmark materials - TiO2, CNP, and MWCNT - after subacute (4 weeks) inhalation with acute (1 week) to sub-chronic (13 weeks) inhalation exposure data. Dose-response relationships in short- and long-term studies revealed that PMN percentage was associated with the lung-retained surface area dose, independent of time post-exposure (Tian et al., 2013).

Once the pathogen-associated molecular patterns (PAMPs) of nanoparticle bind to pattern recognition receptors (PRRs) on the surface of neutrophils, inflammasome-dependent neutrophil activation is initiated (Demento et al., 2009; Najafi-Hajivar et al., 2016). NETosis, a specific cell death of neutrophils, is an alternative for NP to stimulate immune and inflammatory responses (Brinkmann et al., 2004; Fuchs et al., 2007). When NPs stimulate neutrophils to develop NETosis and release neutrophil extracellular traps (NETs), the NPs may be taken up by NETs in a process independent of phagocytosis (Jorch &

Kubes, 2017). A variety of NPs (such as gold, silver, diamond, and Polystyrene, etc.) exposure can induce NETosis (Bartneck et al., 2010; Hwang et al., 2015; Liz et al., 2015; Muñoz et al., 2016).

Aim of the study

As explained above, airborne nanoparticle exposure is a nonnegligible threat to public health, and it is urgent to reveal the toxicological mechanisms to formulate corresponding prevention strategies. AMs are the main immune cell group present in the alveolar cavity. When pathogens enter the alveoli, AMs are the first cells to interact with them and induce an immune response, such as phagocytosis, and secretion of inflammatory-related factors, to maintain the stability of the alveolar environment. While neutrophils are known as one of the main players in the acute inflammatory process, they are the immune cells that primarily recruit and massively infiltrate into the inflammation site (alveolar space). The series of events that trigger NP-induced neutrophilic inflammation has not been fully characterized yet.

Here we applied state-of-the-art intravital microscopy to observe pathophysiological changes and pulmonary innate immune response at the cellular level resolution in animals exposed to NPs by means of ventilator-assisted inhalation of nebulized QDs (fluorescent NPs) and carbon black NP aerosols.

With this in vivo imaging platform, we aimed to visualize immune cells (AMs and neutrophils) and measure the number of alveolar localized neutrophils in mice exposed to NPs. Furthermore, we aimed to observe alterations in the motility status of AMs and neutrophils and by application of specific inhibitors to clarify crucial steps, associated with the innate immune responses to

nanoparticle exposure.

Taken together, this study aimed to uncover the role of AMs and neutrophils in sterile inflammation in a murine model of acute nanoparticle inhalation exposure.

2. Materials and Methods

2.1 Materials

All used laboratory equipment and consumables are listed in the Appendix.

2.2 Methods

2.2.1 In vivo experiment

2.2.1.1 Mice

C57BL/6 (WT) mice were purchased from Charles River (Sulzfeld, Germany) for the respective experiments, Lyz2 mT/mG C57BL/6 mice, IL1r1ko C57BL/6 mice, and Macgreen (Csf1r-EGFP) C57BL/6 mice were originally purchased from the Jackson Laboratory (Bar Harbor, ME, USA) and bred in house. All mice were housed in individually ventilated cages supplied with filtered air in a 12 h light/12 h dark cycle and under a specific double-barrier, pathogen-free unit at Helmholtz Zentrum München. Mice were fed autoclaved rodent feed and water ad libitum. All experiments were performed with female animals at 10 to 16 weeks old. All protocols used were according to the guidelines drafted by and approved by the Regierung von Oberbayern (District Government of Upper Bavaria).

2.2.1.2 Nanoparticle

Quantum Dots (QDs): Qdot™ 655 ITK™ Carboxy, Qdot™ 655 ITK™ Amino

(PEG), and Qtracker™ (PEG) 655 quantum dots (Diameter in water: 22.2-37.5 nm (Rehberg et al., 2012), Emission wavelength: 655 nm) were purchased from Invitrogen Corporation (Karlsruhe, Germany). These QDs are composed of a semiconductor material CdSe core encapsulated with a ZnS shell and an extra layer of polyethylene glycol (PEG-QDs), with additional amine residues (aPEG-QDs) or without any coating carboxyl residues solely without PEG layer (cQDs). The PEG coating itself was composed of short PEG oligomers (1.3 kDa) (Praetner et al., 2010).

Melamine resin particles: MF-FluoRed (Excitation wavelength: 636 nm and Emission wavelength: 686 nm) were purchased from microParticles GmbH (Berlin, Germany). MFs are prepared by an acid-catalyzed polycondensation process in the aqueous solution using melamine resin precursors in presence of red fluorophores. The discrete size is 0.94±0.05 µm.

Printex90 carbon-NPs (CNPs): These commercial carbon NPs were purchased from Degussa (Frankfurt, Germany), (diameter: 14nm; organic content: 1%; surface area: 272 m^2/g) (Ganguly et al., 2009).

2.2.1.3 In vivo labeling of AMs

The method was performed according to a previously published procedure (Neupane et al., 2020). PKH26 phagocytic cell labeling kit (Sigma, Burlington, MA, USA) was purchased from Merck KGaA (Darmstadt, Germany). 0.1 ml PKH dye stock (10^{-3} M) was mixed thoroughly with 0.9 ml p.a. ethanol to

make a 100 µM working solution. The working solution was then freshly diluted in Diluent B to prepare 0.5µM PKH26PCL, which was used as a labeling solution for the respective L-IVM experiments. Mice were applied 75µL of the solution directly into the airway by oropharyngeal aspiration at least 5 days prior to the experiment.

2.2.1.4 Oropharyngeal aspiration

The mice were deeply anesthetized by intraperitoneal injection (i.p.) with a triple compound of medetomidine (0.5 mg/kg body weight), midazolam (5 mg/kg body weight), and fentanyl (0.05 mg/kg body weight) (MMF). Then, mice were attached with their foretooth on a 60° slope in a custom-made platform. The tongue was softly outstretched with toothless blunt forceps and fixed with two gloved fingers. Next, the nose was gently clamped with toothless blunt forceps. When the mice began to breathe deeply, the required volume was pipetted into the back of the throat. After the mice took 10 deep breaths, the nares were reopened. After the antagonist was injected, the mice have been returned to the cage and monitored until they moved normally.

2.2.1.5 In vivo antibody labeling

Direct-labeled antibodies were administered via intravenous injection (i.v., via the medial canthal vein) at least 15min before L-IVM surgery to anesthetized mice (MMF (i.p.)). Neutrophils were labeled with 3µg of anti-mouse Ly6G antibody (Alexa Fluor® 488, clone:1A8, Biolegend, California, USA).

2.2.1.6 Lung Intravital microscopy (L-IVM)

The lung intravital microscope is based on the VisiScope. A1 imaging system (Visitron Systems GmbH, Puchheim, Germany) equipped with an LED light source for fluorescence epi-illumination (CoolLED, U.K.). For QDs excitation the 365nm LED modules (at 50% output power, exposure time 50 ms), and for Melamine resin particles the 655 nm LED module (at 50% output power, exposure time 50 ms) were used. The light was directed onto the sample via a quad-band LED light filter (F66-014, DAPI/FITC/Cy3/Cy5 Quad LED ET Set; AHF Analysentechnik AG, Tuebingen, Germany). Microscope images were acquired by a water dipping objective (20 x, NA 1.0. Zeiss MicroImaging GmbH, Jena, Germany). A beam splitter (T 580 lpxxr, Chroma Technology Corp, Bellows Falls, USA) was used to divide the light from the sample and was acquired with two Rolera EM2 cameras and VisiView Imaging software (Visitron Systems GmbH, Puchheim, Germany). The experimental approach was adapted from the previously described work (49). The mice deeply anesthetized with MMF (i.p.) were kept at 37°C on a mouse heating platform and monitoring system (Harvard Apparatus, Massachusetts, United States). Fluorescent dyes/ antibodies have been applied via the left medial canthal vein using a 1ml insulin syringe (Becton, Dickinson and Company, Franklin Lakes, USA). The surgical sites (neck and left chest) have been locally anesthetized with Bucaine (50µg/site, Puren Pharma) 15 min prior to surgery. The neck tissue was separated, and the trachea was visualized. The anterior

part of the trachea was incised with Castroviejo scissors and a small blunt catheter (20G, Braun, Melsungen, Germany) was threaded <5 mm into the trachea and secured by a ligature. The catheter was then connected with a small rodent ventilator (MiniVent, Harvard Apparatus, Massachusetts, United States) with a 10µl/g bodyweight stroke volume and 150 breaths per minute under 2-3 cm H_2O (~0.1cm/g) positive end-expiratory pressure (PEEP) with 100% oxygen. The mouse was placed on its right lateral decubitus position for left chest surgery. A small surgical incision was made in the skin on the left thorax, thereafter the intercostal muscles between ribs 3 and 4 were carefully incised forming a 5mm opening. The vacuum chamber with an 8mm glass cover slip was carefully inserted between the incision. The lung was stabilized against the coverslip with a 20-25mmHg suction. Negative pressure was generated by a custom-made system consisting of differential pressure gage (Magnehelic. Dwyer Instruments. inc, USA), and a negative pressure pump (Nupro, St Willoughby, USA). Anesthesia was maintained by the administration of half of the initial dose of MMF (i.p.) every hour.

2.2.1.7 Quantum Dots aerosol inhalation

During the experiment, the tube supplying the mouse with oxygen was connected to a small rodent ventilator (Harvard Apparatus, Massachusetts, USA) to control the mouse’s breathing with 150 breaths/min and 10µl/g bodyweight tidal volume. In the inspiration tube, a nebulizer unit consisting of

an AerogenPro nebulizer (Aerogen Small VMD, Kent Scientific Corporation, USA), was inserted to generate liquid aerosol droplets of 3.5-4 µm diameter, composed of NP suspension. For every quantum dot group, the nebulizer was added with 20µl solution containing 4µM quantum dot suspension (1:2 diluted stock suspension) in distilled water with 1% saline providing ions. During NP inhalation, the tidal volume was increased to 15 µl/g. The infrared detector installed on the ventilator detected the tidal volume change and activated the Control Module (Aeroneb® Lab, Kent Scientific Corporation, USA), which triggered the nebulizer activation for 20 ms per inspiration. The entire inhalation process lasted around 2 minutes, after which the tidal volume was reduced back to 10µl/g bodyweight.

2.2.1.8 CNP aerosol inhalation

The inhalation process of CNP (Printex 90) was as described above (3.2.1.7), adding 460 µl CNP (5µg/µl) into the nebulizer for transtracheal inhalation.

2.2.1.9 In vivo blocking/inhibiting experiments

The mice were administered blocking antibodies/isotype control antibodies or inhibitors (Table 1) via the oropharyngeal method into the airway. 3 hours after administration, mice were imaged with L-IVM.

Table 1: List of blocking antibodies or inhibitors applied to the lungs.

Blocking antibody/Inhibitor	Clone	Manufacturer
In vivo mAb anti-mouse LFA-1α	M17/4	Bio X Cell,

		Lebanon, USA
Purified anti-mouse CD54 (ICAM-1) Antibody	YN1/1.7.4	ATCC, Manasses, USA
In vivo mAb anti-mouse/human CD44	IM7	Bio X Cell, Lebanon, USA
Ultra-LEAF™ Purified anti-mouse CD88 (C5aR) mAb	20/70	BioLegend, Fell, Germany
Ultra-LEAF™ Purified anti-mouse CD64 (FcγRI) mAb	W18349F	BioLegend, Fell, Germany
In vivo mAb rat IgG2a isotype control	2A3	Bio X Cell, Lebanon, USA
Ultra-LEAF™ Purified Rat IgG2b, κ Isotype Ctrl antibody	RTK4530	BioLegend, Fell, Germany
NAC(N-Acetyl-L-cystein)	CAS 616-91-1	Merck, Darmstadt, Germany

For i.v. application experiments, mice were pretreated with blocking antibodies/isotype control antibodies or degranulation inhibitors (Table 2) via medial canthal vein injection. 0.5h after administering blocking antibodies, mice were imaged with L-IVM.

Table 2: List of blocking antibodies or degranulation inhibitors applied to the blood circulation.

Blocking antibody/Stabilizer	Clone	Manufacturer	Dose
In vivo mAb anti-mouse LFA-1α	M17/4	Bio X Cell, Lebanon, USA	30 μ g/mouse
Purified anti-mouse CD54 (ICAM-1) antibody	YN1/1.7.4	ATCC, Manasses, USA	30μg/mouse
Mouse CXCL1/GRO alpha /KC/CINC-1 antibody	48415	R&D Systems, Minneapolis, USA	1μg/g(body weight)
Cromolyn sodium salt		Sigma, Burlington, MA, USA	0.2μg/g(body weight)

2.2.1.10 Measurement of blood perfusion velocity

Melamine resin (microParticles, Berlin, Germany) fluorescence particles (50 µl of 0.05 % stock solution, Ex/Em 636 nm/686 nm) were injected into mice by

intravenous injection and imaged at ~2.5 frames per second (fps) with the fast acquisition mode. The pulmonary blood flow velocity of mice is represented by the trajectory (velocity) of MF fluorescence particles. The “Manual Tracking” function of ImageJ (National Institutes of Health, Bethesda, USA) was applied to give a specific coordinate axis to the bead location at each time point. Then, bead velocity was analyzed with the Chemotaxis and Migration Tool software (ibidi GmbH, Gräfelfing, Germany).

2.2.1.11 BAL preparation and cell differentiation

Mice were anesthetized via a mixture of xylazine (110 µg, WDT, Garbsen, Germany) and ketamine (10mg, PharmaWiki, Disentis, Switzerland) (i.p,) and sacrificed by abdominal aorta exsanguination. Immediately after, BAL was performed by tracheal intubation with a 20G cannula (Braun, Melsungen, Germany) and infusing the lungs 8 times with 1.0 ml sterile phosphate-buffered saline (PBS). The total recovered volume was around 8 ml/mouse. The supernatant obtained from the first two BAL centrifugations (400 g, 20 min at 4℃) was pooled for protein or cytokine analysis. The cell pellets were resuspended in 1 ml sterile PBS and the cell number was counted using the trypan blue exclusion method. For this, 20 µl cell suspension was added into 80µl 0.4% trypan blue dye to obtain a 1:5 dilution and mixed by pipetting up and down. The mixture was added to a hemocytometer and all non-blue cells were counted in each large square in each corner of the hemocytometer. The

final cell concentration was calculated by the formula as: Number of cells in cell suspension/ml = total number of cells in 4 large squares/$4\times5\times10^4$.

BAL cell differentials were accomplished on cytospin slides with May-Grünwald- Giemsa staining. 3×10^4 BAL cells were added into different Cytofunnel chambers of Cytospin™ Centrifuge (Cytospin 2, Thermo Shandon Ltd, U.K.) with Cytofunnel and Cytoclips and centrifuged at 400 rpm for 6 min, to concentrate and deposit a monolayer of cells onto the circular area of the slide. The slides were immersed in 100% May-Grunwald for 10 minutes and washed in tap water for 2 minutes. Slides were transferred directly to 5% (diluted in tap water) Giemsa for 15 minutes. Next, the slides were dipped 10 times in tap water quickly and submerged in fresh tap water for 2 minutes. The slides were air-dried at least 2 hours in a ventilated place, then covered with coverslips.

2.2.1.12 Lung tissue frozen section

After the L-IVM experiment, the mouse was sacrificed immediately after the experiment by exsanguination. The trachea was cannulated with a 20G catheter (Braun, Melsungen, Germany), and the lungs were inflated using 1000µl of the mixture of cryo embedding matrix (OCT) (Cellpath, Newtown, England) and 4% Paraformaldehyde (1： 2) via the catheter. Subsequently, the whole lung was isolated and washed in sterile PBS. The lung was then fixed in 4% PFA at 4℃ overnight. The lungs were immersed sequentially in

10% and 30% sucrose overnight. The lung was embedded in OCT and stored at -80°C. 6 µm sections were made in a Hyrax C50 Cryostat (Zeiss, Jena, Germany).

2.2.1.13 Nuclear Staining

Lung cryosections were permeabilized 3 times with PBST (0.1% Tween (Sigma-Aldrich, Burlington, MA, USA) in PBS) for 2 minutes, followed by incubation with DAPI in PBS containing 0.1% (w/vol) bovine serum albumin (BSA) for 1h at room temperature. Afterwards, sections were washed three times with PBST and mounted with DAKO fluorescence anti-fade agent.

2.2.1.14 Murine precision-cut lung slices (PCLS)

Mice were anesthetized via a mixture of xylazine (110 µg, WDT, Garbsen, Germany) and ketamine (10mg, PharmaWiki, Disentis, Switzerland) (i.p,) and sacrificed by abdominal aorta exsanguination. Then, the trachea was cannulated with a 20G catheter (Braun, Melsungen, Germany), and the lungs were inflated with 800µl of a mixture of pre-warmed 2% low melting agarose (Sigma, Burlington, MA, USA) via the catheter. Left lung lobes were cut to a thickness of 100 µm with a vibratome (Hyrax V55; Zeiss, Jena, Germany) using a speed of 10–12 µm·s−1, a frequency of 80 Hz, and an amplitude of 1 mm. Nuclear staining of the PCLs sample was done as described in chapter 2.2.1.12.

2.2.1.15 3D Lung Imaging

Macgreen mice were sacrificed by exsanguination and transcardially perfused with 30 ml sterile PBS at room temperature to flush all blood (EGFP-labeled cells (monocytes, neutrophils, etc.) included) from the lungs. After this, only EGFP-expressing AMs and interstitial macrophages were left in the lung. The lung tissue was stained and cleared as described (Yang et al., 2019). Briefly, samples were fixed in 4% PFA at 4 °C overnight. Next, samples were incubated in PBSG-T (0.2% gelatin, 0.01% thimerosal, and 0.5% TritonX100 in PBS) for 3 days with rotation (70 rpm) at room temperature to block nonspecific antibody binding. Lung samples were incubated with an anti-GFP antibody (clone: ab13970, ABCAM, Waltham, USA) which is diluted in 0.1% saponin in PBSG-T for 7 days with rotation (70 rpm) at 37℃. Afterwards, lung samples were rinsed 6 times with PBST (0.5% Triton in PBS) for 1 hour and incubated with goat anti-chicken secondary antibody (AF647, ABCAM, Waltham, USA) / DAPI diluted in 0.1% saponin in PBSG-T for 3 days with rotation (70 rpm) at 37℃. Samples were washed 6 times again in PBST for 1 hour with rotation at RT to finish the last step of staining. The clearing was performed after dehydration in a concentration gradient of tetrahydrofuran (THF, Sigma, Burlington, MA, USA, 50% v/v tetrahydrofuran/H_2O overnight, 50% THF/H_2O for 1 h, 80% THF/H_2O for 1 h, 100% THF for 1 h, 100% THF overnight, and 100% THF for 1 h) under constant slight shaking. Then samples were incubated in dichloromethane (DCM, Sigma, Burlington, MA,

USA) for around 30−40 min and eventually immersed in dibenzyl ether (DBE, Sigma, Burlington, MA, USA) at least 2h prior to imaging. Imaging was performed in dibenzyl ether with a light sheet fluorescence microscope (Ultramicroscope II, LaVision Biotec) equipped with an sCMOS camera (Andor Neo, Abingdon, United Kingdom) and a 2× objective lens (Olympus MVPLAPO 2×/0.5 NA) equipped with an Olympus MVX-10 zoom body, which provided zoom-out and -in ranging from 0.63× up to 6.3×. Light sheet microscope images were generated with different magnification factors and a step size of 5-10 µm according to the sample size with 470±30 / 640±30 nm ex/em bandpass filters for QDs and 640±30 / 690±50 nm ex/em bandpass filters for AF647 GFP staining. Lung tissue autofluorescence was generally scanned with 520±40 / 585±40 nm ex/em filters to show the microstructure of the lungs. 100 ms exposure time and 95% laser power are typically set with LSFM, where the light sheet microscope has different xy width and numerical aperture (NA) to match the different sample sizes. During the LSFM image acquisition, the sample was immersed in the DBE. Imaris 9.1.0 (Bitplane, Belfast, United Kingdom) was used to perform 2D and 3D rendering and image processing.

2.2.1.16 Fluorescence-based analysis of NP dose in lung homogenates

Mice were sacrificed immediately after L-IVM experiments by exsanguination and then lung perfusion was performed following the protocol above

(2.2.1.15). Subsequently, the whole lungs were removed. The quantification of QDs was based on a previously published method (Robe et al., 2008). Briefly, the lung was immersed in 1 ml tissue lysing solution (Solvable®, Perkin–Elmer, Waltham, USA) at 50 °C for 24 h until the tissue was completely dissolved. NP fluorescence intensity in the samples was measured with a spectrofluorometer (Safire 2, Tecan, Zurich, Switzerland). QDs were detected with BP 400 nm filter for excitation and BP 635nm filter for emission. Calibration standard curves were generated for each QD type by measuring solubilized blank lung samples with known but different amounts of QDs which have been incubated with blank lung tissue in Solvable for 24 hours at 50°C. QD concentrations were calculated via the fluorescence intensities according to the relevant standard curves.

2.2.1.17 Fluorescence Activated Cell Sorting (FACS)

PKH26-labeled mice were sacrificed by exsanguination and the lungs were taken out. Then lung tissue was minced in a 4ml digestion cocktail which was obtained by dissolving 750 ng DNAse (Qiagen, Hilden, Germany), 50 µg Collagenase (Sigma, Burlington, MA, USA), and 80 µg Elastase (Serva, Heidelberg, Germany) in 4ml of Dispase solution (50 caseinolytic U/ml, Corning, New York, America). Next, the mixture was put on a vertical shaker at 37°C for 15-20 min. The mixture solution was gently pressed through a 70 µm filter (Corning, New York, United States) using a 3ml syringe and washed

with an excess volume of 2% fetal bovine serum (FBS) (with 2mM EDTA, Sigma, Burlington, MA, USA). Immediately afterwards, the above filtration step was repeated with a 30μm filter (Corning, New York, United States). The cells were pelleted by centrifugation at 1500 RPM for 10 minutes at 4°C, and the supernatant was discarded. The remaining red blood cells were lysed with 1ml red blood cell lysis buffer (Thermo Fisher Scientific, Massachusetts, USA) for 10 min, then 10ml PBS was added to stop cell lysis. The cells were pelleted by centrifugation at 1500 RPM for 10 minutes at 4℃ and cells were resuspended with 1ml FACS Buffer (0.5% FBS in PBS). The total cell number was counted by a hemocytometer. 10^6 cells were transferred in FACS tubes (Thermo Fisher Scientific, Massachusetts, USA) for each sample, and centrifuged at 300g, 4℃ for 5 min. The supernatant was discarded. To each sample 100uL of the staining solution (anti-siglec F APC 770, clone: REA798, Miltenyi Biotec, Cologne, Germany) was added and incubated at 4℃ for 30min in the dark. After washing and re-suspending in FACS buffer, cells were analyzed on a BD FACSCanto II flow cytometer (BD Bioscienc, New Jersey, USA) with BD FACSDiva software.

2.2.1.18 In Vivo Imaging System (IVIS)

To determine the distribution of fluorescent nanomaterials in the lungs, the IVIS system (Lumina II, Caliper/PerkinElmer, USA), was used for whole organ imaging. In short, the whole lung was placed on a platform located in the

center of the IVIS chamber and imaged with QDs-specific excitation and emission filters (ex/em: 475 nm/ Cy5.5; exposure time: auto; Binning: Medium; F/Stop: 16 and Lamp level: high). The fluorescence/white light images were acquired with the Living Imaging 4.0 software (Caliper, Hopkinton, USA) to determine the fluorescence intensity and the 2D projected geometric area of the lung.

2.2.1.19 Electron Microscopy

The lung electron microscopy images were acquired as described in a previous study (Rehberg et al., 2012). The lung tissue was fixed in 1% PFA, 0.1 M cacodylate buffer (pH 7.4). After dissection, the samples were finally fixed in 2% PFA and 2% glutaraldehyde in 0.1 M cacodylate buffer (pH 7.4) for 2-3 hours at room temperature. The samples were then fixed in 1% OsO_4 containing 1.5% potassium cyanoferrate and embedded in Epon after dehydration. The ultrathin (70 nm) sections of the samples were cut in serial sections (Leica-UC6 ultramicrotome, Vienna, Austria). Except for some sections, which were counterstained with uranyl acetate and lead, sections were not stained. The images were acquired with 80 kV on an FEI-Tecnai 12 electron microscope (FEI, Eindhoven, The Netherlands). The consecutive-stained sections were used to identify organelles. The sections were scanned with a CCD camera (Megaview, Olympus-SIS, Muenster).

2.2.1.20 Quantification of leukocyte kinetics

In order to quantify the neutrophil numbers at different time points after NP exposure (inhalation) (-15min, 0min, 15min, 30min,45min, 60min, 75min, 90min), the short (15s) L-IVM movies were analyzed with Image J software (National Institutes of Health, Bethesda, USA). For neutrophil amount counting, the “Trackmate” function of Image J was used. All neutrophils were automatically counted by the software using the -15min (neutrophil baseline) image for the threshold setting. The same settings were used for subsequent time points, and results were manually corrected if required.

2.2.2 In vitro experiments

2.2.2.1 MH-S cells culture

Murine MH-S alveolar macrophage-like cells were purchased from the American Type Culture Collection (ATCC®, CRL-2019TM) and grown in Roswell Park Memorial Institute (RPMI) 1640 medium with supplements containing 0.05 mM 2-mercaptoethanol, 10 %FBS and 1% penicillin-streptomycin at 37°C and 5 % CO_2. For cell passage, the medium was removed, and cells were washed gently with 20ml pre-warmed sterile PBS. Then cells were incubated with 2ml pre-warmed Trypsin-EDTA (0.25 %, Life Technologies Limited, Paisley, UK) for 4 min at 37 °C. 18 ml pre-warmed MH-S medium was added to stop digestion. After resuspending in the culture medium, MH-S cells were transferred into 50 ml falcon tubes (Thermo Fisher

Scientific, Massachusetts, USA) and re-pelleted by centrifugation (1400 rpm, 5 minutes, 4℃). The cell pellets were resuspended, and 500,000 cells were transferred to a new flask (50 ml, 25 cm², Greiner Bio-One GmbH, Frickenhausen, Germany).

2.2.2.2 ALICE-CLOUD exposure system

500,000 MH-S cells were distributed in 100 μL cell culture medium and then seeded on the 6-well corning insert (0.4 μm pores), with 1.7 mL basal medium in the bottom wells. The basal medium was changed with the aspiration of the apical medium 24h after cell seeding, and then the cells were equilibrated at an air-liquid interface (ALI) condition for 2h. The AerogenPro nebulizer (Aerogen Small VMD, Kent Scientific Corporation, USA) was added with 20μl solution containing 4μM quantum dot suspension (1:2 diluted stock suspension) in distilled water with 1% saline providing ions to generate QDs liquid aerosol droplets of 3.5-4 μm diameter. Cells were exposed to the QDs at the ALI conditions for 2h or 24h after complete sedimentation of the particles and then washed with PBS to remove the un-attached particles.

2.2.2.3 Water-soluble tetrazolium salt (WST) cell viability assay

MH-S cells were seeded in 24-well plates at a density of 10^5 / well and cultured overnight. Cells were exposed to QD particles (8nM) and vehicle as a control group in 500μl cell culture medium in submerged conditions for 1h. The supernatant was removed, and the cells were incubated with 10 % Roche

WST reagent for 15min at 37℃ and 5% CO2. After 15 min of incubation at 37 °C and 5 % CO2, WST samples were then collected and centrifuged at 14,000 rpm, 10min at room temperature. Absorbance at 450nm of 200µl solution was measured in 96-well plates with the Tecan reader (TECAN Trading AG, Männedorf, Switzerland). Each sample was measured with 2 duplicated wells, and the absorbance value was corrected with a blank sample (WST solution non-incubated with cells). The cell viability of each sample was compared with the control group according to the following equation:

Cell viability= (sample OD – blank OD) / (control OD – blank OD) ∗100%

2.2.2.4 Analysis of cell phagocytosis with FACS

MH-S alveolar macrophage-like cells were seeded respectively in a 24-well plate at a density of $25*10^4$ cells / well. The cells were pre-treated with anti-ICAM-1, anti-LFA-1, anti-CD44, anti-CD64, anti-CD88 and isotype (10µg/ml) antibodies, cromolyn (4 µg/ml), NAC (10µg/ml) or vehicle-control separately up to 3h at 37 °C and 5 % CO_2 (Table 3). Then pHrodo™ Green E. coli BioParticles (5 µg/ml) were added to the supernatant for 1h. The medium was removed, and cells were washed gently with 1ml sterile pre-warmed PBS. The cells were incubated with 100µl pre-warmed Trypsin-EDTA for 4 min at 37 °C, the digestion was stopped by the addition of 900µl pre-warmed MH-S medium. MHS cells were transferred into the FACS tubes (Thermo Fisher

Scientific, Massachusetts, USA) and re-pelleted by centrifugation (1400 rpm, 5 minutes, 4℃). After washing and re-suspending in FACS buffer, cells were analyzed by a BD FACSCanto II flow cytometer (BD Bioscienc, New Jersey, U.S.) with BD FACSDiva software.

Table 3: List of blocking antibodies or inhibitors applied in vitro.

Blocking antibody/Inhibitor	Clone	Manufacturer
In vivo mAb anti-mouse LFA-1α	M17/4	Bio X Cell, Lebanon, USA
Purified anti-mouse CD54 (ICAM-1) antibody	YN1/1.7.4	ATCC, Manasses, USA
In vivo mAb anti-mouse/human CD44	IM7	Bio X Cell, Lebanon, USA
Ultra-LEAF™ Purified anti-mouse CD88 (C5aR) mAb	20/70	BioLegend, Fell, Germany
Ultra-LEAF™ Purified anti-mouse CD64 (FcγRI) mAb	W18349F	BioLegend, Fell, Germany
In Vivo mAb rat IgG2a isotype control	2A3	Bio X Cell, Lebanon, USA
Ultra-LEAF™ Purified Rat IgG2b, κ Isotype Ctrl antibody	RTK4530	BioLegend, Fell, Germany
NAC(N-Acetyl-L-cystein)	CAS 616-91-1	Merck, Darmstadt, Germany

2.2.2.5 Analysis of MH-S QDs internalization with FACS

MH-S cells were seeded respectively in a 24-well plate (25*10^4 cells/well). The cells were pre-treated with anti-CD64, anti-CD88, and isotype (10µg/ml) blocking antibodies or vehicle-control separately up to 3h at 37 °C and 5 % CO2 (Table 3). Then cQDs and aPEG-QDs (2 pM) mixed with Surfactant were added to the supernatant for 1h. The FACS process of cQDs internalization M-HS was as described above (2.2.2.4).

2.2.3 Statistical analysis

All data were presented as mean ± standard error of the mean (SEM) and plotted with GraphPad Prism 8 (GraphPad Software Inc., La Jolla, USA), with the sample sizes and the number of repeats indicated in the figure legends. Comparison of results between two groups for normally distributed data was analyzed using the two-sided student t-test and for nonparametric data the Mann-Whitney rank-sum test. Comparisons among multiple groups were performed using a one-way ANOVA with Tukey's comparisons test. Significances are defined as 0.05 ($P < 0.05$, *), 0.01 ($P < 0.01$, **), 0.001 ($P < 0.001$, ***) and 0.0001 ($P < 0.001$, ****), while p value ≥0.05 was considered not significant (ns).

3. Results

3.1 Characterization of QD deposition and distribution after QD aerosol inhalation

3.1.1 Distribution of different QDs diluted in distilled water.

We used distilled water to dilute cQDs, aPEG-QDs, and PEG-QDs at a 1:1 ratio as working solutions (4μM) for the nebulizer. Electron microscopic images of QD solutions (distilled water) show (Figure 4), that these three QDs are monodisperse particles without agglomeration.

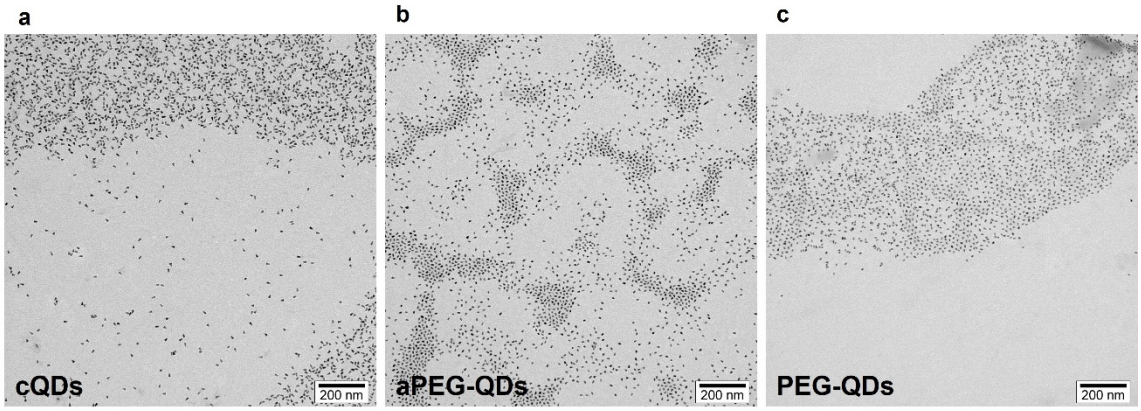

Figure 4 Size and distribution of cQDs, aPEG-QDs, and PEG-QDs in distilled water. (a: cQDs, b: aPEG-QDs, and c: PEG-QDs, scale bar: 200 nm)

3.1.2 Quantitative Analysis of lung deposited QD dose

The ventilator-assisted nebulizer (Aerogen Small VMD, Kent Scientific Corporation, USA) generates liquid aerosol droplets (3.5-4 μm) containing QD suspensions. For every mouse, 20μl of a 4μM QDs suspension was added into the nebulizer for inhalation. Mice were sacrificed immediately after NP application and lung tissue was removed and homogenized to measure the QDs deposited dose in the lungs. Figure 5 depicts the standard curve obtained

from mice lung homogenate incubated with known cQDs dose (R^2 > 0.99). From the standard curve, the cQDs deposited dose has been calculated as 2.12±0.31 pmol/g amount of substance(n)-NPs / mass-lung, and 2.04±0.68 pmol/g amount of substance(n)-NPs / mass-lung for aPEG-QDs. The average cQDs deposition efficacy was 0.53±0.08 %, which is equal to the delivery efficacy of aPEG-QDs (0.51±0.17%), indicating that the delivery efficiencies for these different surface-modified QDs are similar.

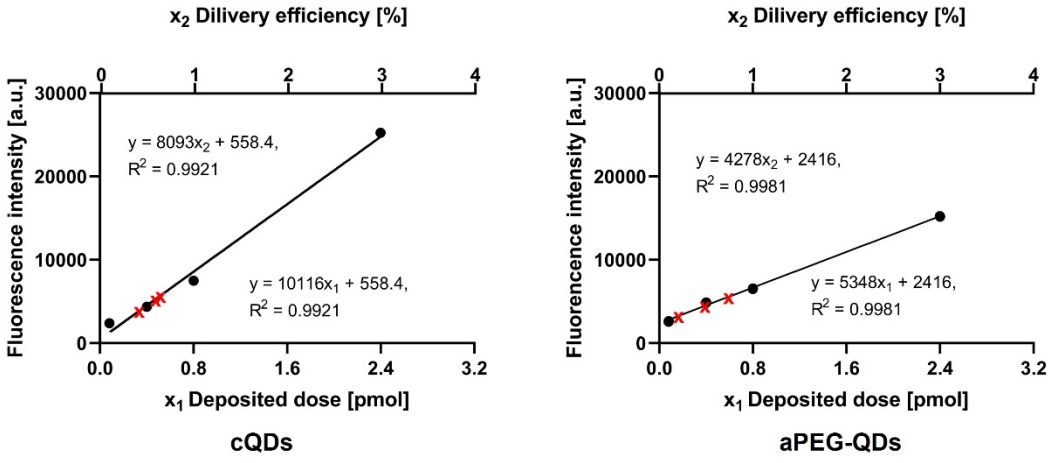

Figure 5 QDs fluorescence intensity−delivery efficiency correlation curve in mouse lungs after inhalation. cQDs/aPEG-QDs delivery efficacy was calculated according to the linear fluorescence intensity− standard curve (R^2 > 0.99) obtained from blank lung homogenates supplemented with known cQDs/aPEG-QDs doses (black spots). Red crosses indicate the QDs doses detected in mice lung homogenates of 3 independent inhalation applications, n=3.

After 80 pmol was exposed through the trachea inhalation method (0.53% cQDs delivery efficiency), and QDs were. The deposited dose was calculated for the cQDs (regarded as spheres with a diameter of 20 nm) from 0.53% delivery efficiency of the initial 80 pmol as 16 cm^2/g (geom. surface area of NPs / mass-lung). Because the size and delivery efficiency of aPEG-QDs is similar to that of cQDs, the deposited dose is also around 16 cm^2/g (geom. surface area of NPs / mass-lung).

3.1.3 QDs distribution in whole murine lungs

After establishing the delivery efficacy of the Aerogen Pro-Minivent nebulizing device, we next investigated whether homogenous NP distribution in the lungs was achieved. For this, the In Vivo Imaging System (IVIS) was used to check the distribution of NPs after inhalation, by ex-vivo imaging of entire mouse lungs pre- and post-QDs inhalation. The imaging of cQD and aPEG-QD fluorescence indicated that both surface modified QDs are uniformly distributed in the whole lungs after inhalation (Figure 6 a-c). Accumulation of QDs inevitably appeared in the trachea and large bronchi during inhalation, as indicated by the high fluorescence signal in these parts.

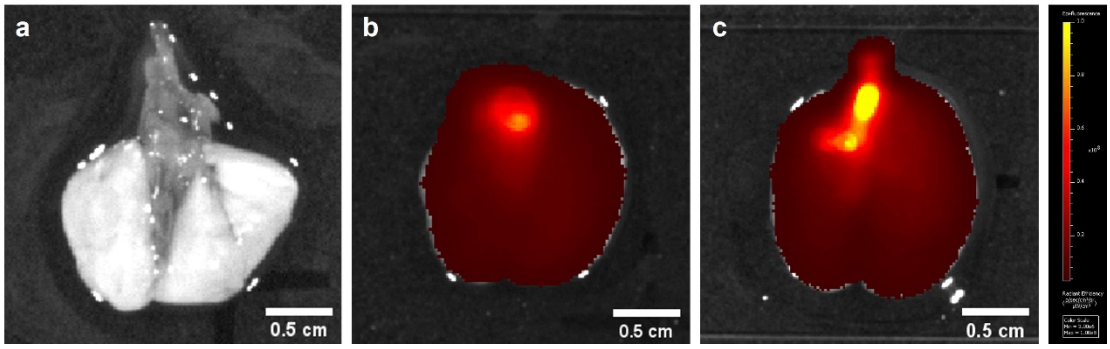

Figure 6 Analysis of QD distribution in lungs using IVIS. Typical ex-vivo lung images from mice treated with 16 cm^2/g (geom. surface area of NPs / mass-lung) cQDs and aPEG-QDs via ventilator-assisted inhalation for 2h and compared to untreated controls measured by IVIS (a: Ctrl, b: cQDs, c: aPEG-QDs).

3.1.4 3D pulmonary mapping of QD distribution

Tissue clearing drastically decreases tissue−light interactions (absorption, scattering). Thereby 3D imaging of the unlabeled lung structure and the NP distribution in the whole mouse lung by light sheet microscopy is possible (Yang et al., 2019). Merged images of maximum intensity projections (MIP) of QD fluorescence signals with the 3D lung structure confirm that cQDs as well as

aPEG-QDs exhibited a uniform distribution in the lungs in the overall view (Figure 7a-b). However, some local differences existed at the microscopic scale. After cQDs exposure, preferential central acini (blue arrow) exhibited strong cQD fluorescence while in the great majority of the peripheral acini (yellow arrow) fewer cQDs were deposited (Figure 7a,c). Conversely, after aPEG-QDs inhalation, the distribution of aPEG-QDs was similar in central or peripheral areas of the lungs (Figure 7b,d). This distribution pattern difference was also observed in confocal microscopy images of precision cut lung slice (PCLs) samples from cQDs (Figure 7e) and aPEG-QDs (Figure 7f) exposed mice.

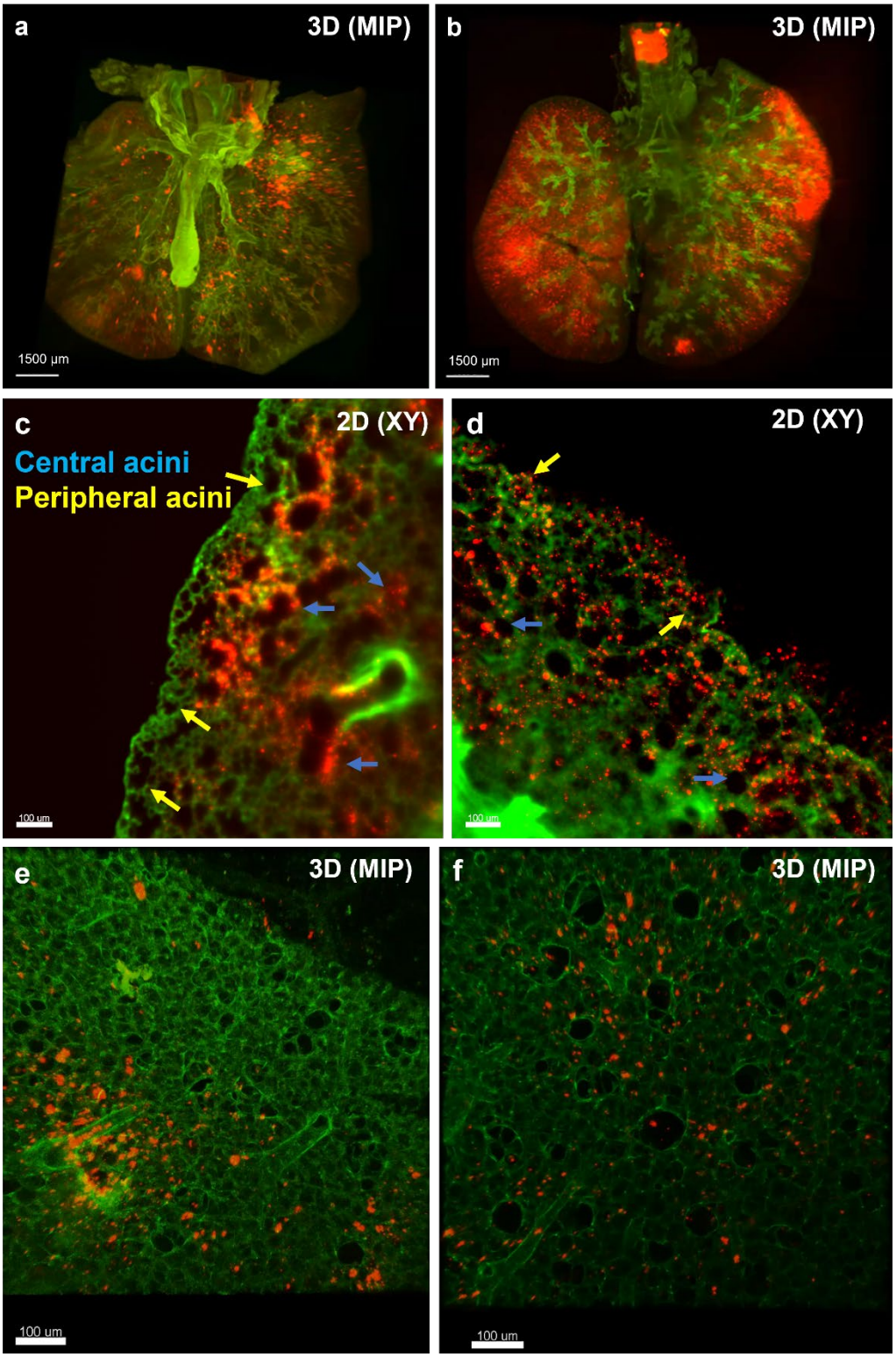

Figure 7 (a)-(d) 3D mapping of different QD distribution modes in entire mouse lungs upon QD delivery by ventilator-assisted NP aerosol inhalation. The distribution of QDs (red) in the Z-stack images of entire cleared lungs obtained by light sheet microscopy (panel a and b: 3D MIP, a: cQDs and b: aPEG-QDs, scale bar: 1500 µm) and in single z-planes (panel c and d: 2D xy slice, c: cQDs and d: aPEG-QDs, scale bar: 200 µm) of the tissue structure (autofluorescence, green) after inhalation of different types of (16cm^2/g) QDs. (e)-(f) Confocal microscopic 2D images of QDs (red, e: cQDs and f: aPEG-QDs) exposed PCLs sample (autofluorescence: green). Scale bar: 100 µm.

3.1.5 Inhaled NPs are rapidly detected by L-IVM

To investigate the dynamics of NPs and to determine whether inhaled particles can be detected in the uppermost alveolar layer of the lung, which is accessible by IVM, two types of fluorescent particles, NPs (cQDs, aPEG-QDs, PEG-QDs; diameter: 15-20nm) and microparticles (melamine resin particles (MF); 0.94µm ± 0.05µm) were delivered by ventilator assisted inhalation and simultaneously imaged. Both types of particles reached the surface of the lung some seconds after the onset of inhalation ("delay" mainly due to passage time through nebulizing device and tubing) and were immediately detected as distinct fluorescent spots by LIVM (cQDs: 5.25 ± 0.75s, aPEG-QDs: 8.33 ± 0.96s, PEG-QDs: 6.67 ± 1.44s and MF: 6.33s ± 1.15s; P=0.37) (figure 8a-b).

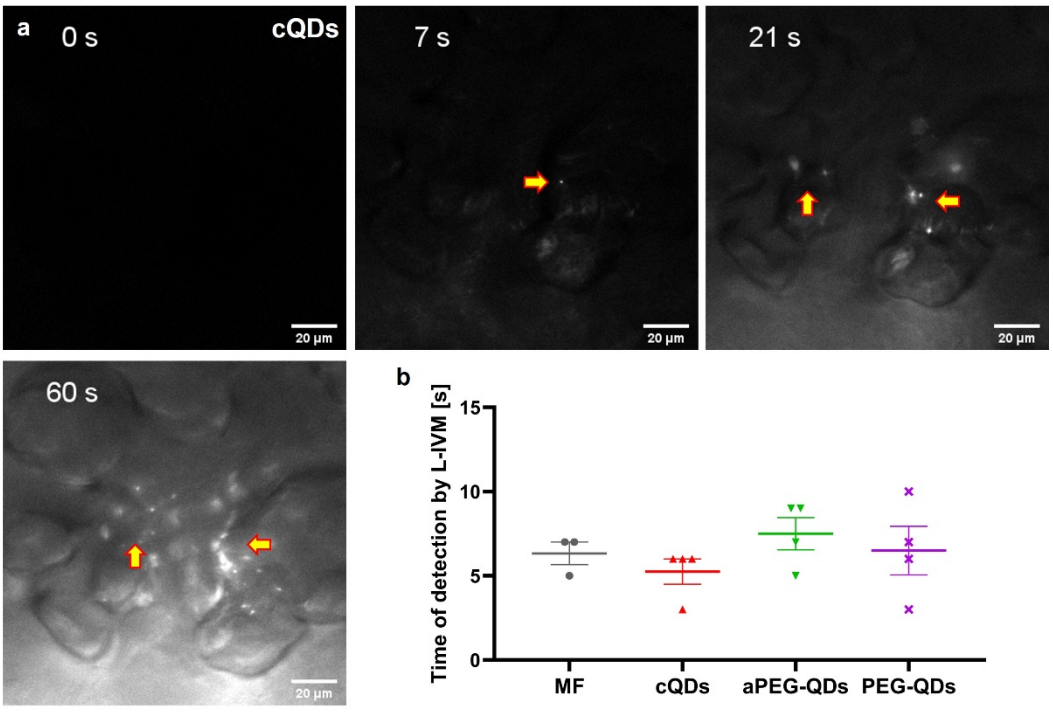

Figure 8 Fluorescent NPs were rapidly detected by L-IVM. (a) cQDs were rapidly detected by L-IVM as distinct fluorescent spots (white dots) in single alveoli upon ventilator-assisted inhalation and gradually deposited. Scale bars: 50 µm. (b) cQDs, aPEG-QDs, PEG-QDs NPs (15-20 nm), and melamine resin (MF) microparticles (0.94µm ± 0.05µm), were detected by LIVM in a similar time after the onset of inhalation by LIVM (n = 3-4 mice/group, One-way ANOVA test).

3.1.6 L-IVM analysis of QD distribution patterns on the lung surface

After 5 minutes of inhalation, L-IVM images show strong fluorescence spots for cQD, aPEG-QD as well as PEG-QDs in the alveolar space on the surface of the lungs (Figure 9a-c). Visual inspection indicated that more aPEG-QDs were deposited in the field of observation (peripheral regions of the lung) compared to cQDs or PEG-QDs (Figure 9a-c). Quantification of the mean fluorescence intensity of the whole observation area, revealed that the fluorescence intensity in the aPEG-QDs group was approximately twice that of the cQD and PEG-QD groups, which might indicate that aPEG-QDs NPs are deposited at terminal bronchi or peripheral alveoli more easily (Figure 9d). Notably, not all alveoli in the field of views exhibited deposited QDs. For example, on average 31.47±2.22 % of alveoli received cQDs.

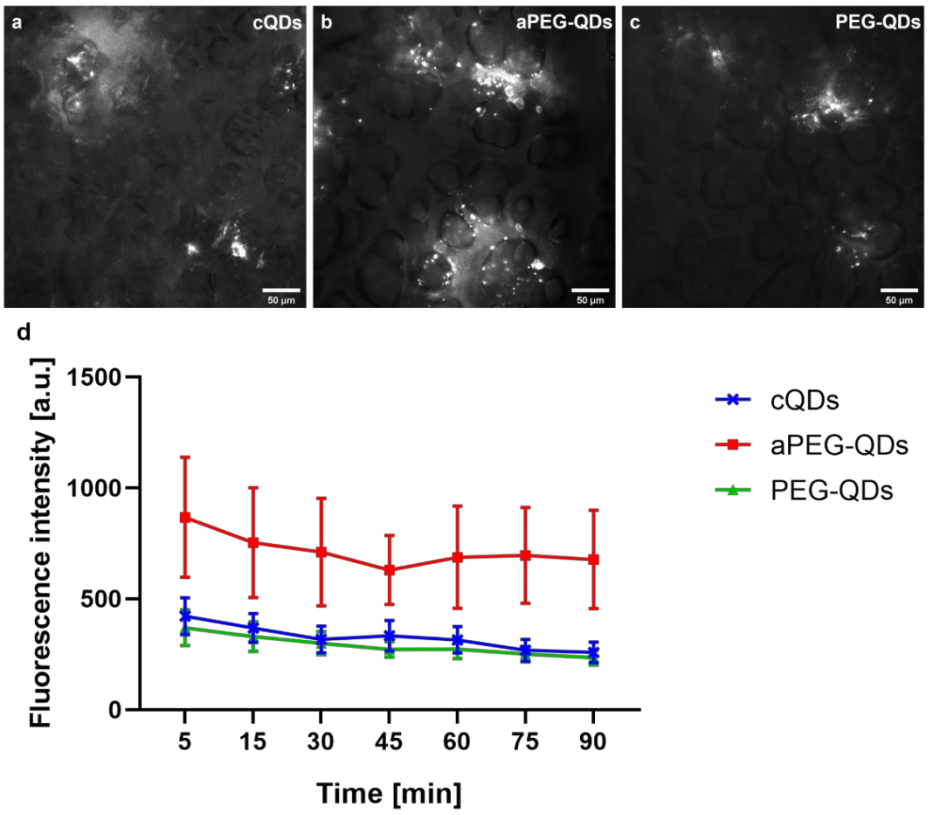

Figure 9 QDs reach the alveolar compartment at the lung surface. (a)-(c). L-IVM images of different QDs (a: cQD; b: aPEG-QD; c: PEG-QD) distribution pattern on the surface of the lungs 5 min after pulmonary NP inhalation. QDs are shown in white. Scale bars: 50 μm. (d) Average QD fluorescence intensity in the whole L-IVM images at consecutive time points after different QDs applications. (Means ± SEM, n= 3 mice/group)

3.2 NP-inhalation increased neutrophil accumulation in the lung

3.2.1 Dose effect on cQDs-induced neutrophil recruitment

A previous study of our group revealed that i.v. injection of cQD NPs into the blood circulation, induced acute neutrophil recruitment 15min upon administration (Rehberg et al., 2010). We aimed to further investigate the potential pro-inflammatory response of NPs in the alveolar region. Using lung intravital imaging, the recruitment of neutrophils (immunolabeled with fluorescent anti-Ly6G mAbs) upon ventilator-assisted inhalation of cQDs in pulmonary blood vessels was observed and quantified. Because of the mechanical trauma from the surgical operation (surgical incision, negative pressure suction, etc.), a mild inflammatory response occurred in the lung tissue at baseline situations during the course of the experiment, which is characterized by a slight increase in neutrophil numbers (Figure 10). The neutrophils present at baseline are due to the lung-marginated pool of neutrophils (Doerschuk, 2000).

To investigate whether cQD-evoked neutrophil recruitment is dose-dependent, we used two doses of cQDs for inhalation (deposited dose: 16cm^2/g and 32cm^2/g, mass-specific geometric surface area). In the first group, 16cm^2/g

cQD inhalation, already at 30 min, elicited an increased number of neutrophils in the observation areas, as compared to the control group, which became significant at 60 min (5.39±0.49 /10^4µm^2 vs 3.74±0.44 /10^4µm^2, P<0.05). Increasing the deposited dose (from 16cm^2/g to 32cm^2/g) of cQDs did not cause a significant difference in the numbers of recruited neutrophils, as determined by semi-automated quantitative detection of fluorescent neutrophils (After 90 min exposure: 16cm^2/g: 6.25±0.39 /10^4µm^2 and 32cm^2/g: 6.76±0.61 /10^4µm^2, P=0.61) (Figure 10).

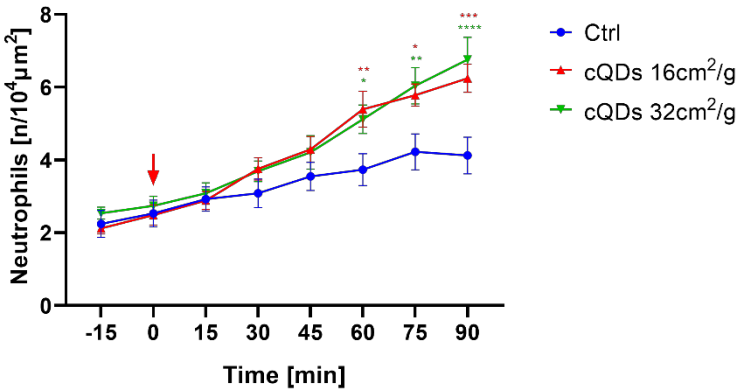

Figure 10 Quantitative analysis of neutrophil numbers after QD inhalation. Neutrophil numbers were quantified in the alveolar region using lung intravital microscopy upon ventilator-assisted inhalation of cQDs and vehicle (NPs inhalation started at 0 min (arrow), Means ± SEM, n=6 mice/group, Two-way ANOVA test, red * cQDs (16 cm^2/g) vs vehicle-control, green * cQDs (32 cm^2/g) vs vehicle-control).

3.2.2 Effect of carbon NPs (CNP) on neutrophil recruitment

In order to investigate whether leukocyte recruitment dynamics obtained for cQDs are comparable to the inflammatory response induced by environmental air pollution, we investigated neutrophil dynamics after CNP inhalation, which is a typical exposure model to study the effects of urban air pollution (Chen et al., 2016). The original diameter of Carbon Black Printex 90 is 14 nm, and it is listed as a potential human-related carcinogen (group 2B) by the International

Agency for Research on Cancer (Baan et al., 2006). We referred to a meta-analysis (Schmid & Stoeger, 2016) on the relationship between deposited NP surface area and lung inflammation, from which we calculated the CNP dose predicted to be required to cause similar lung inflammation levels as caused by cQDs. Therefore C57BL/6 mice were exposed to 75cm^2/g and 172.5cm^2/g (mass-specific geometric surface area) CNP by ventilator-assisted inhalation. As compared to the control group, 60 minutes after particle inhalation, a large number of neutrophils accumulated in the lung in the 172.5m^2/g CNP group (5.12±0.20/10^{4}μm^2 vs 3.74±0.44/10^{4}μm^2, P<0.05, Figure 11), a cell number which is comparable to neutrophil recruitment, observed in cQDs-exposed animals (Figure 10). Similarly, if the deposited CNP dose was reduced to 75m^2/g, the neutrophil counts were still higher than in the control group at 90 minutes (5.62±0.75/10^{4}μm^2 vs 4.12±1.23/10^{4}μm^2, P<0.05). In short, increasing the deposited dose of NPs (cQDs: from 16cm^2/g to 32cm^2/g and CNP: from 75cm^2/g to 172.5cm^2/g) maintained a stable increased tendency in the number of recruited neutrophils (Figure 10-11).

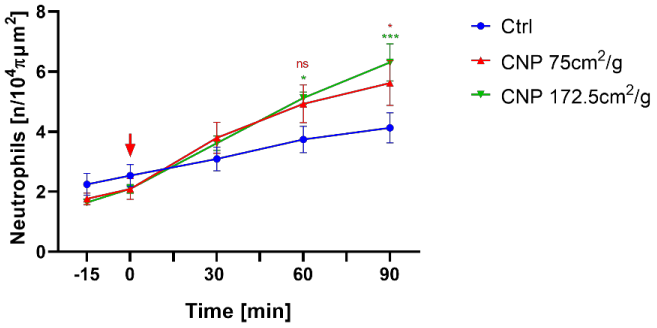

Figure 11. Quantitative analysis of neutrophil numbers after CNP inhalation. Alterations in the amounts of neutrophils over time under L-IVM were compared between two different doses of CNP NP inhalation (NP inhalation starting at 0 min (arrow), Means ± SEM, n= 4-6 mice/group, Two-way ANOVA test, red * or ns CNP (75 cm^2/g) vs vehicle-control, green * cQDs (172.5 cm^2/g) vs vehicle-control).

3.2.3 PEG-surface modification of QDs inhibited QD-induced rapid recruitment of neutrophils

Depending on their surface properties, proteins and other biomolecules accumulate / bind on NP surfaces, thereby forming a bio-molecule corona (Hellstrand et al., 2009; Röcker et al., 2009), once in contact with biological fluids (serum, alveolar lining fluid, etc.), thus determining NP interactions as well as NP clearance (Aggarwal et al., 2009; Owens & Peppas, 2006). Using intravital microscopy on the mouse cremaster muscle, Rehberg and colleagues studied leukocyte dynamics caused by QDs with different surface coatings. They revealed that cQDs-induced significant neutrophil recruitment, already 15min after cQDs application in blood vessels, while PEG-QDs or aPEG-QDs both with polyethylene glycol (PEG) coating did not. This has been attributed to the largely diminished biomolecule corona of the NPs, since PEG sterically prevents protein binding (Gref et al., 1994).

We resorted QDs (deposited dose: 16cm^2/g) of the same size but with different surface modifications (carboxyl-, animo-PEG- (aPEG-), and PEG-) to evaluate whether these modifications affect neutrophil recruitment after inhalation exposure. In the control group, the number of neutrophils slightly increased from 2.24±0.37/$10^4$$\mu m^2$ at baseline, 15 minutes before inhalation to 4.12±1.23/$10^4$$\mu m^2$, 90 minutes after inhalation of vehicle, as determined by semi-automated quantitative detection of fluorescence neutrophils. Neutrophil numbers in the area of observation after aPEG- and PEG-QDs inhalation

matched those of control conditions (90min: 3.83±0.55/10^4µm^2 for aPEG-QDs, 4.47±0.28/10^4µm^2 for PEG-QDs and 4.12±0.50/10^4µm^2 for the control group). In contrast, a significant increase in neutrophil numbers was observed 90min (6.25±0.39/10^4µm^2) upon application of cQDs (Figure 12a). The initial increase in neutrophil numbers is clearly visible at 30 min, in the graph, although the values are not yet significant, indicating a very rapid neutrophil response after cQD exposure. In order to further correct the differences in neutrophils between experimental animals, the numbers of neutrophils at 15 min before inhalation have been normalized to one and used as the baseline to calculate and depict the neutrophil cumulative curve (Figure 12b), and it also matched changes in the number of neutrophils (Figure 12a). We hence determined that not the deposited dose alone, but also the surface of NPs determines their pro-inflammatory potential. This could possibly be mediated by their ability to bind to biomolecules present in the alveoli, their potential to interact with cells, or cellular receptors.

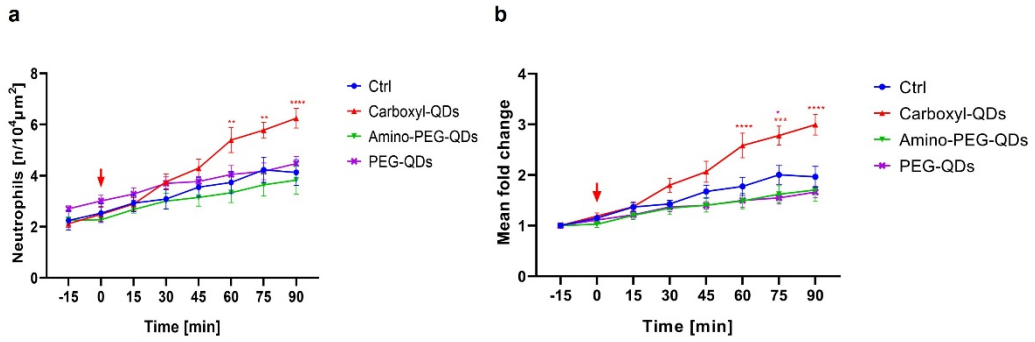

Figure 12 Quantitative analysis of the impact of QD surface modifications on neutrophil numbers after QD inhalation. a. Neutrophil numbers were quantified in the alveolar region using L-IVM under baseline and upon ventilator-assisted inhalation of either cQDs, aPEG-QDs, PEG-QDs, or vehicle (NPs inhalation starting at 0 min, red arrow,) at 16 cm^2 /g (geom. Surface area of NPs / mass-lung). b. Results are presented as mean fold change of the neutrophil amounts 15 min prior to NP inhalation to baseline condition. (Means ± SEM, n=6 mice/group, Two-way ANOVA test, red ⁎ cQDs vs vehicle-control, purple ⁎ PEG-QDs vs vehicle-control).

3.2.4 Effect of NP inhalation on blood flow velocity

Inflammation often induces changes in pulmonary microhemodynamics (such as blood flow velocity decrease and shear rates (Ueki et al., 2018)), which may be related to neutrophil recruitment. To determine whether NP inhalation affects blood flow in the alveolar microcirculation, we measured the blood perfusion velocity in the lungs of cQDs-exposed mice via tracing of i.v. injected fluorescent melamine resin particles (MF) microbeads (diameter: 0.94μm±0.05μm) (Figure 13). The blood flow velocity was decreased in cQD-inhaled mice 2h after particle exposure to 119.25±8.60 μm/s, as compared to 190.06±13.27 μm/s in control mice. In contrast, in the aPEG-QDs and PEG-QDs groups, blood flow speed did not change significantly (218.37±21.19μm/s for aPEG-QDs and 214.86±16.93 μm/s for PEG-QDs) and remained around the same level as in the control mice. Interestingly, these effects of the different QDs on blood perfusion (Figure 13a) match their effects on neutrophil amount changes in the lung (Figure 12a). Similarly, pulmonary blood flow velocity was also significantly decreased in mice exposed to 32cm^2/g cQDs (Figure 12b). These results suggest that cQDs-exposure affects the pulmonary microvascular system after neutrophil recruitment. Finally, we tested if CNP inhalation also affects microvascular perfusion. Indeed, CNP-inhalation reduced blood flow velocity as compared with vehicle exposed mice at 120 min (Figure 12c).

To ensure the comparability of all experimental groups, the inner diameters of 10 random blood vessels were measured in each mouse. The diameters of pulmonary blood vessels in the fields of view were similar (Figure 12d-f), excluding the influence of blood vessel size on blood perfusion velocity and furthermore ruling out an effect on blood vessel diameter (vessel constriction or dilatation) by NP inhalation.

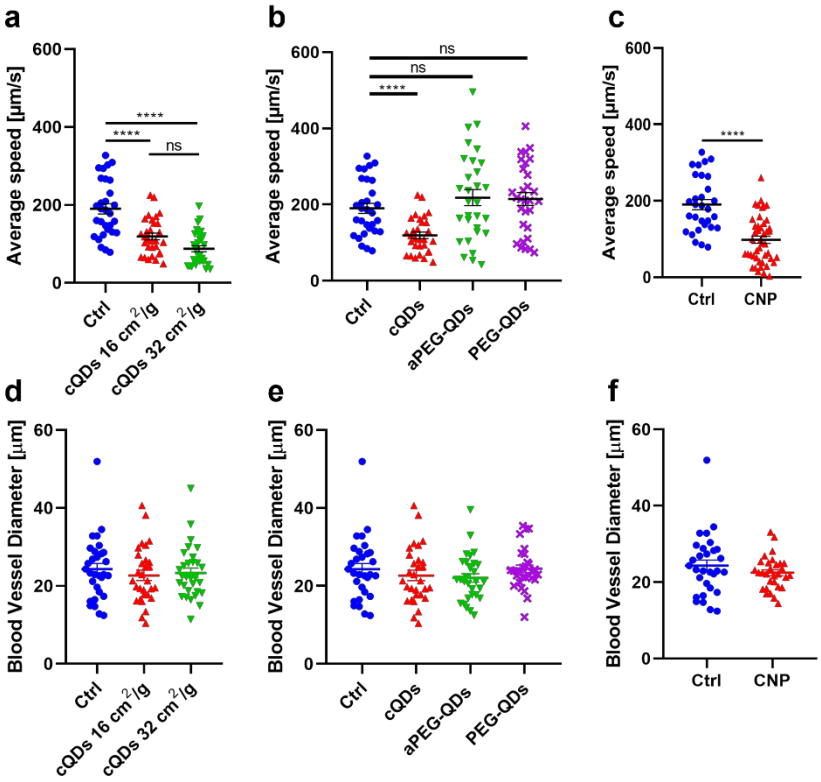

Figure 13 Altered blood perfusion speed in the pulmonary blood vessel of NP-exposed mice. Determination of blood perfusion speed by i.v. injection of fluorescent beads (Diameter = 1 µm) into the mice during image acquisition and subsequent tracking to measure their speed. Each dot represents the data obtained from one fluorescent bead in blood vessels and in each mouse the speed of 10 fluorescent beads was measured. (a) Analysis of blood perfusion velocity in alveolar microvessels upon inhalation of different doses of cQDs. (b) Blood perfusion speeds in different kinds of QDs-exposed lungs. (c) Blood perfusion speeds in CNP-exposed lungs. (d)-(f) Vessels in the observation area were similar in size. (a)-(f) Data are presented as Means ± SEM, n= 3 mice/group, a,b,d,e: One-way ANOVA test, c,f: paired Student's t-test).

3.2.5 The deposition of cQDs and CNPs in the lung caused similar levels of inflammation

As presented above, we found that fluorescent cQD NPs and combustion-derived CNPs-induced similar recruitment processes in the lung after inhalation exposure: (1) significant recruitment occurred at 1 hour after inhalation, (2) 90 minutes after NP exposure neutrophil levels were equivalent. Therefore, we put the above-deposited doses of NPs that can cause neutrophil recruitment into the graph of the relationship between the dose (geometric surface area) and the ratio of neutrophils in BAL after 16-24 h NP exposure, taken from a meta-analysis conducted by Stoeger and Schmid (Schmid & Stoeger, 2016). CNPs were classified as low-solubility, low-toxicity (LSLT) particles, while cQDs were classified as metal oxide NPs because of their CdSe core and ZnS shell. Thereby we found that the two NPs theoretically cause a similar acute influx of neutrophils (Figure 14). To further clarify the dose correlation of the two NPs, we collected 2h and 24h of BAL from mouse lungs.

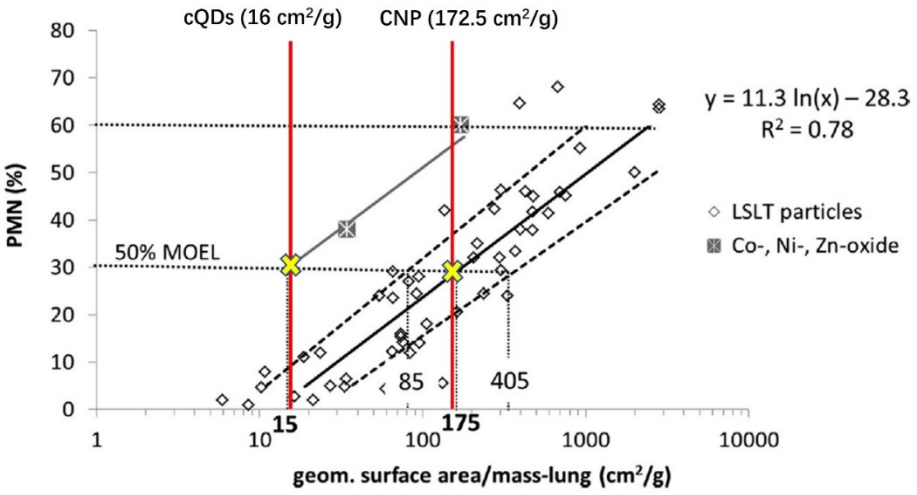

Figure 14 The relationship between NP-induced proportion of neutrophils in BAL and NPs exposure dose (geometric surface area). Adapted from (Schmid, Stoeger; J Aerosol Sci., 2016).

BAL cell analysis was applied to define the different inflammatory responses of cQDs or CNP inhalation with cytospin analysis of May Grunwald-stained BAL cells. At 2h after cQDs inhalation, a small number of 0.4 × 10^4 neutrophils was detected, while neutrophils were almost undetectable in control animals (Figure 15 a). As compared to the control group, the amounts of total cells, AMs and lymphocytes were at similar levels in the cQDs- as well as the CNP-exposed group (Figure 15 a,b). Similarly, in the CNP-exposed group, neutrophil levels are elevated, although not significant, upon 2h exposure (Figure 15b).

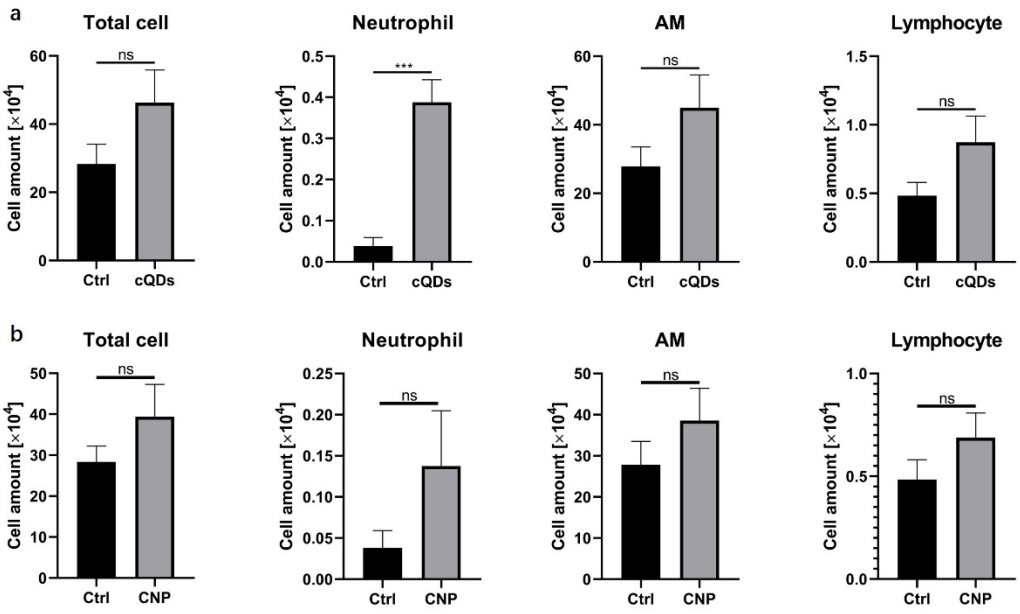

Figure 15 BAL cell analysis 2h after NPs inhalation. (a) The amounts of total cells, AMs, neutrophils, and lymphocytes were determined within May Grunwald-stained BAL cells (Cytospin) of mice 2h after inhalation of cQDs (16 cm^2/g geom. surface area of NPs / mass-lung), (b) 2h after inhalation of 172.5 cm^2/g CNP and compared to untreated controls (Means ± SEM, n= 4-6 mice/group, paired Student's t-test).

In order to further study the NP-induced neutrophil recruitment, we collected the BAL of the mice upon 24h cQDs and CNP-inhalation. A large number of neutrophils ((2.68±1.35)*10^4 vs ((0.16±0.04)* 10^4) and lymphocytes ((0.51±0.07)*10^4 vs (0.22±0.08)*10^4) infiltrated into the airways of cQDs-

exposed mice, while these cells were almost undetectable in the BAL of the control mice (figure 16a). Similar, the number of recruited neutrophils ((1.65±0.71)*10^4 vs ((0.16±0.04)*10^4, P<0.01) and lymphocytes ((0.64±0.1)*10^4 vs (0.22±0.08)*10^4, P<0.05) was also significantly increased in CNP-exposed mice 24h after inhalation of CNP as compared to control mice (figure 16b). Taken together, BAL analysis revealed an acute inflammatory response induced by cQDs and CNPs, with a prominent accumulation of neutrophils and lymphocytes, at 24 h after exposure.

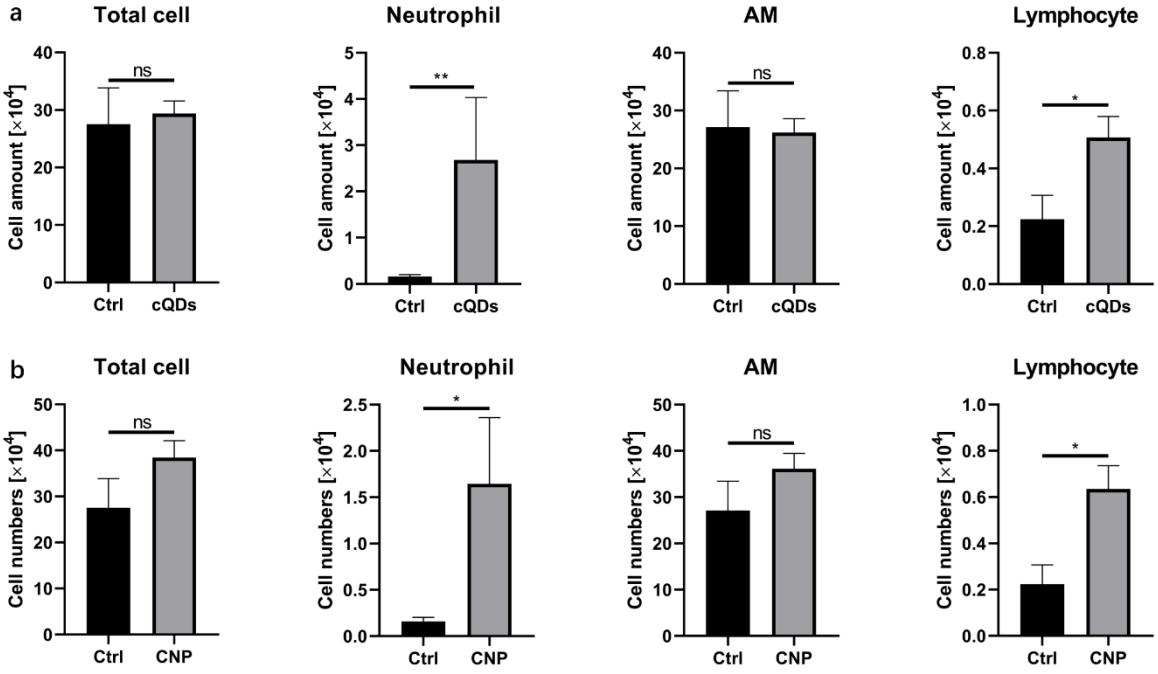

Figure 16 BAL cell analysis 24 h after NP inhalation (a) The amounts of total cells, AMs, neutrophils, and lymphocytes were determined with May Grunwald-stained BAL cells (Cytospin) of mice 24h after inhalation of cQDs (16 cm^2/g geom. surface area of NPs / mass-lung) and (b) of 172.5 cm^2/g CNP and compared to untreated controls (Means ± SEM, n= 3-6 mice/group, paired Student's t-test).

3.3 Infiltrated neutrophils in close proximity are vital for capture of inhaled, deposited NPs

3.3.1 Recruitment of neutrophils occurs in close proximity to inhaled, deposited NPs

Close inspection of long-term recordings of neutrophil dynamics upon cQD inhalation revealed that neutrophils preferentially arrested in microvessels in close proximity to the alveolar deposited cQDs, where they often exhibited a probing/crawling behavior (Figure 17a).

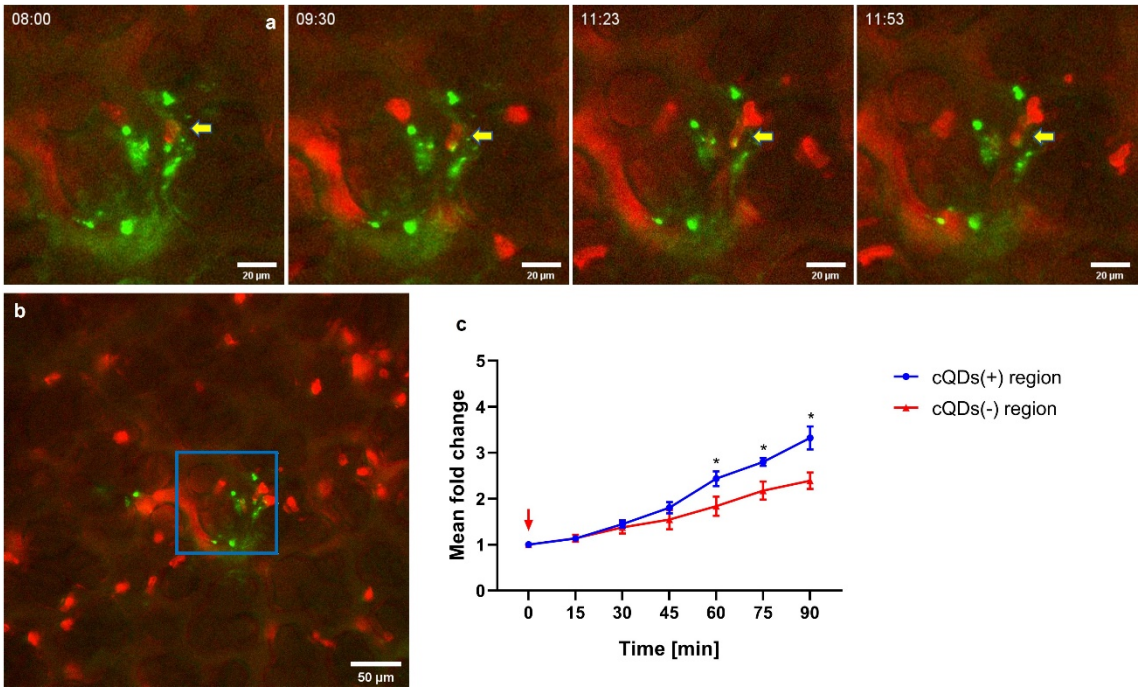

Figure 17: Recruitment of neutrophils occurred in close proximity to inhaled, deposited NPs. (a) Time-lapse of probing neutrophils in a cQD-abundant area starting 8 min after inhalation. cQD-exposed (green) mice injected with anti-Ly6G to label neutrophils (red), Scale bars, 20 µm. (b) A large number of neutrophils accumulate in the NP-enriched area (a square with 100 µm side length indicates the region of cell number analysis). Scale bars: 50 µm. (c) Data of cQDs abundant and cQDs deficient regions were presented as mean fold change from baseline (-15 min) (NPs inhalation starting at 0 min (red arrow), Means ± SEM, n=3 mice/group, Two-way ANOVA test).

Therefore, neutrophil numbers close to deposited cQDs have been quantified in square areas (100µm side length) with cQDs hotspots in the center (Figure 17b) and have been compared to neutrophil amounts in cQDs-deficient areas.

Neutrophil aggregation seemed to be centered around cQDs-rich areas. Comparing the changes in the cQDs-deficient areas, the rise of the neutrophil amount was faster than in the cQDs-rich square areas (Figure 17c, cQDs(+): 2.43±0.16 folds vs cQDs(-): 1.83±0.21 folds (60 min)).

3.3.2 Neutrophils rapidly accumulate and infiltrate into the alveoli upon inhalation of NPs

In intravital imaging, the structure of the lungs was well presented by autofluorescence and the outline of alveoli was determined clearly (Figure 18a). These imaging properties facilitate the clear discrimination of airspace and microvessels, thus also discrimination between alveolar and microvessel localized neutrophils (Figure 18b-e). As early as 30 min upon cQD (16cm^2/g) inhalation increased alveolar localized neutrophil numbers could be detected as compared to control mice, which turned significant at 60 min (1.08±0.21/$10^4$$\mu m^2$ vs. 0.43±0.08/$10^4$$\mu m^2$, $P<0.05$) (Figure 18f). The proportion of air space localized neutrophils vs. all neutrophils in cQD-treated animals increased from the baseline value of 5.65±0.83 % alveolar localized neutrophils to 18.52±3.66 % at 60 min and compared to 5.50±1.42 % at baseline value and 9.49±1.28 % at 60 min in control animals (Figure 18g). Taken together, these data indicate that neutrophil influx into the air space occurred at 1h after cQDs administration.

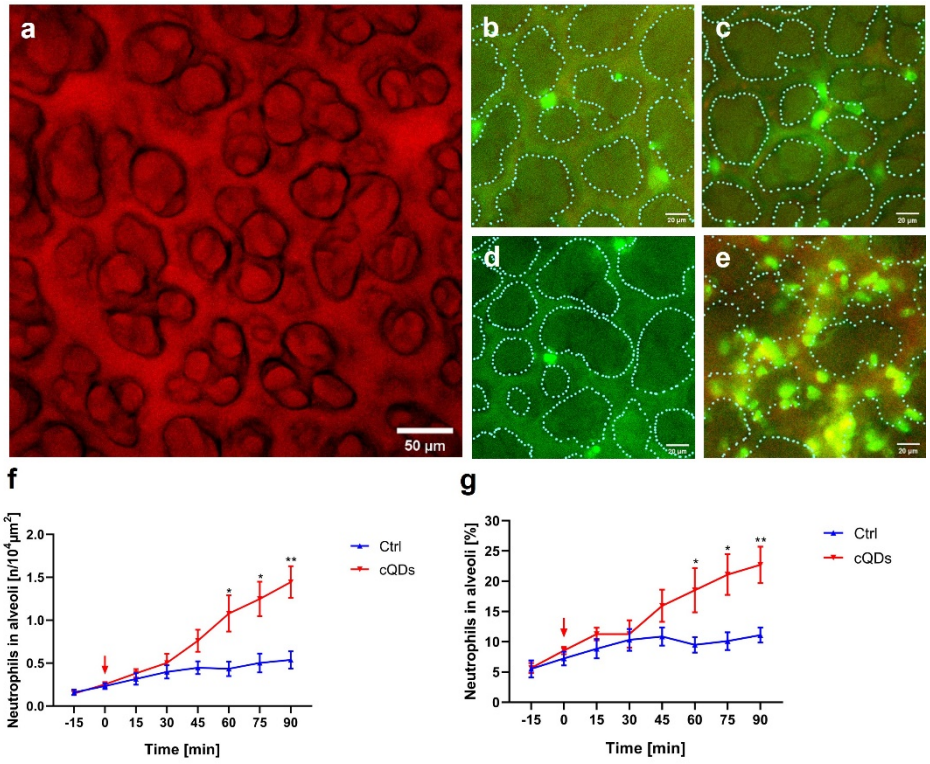

Figure 18 Neutrophil infiltration upon cQDs inhalation. (a) Visualization of lung micro-structure using L-IVM with reflected light (light excitation wavelength: 655nm, scale bars: 50 µm). (b-e) L-IVM of Ctrl and cQDs-exposed neutrophil-labeled mice (anti-Ly6G mAbs, i.v., green), alveolar structure visualized by reflected light (red). Dotted lines represent alveolar boundaries. (panel b: Ctrl group -15min, panel c: Ctrl group 90min, panel d: cQDs group -15min, panel e: cQDs group 90min, scale bars: 50 µm). (f) Neutrophil numbers infiltrated into alveoli over the time-course of L-IVM after cQDs inhalation (g) Percentage of alveolar localized neutrophil after cQDs application (QDs inhalation starts at 0 min, mean ± SEM, n=3 mice/group, Two-way ANOVA test.)

3.3.3 Neutrophils internalized cQDs in the alveoli

In LIVM images obtained 1 hour after cQDs (16cm^2/g) inhalation, some alveolar localized neutrophils were found to be associated with cQDs, indicating QDs uptake (Figure 19a). Analysis of bronchoalveolar lavage fluid obtained 24h after cQD (16cm^2/g) application, NPs were not only found in macrophages, but also in neutrophils (Figure 19b-d). 15.35±2.97% of BAL neutrophils contained cQDs (Figure 19b).

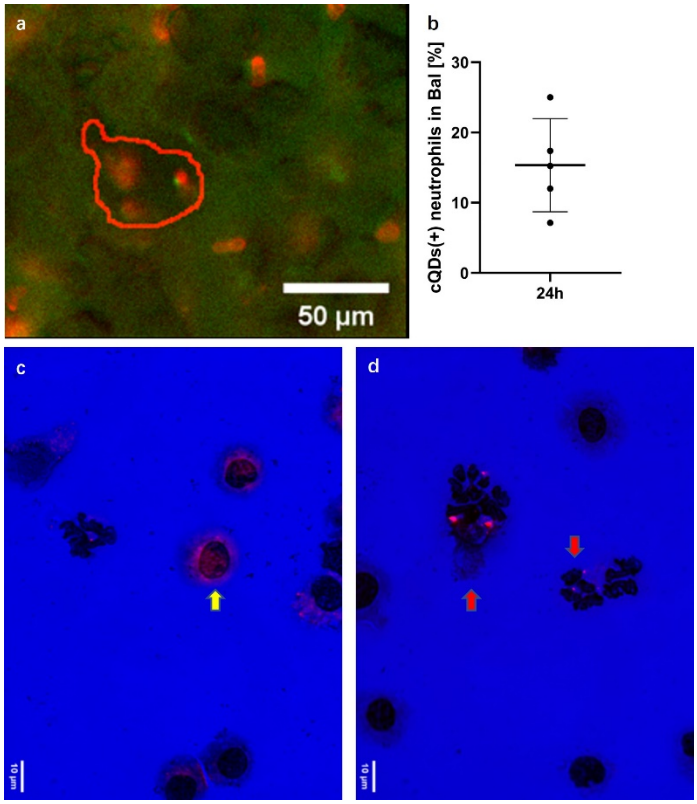

Figure 19 In addition to AMs, neutrophils also ingest inhaled NPs in the alveoli. (a) L-IVM image at 60 min after cQDs-inhalation (green) neutrophils (red; anti-Ly6G mAbs, i.v., Scale bar: 50 µm). (b) Quantification of cQDs(+) neutrophils in BAL from cQDs 24h exposed mice. (c) and (d) May Grunwald-stained BAL cells (Cytospin, 24h after cQD exposure) indicated that neutrophils infiltrated into alveoli and assisted in NP clearance. cQDs (red) are found in (c) AMs (yellow arrow) and (d) neutrophils (red arrows), and cells are visualized by phase contrast microscopy (scale bar: 10 µm).

To record the interaction between neutrophils and cQDs in lung tissue sections of mice 90 min after cQDs (16cm^2/g) inhalation, immunofluorescence staining of frozen 6µm slides stained with Ly6G as a neutrophil marker and DAPI (Figure 20a-d) was performed. The images depict pulmonary localized neutrophils with internalized NPs. Thereby, these data indicate a contribution of neutrophils in the alveolar clearance of NPs.

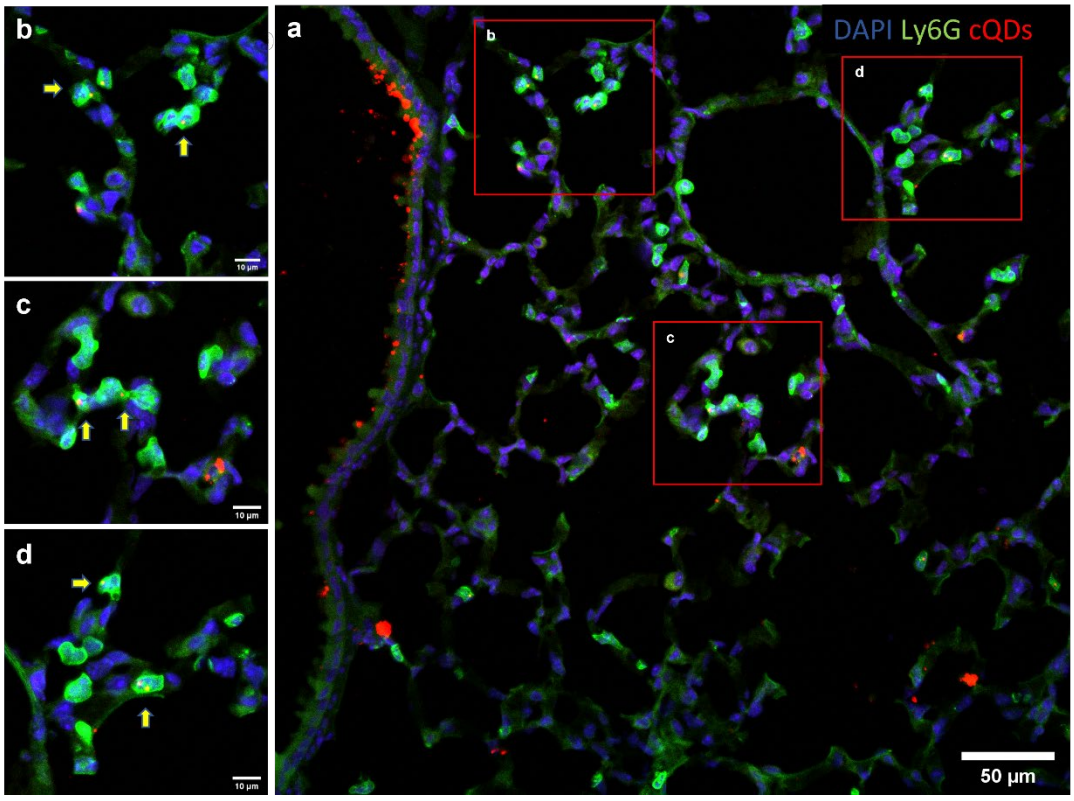

Figure 20 (a) Fluorescence confocal microscopy of mice lungs 90min after cQDs (red) inhalation. Neutrophils were labeled with anti-Ly6G antibody (green). Nuclei were stained by DAPI (blue) (Scale bar: 50 µm). The neutrophils in the alveoli gather in the NP-abundant areas. (b)-(d) Magnification of particle-laden neutrophils from (a) (Scale bar: 10 µm).

3.4 NPs-evoked neutrophil recruitment is mediated by cellular degranulation

3.4.1 cQD-induced neutrophil recruitment is diminished by inhibiting cellular degranulation

As previously reported, cQDs application in the blood circulation induced rapid neutrophil recruitment, this process was inhibited by the application of cromolyn which inhibits cellular degranulation (Rehberg et al., 2010). Cromolyn is generally considered a mast cell stabilizer, but it also decreased radical production by AMs in response to zymosan (Sadeghi-Hashjin et al., 2002). AM-derived microvesicles (MVs), which are mediators of intercellular

communication, carry bio-active substances, like tumor necrosis factor (TNF) was reported to play a vital role in initiating acute lung injury (ALI) (Soni et al., 2016).

To test whether cellular degranulation is involved in initiating NP-induced neutrophil recruitment, the mice were pretreated via i.v. injection with 0.2 mg/kg (BW) cromolyn 30 min before inhalation. In cromolyn-pretreated mice, cQD (16 cm^2/g) as well as CNP (172.5cm^2/g) induced neutrophil recruitment (cQDs: 3.31±0.26/$10^4 \mu m^2$ and CNP: 3.54±0.17/$10^4 \mu m^2$) was found to be significantly reduced at 60min compared to cQD- and CNP-exposed mice (cQDs: 5.39±0.49/$10^4 \mu m^2$ and CNP: 5.12±0.20/$10^4 \mu m^2$) without cromolyn treatment. The pretreatment of cromolyn reduced the number of neutrophils after inhalation of cQDs and CNPs to the levels of the control group (3.74±0.44/$10^4 \mu m^2$) (Figure 21a,d). These important findings underline that cellular degranulation is involved in the initiation of the cQD- and CNP-elicited neutrophil response. Importantly, pretreatment with cromolyn significantly reduced neutrophils infiltration into alveoli after 24 hours of NP exposure, as determined by BAL analysis (Figure 21b,c,e,f).

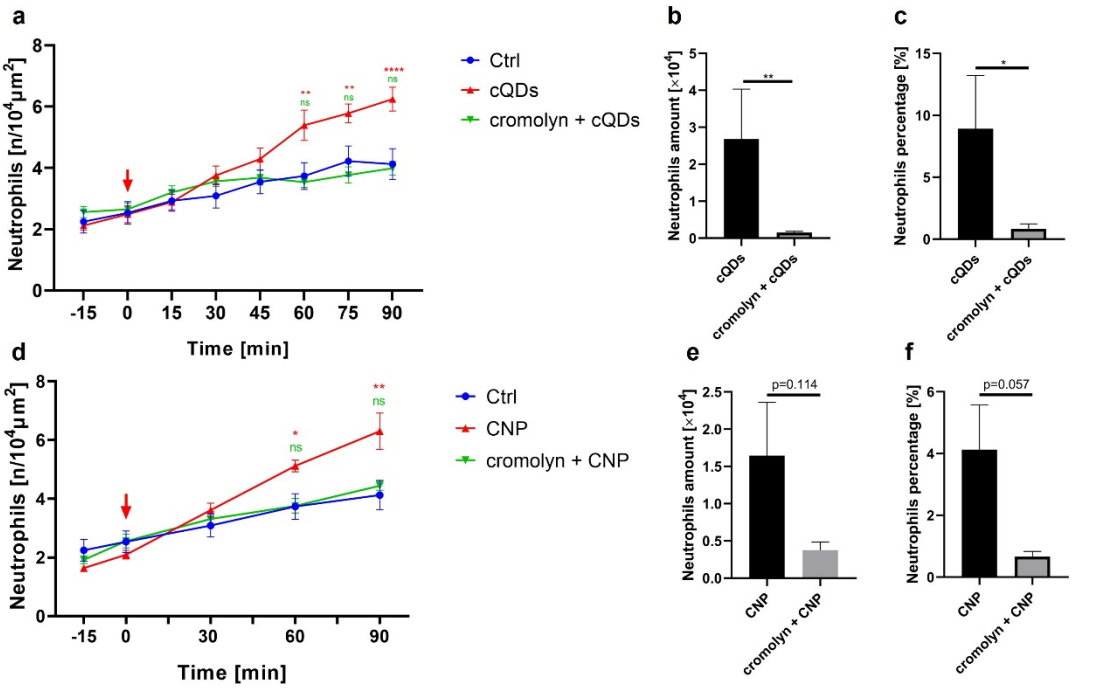

Figure 21 Inhibition of cellular degranulation reduces cQD- and CNP-evoked neutrophil recruitment. (a) and (d) Alterations in the amounts of neutrophils over time during L-IVM were compared between mice receiving cromolyn (iv. injection 0.2 mg/kg BW 30 min prior to NP inhalation), an inhibitor of cell degranulation prior to inhalation of (a) cQDs, (d) CNP or vehicle-control. (b) and (c) The numbers and percentage of total BAL cells, AMs, neutrophils, and lymphocytes were determined with May Grunwald-stained BAL cells of mice pretreated with cromolyn prior to inhalation of cQDs or CNP (e) and (f) for 24h and compared to corresponding controls (NPs inhalation starting at 0 min (red arrow), Means ± SEM, n=4-6 mice/group, a,d: Two-way ANOVA test, b,c,e,f: parametric data used paired Student's t-test and nonparametric data used Mann-Whitney rank-sum test, n=3-6 mice/group, a: red * cQDs vs vehicle-control, green * cQDs vs cromolyn + cQDs, d: red * CNP vs vehicle-control, green * CNP vs cromolyn + CNP).

In order to further study the effect of cromolyn on cQDs-induced neutrophil recruitment, we compared the neutrophil crawling velocity along the microvessel walls. After cQDs exposure, the speed of neutrophil movement along the blood vessel walls decreased in close vicinity to deposited cQDs (from 15 min on). However, pretreatment with cromolyn considerably increased in cQD-exposed mice neutrophil crawling speed, to an even higher level than in the control group (Figure 22a-d), especially in the 15-30 minute period (cromolyn pretreated and cQDs: 0.359±0.043µm/s vs cQDs: 0.146±0.024µm/s, $p<0.0001$) (Figure 22b). This suggests that cellular degranulation slows down

neutrophils in close proximity to deposited NPs, which might intensify crawling and probing behavior and subsequent leukocyte recruitment to the airspace in these areas.

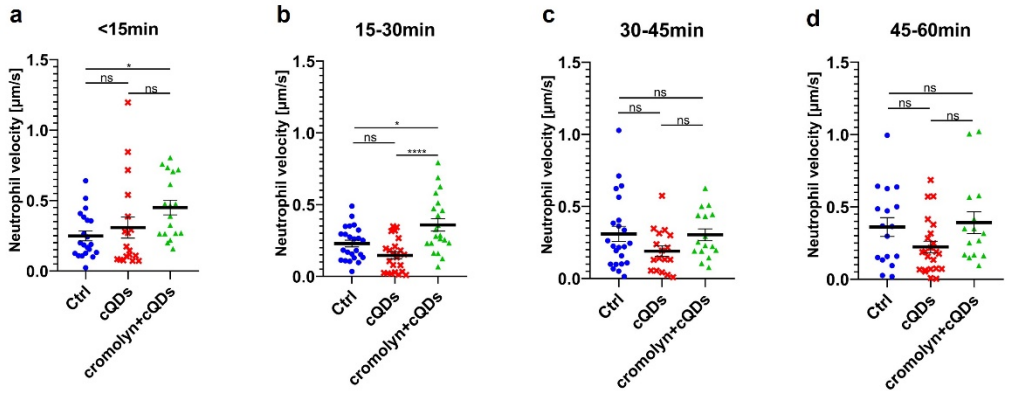

Figure 22 Analysis of neutrophil crawling velocity. (a)-(d) The movement speed of long-staying (>5 min) neutrophils in and around cQDs-abundant areas (distance < 100 µm) in mice with or without cromolyn-treatment was analyzed after inhalation of cQDs or vehicle-control. (Means ± SEM, n=3 mice/group, One-way ANOVA test).

As presented above (Figure 13a), blood flow velocity was decreased 2 hours upon cQDs exposure. Cromolyn pretreatment restored blood flow velocity in cQDs-exposed mice back to control levels (119.25±8.60 µm/s of cQDs vs 190.06±13.27µm/s of control group vs 175.13±11.67 µm/s of cromolyn pretreatment group) (Figure 23a). Pulmonary vessel diameters were not affected by cromolyn treatment. (Figure 23b).

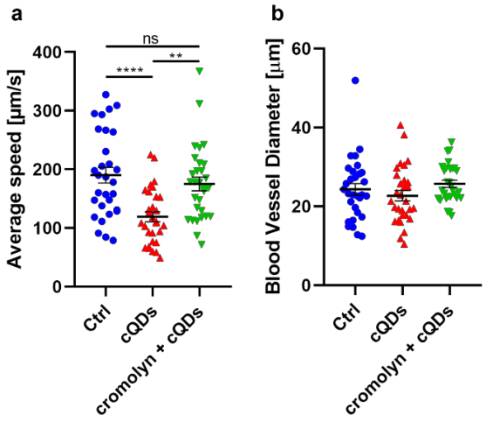

Figure 23. Cromolyn restored the decrease of blood perfusion speed in the pulmonary blood vessels of cQD-exposed mice. (a) Blood perfusion speed in pulmonary microvessels of mice with or without cromolyn-treatment prior

to inhalation of cQDs. (b) Blood vessel diameter in the fields of view in the different treatment groups (Means ± SEM, n=3 mice/group, One-way ANOVA test).

TNF contained in microvesicles, derived from AMs, was shown to be important in the immune response during ALI (Soni et al., 2016). TNFα neutralization by oropharyngeal aspiration of anti-TNFα mAbs 3h prior to cQD or CNP inhalation resulted in significantly reduced neutrophil accumulation 60 min after cQDs inhalation (Figure 24a), as well as after CNP-inhalation (Figure 24b). These results indicate that TNFα is involved in the rapid neutrophil recruitment encounter and might be released during cellular degranulation upon NPs exposure.

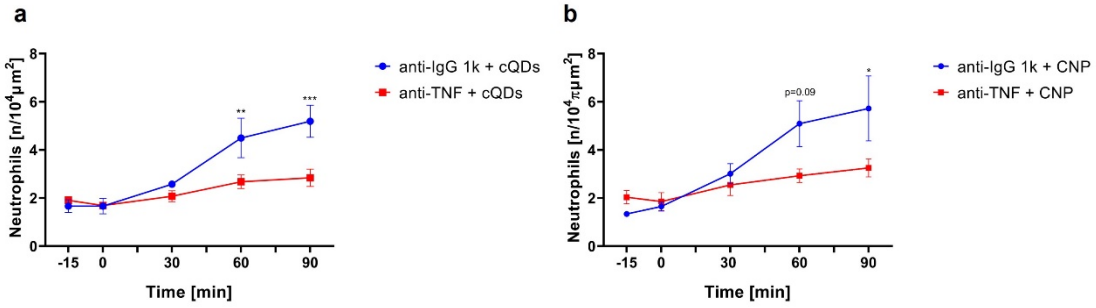

Figure 24 TNFα neutralization prevented cQD- and CNP evoked neutrophil recruitment. (a) and (b) Alterations in the amounts of neutrophils over time under L-IVM were compared between mice pretreated with anti-TNFα mAb or isotype mAb followed by cQD (a) or CNP (b) inhalation. NPs inhalation started at 0 min, red arrow, Means ± SEM, n=3-4 mice/group, Two-way ANOVA test.

3.4.2 cQD-induced neutrophil recruitment is not mediated by the IL-1 family

IL-1α has been reported to play an important role in pulmonary neutrophilic inflammation induced by inhaled NPs (silica) (Rabolli et al., 2014). The function of IL-1α is mediated by the interleukin 1 receptor 1 (IL-1r1) (Boraschi & Tagliabue, 2013). To achieve a better understanding of the implication of IL-1 in the pulmonary inflammatory response to cQDs the function of IL-1 in the

development of cQDs-evoked pulmonary inflammation was assessed in IL1r1-ko mice. The deposition of cQDs caused a large number of neutrophils to be recruited in the lungs of IL1r1-ko mice, close to numbers obtained in WT mice (IL1r1-ko mice and WT mice: 4.93±1.18/10^4μm^2 vs 5.39±0.49/10^4μm^2 (60min), 5.20±0.89/10^4μm^2 vs 6.25±0.39/10^4μm^2 (90min), Figure 25). These results indicated that IL-1 did not play a vital role in cQDs-evoked early neutrophil recruitment.

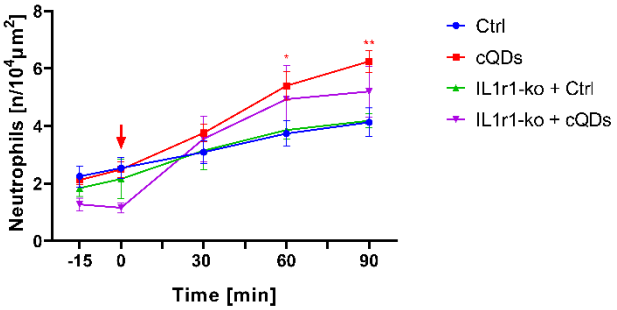

Figure 25 IL1r1 knockout has no effect on cQDs-evoked recruitment of neutrophils. Alterations in the amounts of neutrophils over time under L-IVM were compared between WT mice and IL1r1-ko mice after inhalation of cQDs or vehicle-control. (NPs inhalation starting at 0 min, Means ± SEM, n=3 mice/group, Two-way ANOVA test, red * cQDs vs vehicle-control).

3.4.3 cQD positive AMs are correlated with a higher number of neutrophils in their close vicinity

Since we established that neutrophil recruitment preferentially occurs close to NP “hotspots” (Figure 20c) and inhibition of cellular degranulation (Figure 21a, d) abolishes neutrophil recruitment, we analyzed next, whether AMs could be involved in initiating local (alveolar) immune response. In a new set of experiments, we administered PKH26 dye (AMs labeling efficiency: 90%) into the mice airway directly (at least 5 days prior to NPs inhalation) in order to achieve visualization of AMs (Neupane et al., 2020) and to compare whether

the uptake of cQDs by AMs is correlated to the aggregation of surrounding neutrophils. For this neutrophils in a radius of <30μm around PKH26-labeled AMs exhibiting cQD fluorescence (cQD+), or no QD signals (cQD-) and in AM free control areas (blank) have been determined at 5, 30, 60 and 90 min after cQD inhalation (Figure 26a). Within the first hour after cQDs inhalation, the number of neutrophils around cQDs(+) AMs and cQD(-) AMs and control areas were comparable. However, 60 and 90 min after cQDs inhalation, more neutrophils ($0.278\pm0.027/\pi10^2\mu m^2$ at 60min and $0.296\pm0.034/\pi10^2\mu m^2$ at 90min) gathered around cQDs(+) AMs, compared to cQD(-) and control areas ($0.193\pm0.020/\pi10^2\mu m^2$ at 60min and $0.194\pm0.018/\pi10^2\mu m^2$ at 90min) (Figure 26b). In addition, we compared the effects of different distances on the attraction of neutrophils by cQDs-positive AMs. As the distance increases (30 –50 μm), the tendency of neutrophils to gather around AMs with phagocytosed cQDs disappeared ($0.226\pm0.025/\pi10^2\mu m^2$ of 30–50μm) and matched the cell numbers in control areas ($0.194\pm0.018/\pi10^2\mu m^2$) at 90min (Figure 26d). To rule out a direct NP effect without the need for cellular uptake, or a contribution of epithelial cells, neutrophil numbers around cQDs(+) AMs or cQDs directly deposited on epithelial cells were compared. From 60 min, significant neutrophil aggregation appeared around QDs internalized by AMs compared to cQDs not internalized by AMs (Figure 26c). Taken together, this data suggests that the cQD-induced recruitment of neutrophils is not initiated by “cell-free” cQDs and is indeed mediated by AMs, not alveolar epithelial cells.

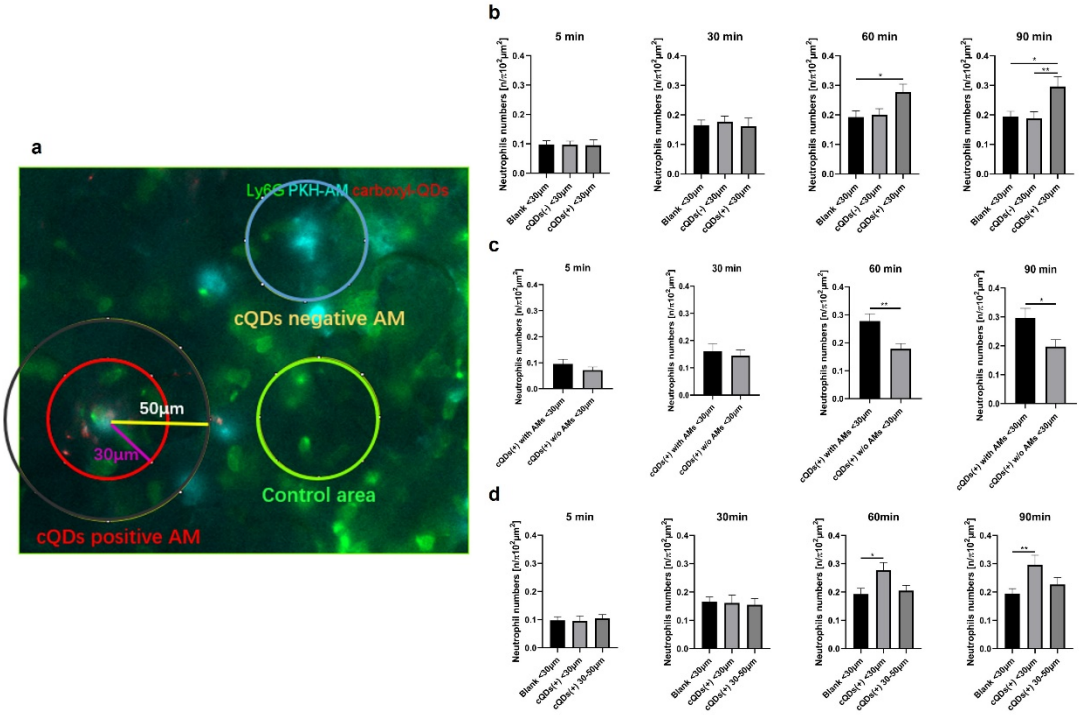

Figure 26 Analysis of neutrophil accumulation close to AMs (a) Regions were divided according to whether AMs phagocytosed cQDs. Green circle: Control/Blank area, red circle: cQDs(+) AM area, blue circle: cQDs(-) AM area. (b) Neutrophils accumulate around AMs that phagocytose cQDs. The number of neutrophils around cQD(+) AMs, cQD(-) AMs and blank areas were determined. Neutrophils accumulate around AMs that phagocytose cQDs. (c) The number of neutrophils around AMs containing cQDs, and "cell-free" cQD areas were calculated. (d) Analysis of neutrophil numbers at different distances from AMs that phagocytosed cQDs (distance < 30 μm and 30 μm < distance < 50 μm, n=3 mice, One-way ANOVA test).

3.4.4 Intravascular application of anti-CXCL1 has no effect on the cQDs-induced recruitment of neutrophils.

Neutrophil recruitment in the lung, a pathophysiological feature of lung diseases such as COPD and severe asthma, is mainly regulated by CXCL1 and CXCL8 (Planagumà et al., 2015). Therefore, we aimed to investigate whether CXCL1 is involved in the regulation of NP-induced neutrophil recruitment in vivo. An anti-mouse CXCL1 mAbs was administered into the circulatory system of WT mice, followed by cQDs inhalation exposure. Similar numbers of neutrophils in the lung of anti-CXCL1 treated mice were found as compared to untreated

animals from 60 min after cQD inhalation (6.66±0.48/10^4μm^2 vs 5.39±0.49/10^4μm^2, P=0.39) (Figure 27a). Injection of anti-CXCL-1 did not inhibit neutrophil recruitment in vivo and had no rescuing effect on cQDs decreased blood circulation velocity (Figure 27b-c).

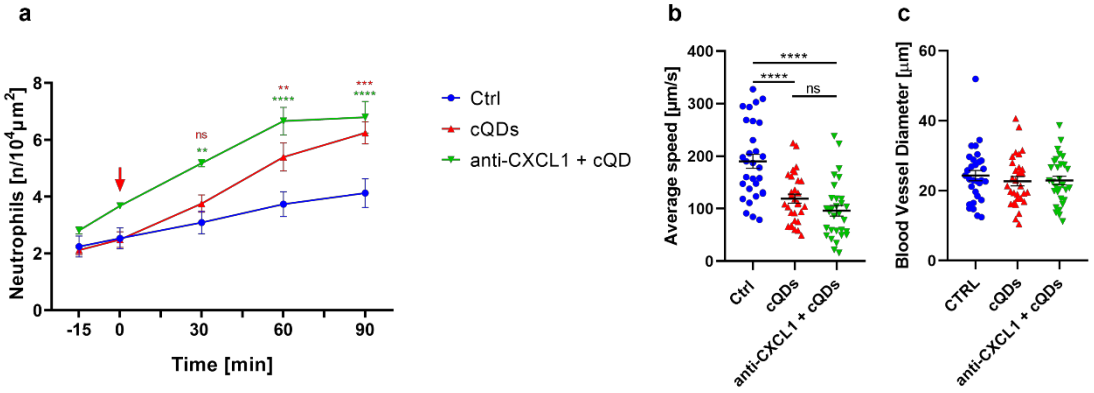

Figure 27 Blocking of intravascular CXCL1 has no effect on cQDs-evoked recruitment of neutrophils. (a) Alterations in the amounts of neutrophils over time under L-IVM were compared between mice receiving CXCL-1 blocking antibody prior to inhalation of cQDs or vehicle-control. (NPs inhalation starting at 0 min, means ± SEM, n=3 mice/group, Two-way ANOVA test, red * cQDs vs vehicle-control, green * anti-CXCL1 + cQDs vs vehicle-control). (b) Blood perfusion speed in the pulmonary vessels of mice with or without CXCL1-blocking prior to inhalation of cQDs or vehicle-control (Means ± SEM, n=3 mice/group, One-way ANOVA test). (c) Blood vessel diameter in the fields of view in the different treatment groups. (Means ± SEM, n=3 mice/group, One-way ANOVA test).

3.5 Inhaled NPs affect the patrolling speed of AMs

3.5.1 PKH26 labeled AMs with high specificity

AMs are the main phagocytic cells in the alveolar lumen cavity (Barletta et al., 2012). They have a strong phagocytic capacity for pathogens (bacteria, viruses, and NPs, etc.) inhaled in the respiratory tract, and maintain homeostasis in the lungs (Guilliams et al., 2013; Kopf et al., 2015). As early as 3 h after CNP exposure, 50% of AMs were shown to be loaded with particles (Chen et al., 2016). AMs patrol within and between alveoli for bacteria or endogenous cellular debris clearance (Neupane et al., 2020). Above (Chapter

4.3.5) we demonstrated that more neutrophils aggregated around AMs that had phagocytosed NPs. Next, we analyzed the effects of NPs on AM dynamics. First, we determined the immune cell composition in BAL of naive mice with May Grunwald-stained BAL cells (Cytospin). The alveolar cavity is filled with AMs (98 ± 0.64 %, Figure 28a). Flow cytometry confirmed that 90.1% of AMs were labeled with PKH-26 (Figure 28b). Lung intravital microscope images indicated that not every alveolus contained an AM (Figure 28c), and we detected each AM protecting roughly three alveoli (Figure 28d). This ratio was in line with the very recent data from Neupane et al (AS., 2021), indicating that the staining is AM specific (as has been demonstrated in Neupane (Neupane et al., 2020)) also in our hands.

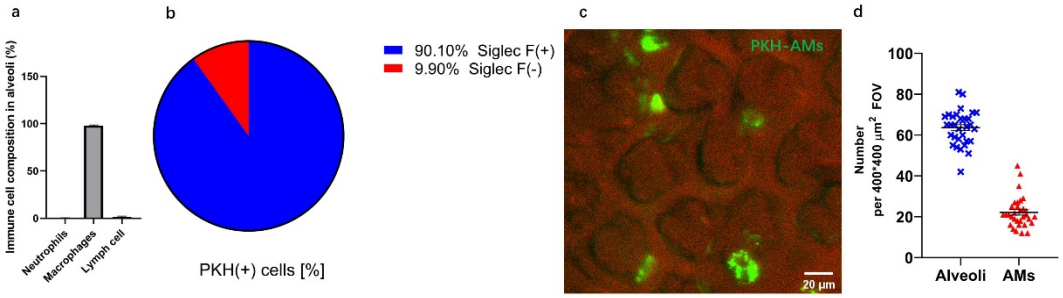

Figure 28 PKH-26L labeling of AMs. (a) The numbers of AMs, neutrophils, and lymph cells in naïve mice were determined by BAL cell differentiation of May Grunwald-stained BAL cells (Cytospin). (b) Quantification of PKH26+ cells in the lungs of PKH-labeled mice (n=3). (c) L-IVM image of PKH26 pretreated mouse lung. PKH-AMs are shown in green, and lung microstructure (red) was depicted by reflected light. Scale bar: 20 µm. (d) Quantification of the ratio of AMs to alveoli in the fields of observation (Means ± SEM, 32 fields of observation, n= 3 mice).

3.5.2 NP exposure alters AM velocity

To our knowledge, only one previous research has investigated AM migration patterns during their patrolling through the lungs in vivo, when Neupane et al investigated the effect of pathogens on AM motility (Neupane et al., 2020). The ability of PKH-AMs to crawl in the alveolar space in influenza-infected

mice was significantly defective, thereby reducing AM ability to capture P. aeruginosa and S. aureus, thereby aggravating the bacteria-induced lung inflammation (Neupane et al., 2020). From our own above-presented data, we deduced that AMs may be effector cells for NP-induced neutrophil recruitment. Therefore, we suspected that the rapid neutrophil recruitment induced by NPs may be related to AM migration and no research has investigated AM movement in NP-exposed mice lungs.

Therefore, tracking of PKH-labeled AMs has been performed. Intriguingly, as compared to control values (0.46±0.03μm/min), cQDs as well as CNPs (1.04±0.04μm/min) increased the migration velocity of PKH-labeled AMs (0.74±0.05μm/min) in the alveoli of the respective mice, whereas aPEG-QDs decreased AM crawling velocity (0.29±0.03μm/min) (Figure 29a-b). Importantly, 24h after cQDs and CNP exposure, AMs remained in a particularly active state in alveoli, i.e., AM velocity was still increased compared to controls (Figure 29c).

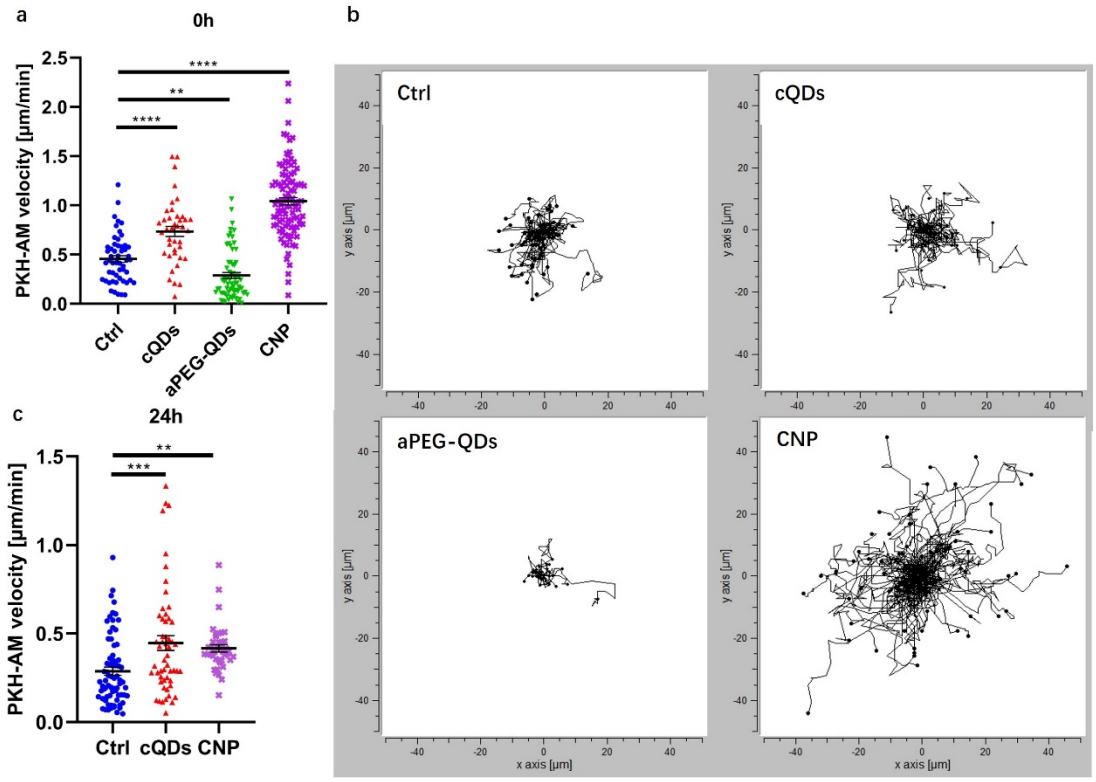

Figure 29 In vivo dynamics of AMs. (a) Average track velocity (µm/min) of AMs in different NP-exposed mice (0h) during a 1h L-IVM imaging session. Each symbol represents the migration velocity of a randomly selected individual AM, n=4-6 mice/group (Means ± SEM, n=4-6 mice/group, One-way ANOVA test). (b) Spider plot of randomly chosen PKH-AM migration paths in the alveoli of mice after different NP exposures during a 1h L-IVM imaging session. (c) Average track velocity (µm/min) of AMs in different NP-exposed mice 24h after inhalation during a 1h L-IVM imaging session. n=4-6 mice/group (Means ± SEM, n=4-6 mice/group, One-way ANOVA test).

3.5.3 NP exposure did not cause AM death

Intratracheal instillation of silica salts and silica particles induced AM cell death and release of IL-1a, which caused lung inflammation (Kuroda et al., 2016). To further investigate whether the alteration of AM patrolling movement is due to altering cell viability upon NPs exposure, we exposed M-HS cells to cQDs and aPEG-QDs (8nM) for 1h respectively and measured the cell viability by WST-assay. The results showed that the exposure of the two kinds of QDs did not alter the viability of AMs in this period of time (Figure 30a). In addition, after 90 min of cQDs inhalation in vivo, AM cell numbers remained at

the pre-exposure levels (-15min) (Figure 30b). From this, we concluded that QDs exposure did not affect AM viability or even induced cell death.

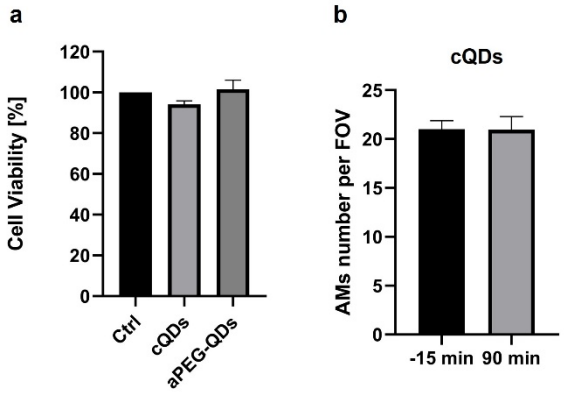

Figure 30 QDs exposure did not alter AM viability. (a) M-HS cells were exposed to cQDs and aPEG-QDs (8nM) for 1h and cell viability was measured by WST assay. (b) Quantification of AMs number in cQDs-exposed mice using L-IVM, 7 FOVs / time point. (Means ± SEM, n=4, paired Student's t-test).

3.5.4 PEGylation prevents QD NPs from being internalized by AMs

Next, we tested whether NPs' surface modifications were important for the capture/uptake of inhaled QDs by AMs in vivo. Our data shows that AMs increasingly internalized cQDs over the observation time of 90 min. The QDs are visible as early as 5 min after inhalation in/at AMs, the values increase from 3.67±0.86 % positive cells to 11.11±1.28 % after 90 min, whereas only little aPEG-QDs uptake was detected (Figure 31a-c). To further explore this, we administered cQDs and aPEG-QDs (8 µM) respectively into the medium of AMs-like cells (MHS cells) for 1 hour. Almost all MHS cells (94.90%±1.62%) internalized cQDs particles, while fewer MHS (10.23%±2.72%) phagocytosed aPEG-QDs particles, as determined by FACS analysis (Figure 31d).

In addition to a missing "opsonization" of PEGylated QDs which aggravates cellular uptake, also the altered migratory behaviors of AMs after NP exposure

may contribute in vivo. In accordance with this, in the first hour of imaging, several AMs were observed to crawl toward and engulf nearby NPs in alveoli (Figure 31e). More interestingly, AMs also share overloaded NPs with other AMs (Figure 31f).

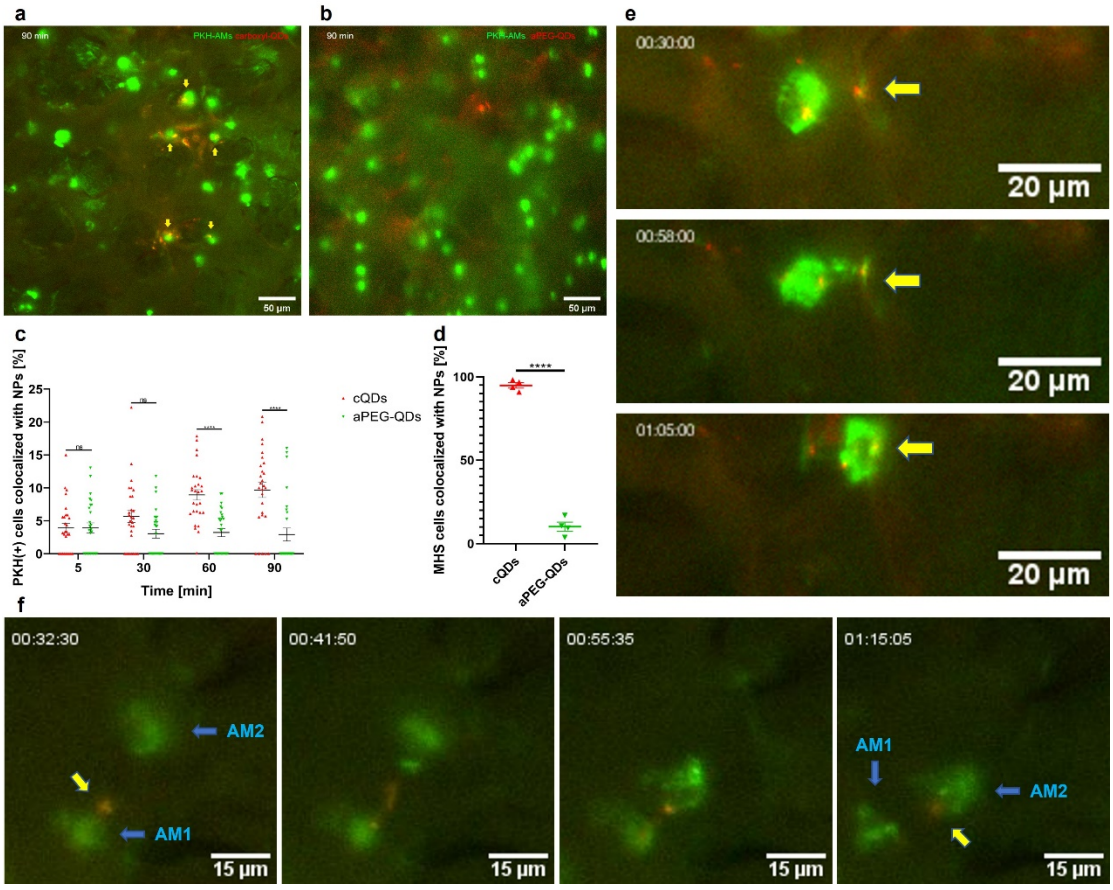

Figure 31 After 60 minutes upon NPs exposure, more cQDs were taken up by AMs than aPEG-QDs. L-IVM image at 90 min after (a) cQDs and (b) aPEG-QDs-exposure (red). PKH26L has been applied 5 days prior to the experiment to label AMs (green) (Scale bar: 50 µm). (c) Quantification of AMs colocalized with QDs, indicating cellular uptake in cQDs-exposed and aPEG-QDs-exposed mice using L-IVM (NPs inhalation starting at 0 min, Means ± SEM, 7 random observed fields per time point per mouse, n=3 mice/group, Two-way ANOVA test). (d) Quantification of MHS cells incubated with QDs for 1h in cell culture medium by FACS analysis (Means ± SEM, n=4, paired Student's t-test). (e) Time-lapse of PKH-AM (green) crawling towards and engulfing cQDs (red, arrows). Scale bar: 50 µm (f) QDs (red) are exchanged between two AMs (green). Scale bar: 50 µm.

Next, we utilized tissue clearing to achieve co-imaging of AMs from Macgreen mice (Csf1r-EGFP is expressed selectively in macrophage and monocyte cell lineages) after transcardial perfusion for flushing out all of Csf1r-EGFP

labeled blood cells. The positional relationship between the fluorescent NPs (cQDs and aPEG-QDs) and Csf1r-EGFP cells (macrophages) revealed information regarding the NPs internalization. In accordance with the LIVM results (figure 31c), higher numbers of NP+ AMs (Figure 32a, yellow arrows) were observed in cQDs-exposed lungs compared with aPEG-QDs-exposed mice (Figure 32b). Similar, in Precision Cut Lung Slices (PCLs) images, after 2h of cQDs inhalation, NPs were mostly collected by AMs (Csf1r-EGFP) rather than deposited on the endothelial cell surface (figure 32c-g).

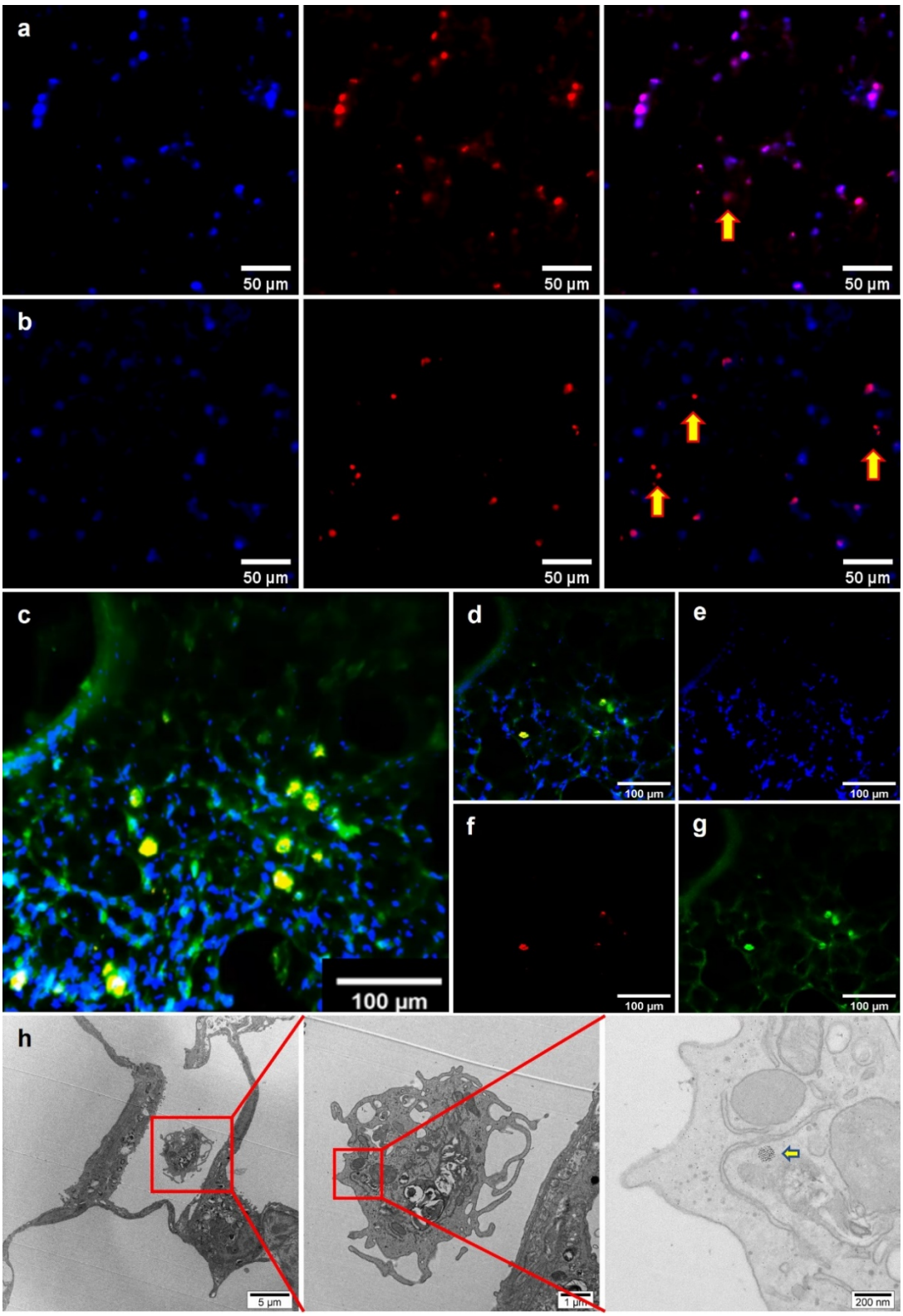

Figure 32 (a)-(b) 2D images from light sheet microscope images of cQDs and aPEG-QDs exposed mice. Csf1r-1(+) AMs are shown in blue, QDs are shown in red and AMs uptaking QDs are shown in purple. (panel a: cQDs, panel b: aPEG-QDs, Scale bar: 50 µm). (c)-(g) 3D (c) and 2D (d-g) The images of PCLs sample (covering 100 µm in z) from cQDs exposed lungs from the confocal microscope. Nucleus (DAPI-labeled) are shown in blue, cQDs are shown in red and cQDs uptaking PK-AMs (green) areshown in yellow, scale bar: 100 µm. (e) Transmission electron microscopy of the cQDs-exposed lung (1h) showed that NPs accumulated abundantly in AMs and surfactants. Aggregates of cQDs were found within the cytoplasm of AMs.

To further investigate the distribution of NPs at the subcellular level, electron microscopy was applied to obtain subcellular structural information of the lungs of mice that have been exposed to cQDs, aPEG-QDs or PEG-QDs for 2 hours respectively. Some cQDs clusters were identified within the cytoplasm or in endosomes of AMs, whereas no such aggregated QDs could be clearly identified in AMs in the PEG-QD or aPEG-QD groups (Figure 32h). Ultrastructurally, pulmonary surfactants are composed of several subtypes: freshly secreted lamellar body-like forms, tubular myelin sheaths, alveolar linings, and small unilamellar vesicles (Ochs et al., 1999). As described in (Fehrenbach et al., 1998), cQDs were found to be attached to or agglomerated with alveolar surfactant (tubular myelin) within the alveolar space of cQDs-exposed mice, which was not observed for aPEG-QDs and PEG-QDs (Figure 33a). Besides, C5aR1 blockade reduced phagocytosis of cQDs and surfactant mixtures by AMs, but FcγRI blockade did not (Figure 33b-e).

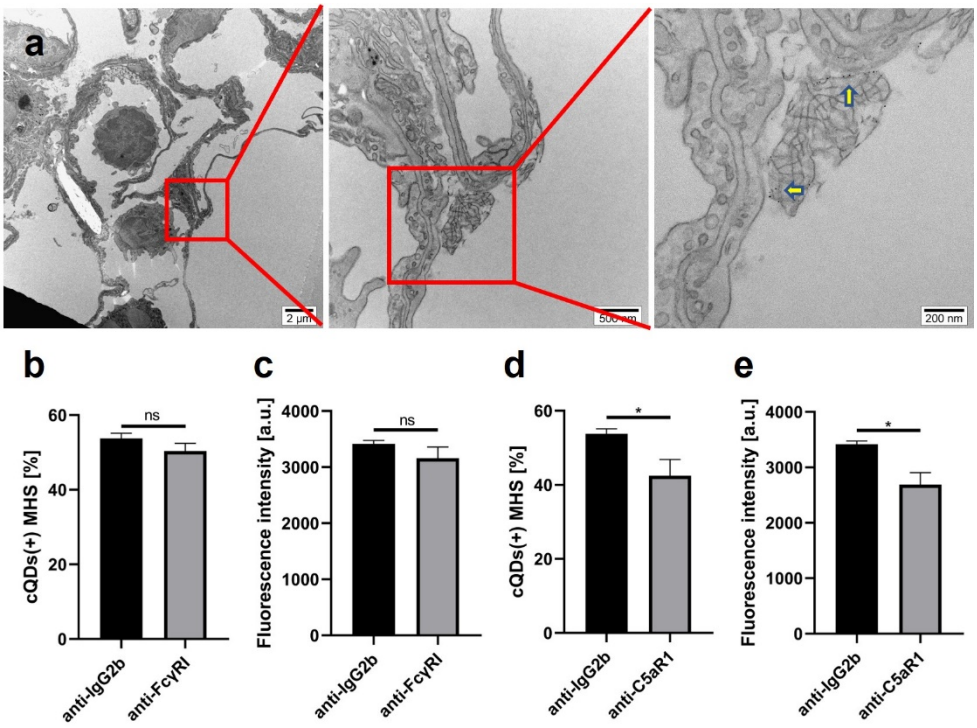

Figure 33 cQDs accumulated abundantly in AMs and surfactants. (a) Transmission electron microscopy of the cQDs-exposed lung (1h) showed that NPs accumulated abundantly in AMs and surfactant. cQDs and surfactant aggregates existed in the alveoli. (b)-(e) MHS cells phagocytosing cQDs co-incubated with surfactant were analyzed by flow cytometry of MHS cell treated with C5aR1- and FcγR I-blocking mAb or isotype mAb control 3h prior to cQDs (2nM) application for 1h, n=3-4.

3.5.5 NP-induced enhanced macrophage patrolling and rapid neutrophil recruitment are mediated by LFA-1

The above experiments indicate that cQDs or CNP deposition in the lungs can induce two acute responses: (1) a large number of neutrophils accumulate in the pulmonary microvessels and transmigrate rapidly into the alveoli (airspace); (2) AM “patrolling” (motility) in the alveoli is stimulated.

LFA-1 is highly expressed on PMNs, which is crucial in promoting the PMNs recruitment cascade (Ley et al., 2007). Recently, it was revealed that LFA-1 is also one vital adhesion molecule utilized by AMs for patrolling within the alveoli (Neupane et al., 2020). To study the relationship between (1) and (2), we administered LFA-1 blocking antibodies by oropharyngeal aspiration 3h prior to

NP-inhalation into mice lungs to significantly reduce the motility of macrophages in the alveolar cavity, analogous to the recently published approach by the Kubes lab (Neupane et al., 2020). Indeed, the AM motility in LFA-1-mAb treated mice was significantly decreased compared with isotype-antibody treated control mice upon cQD inhalation (0.15±0.01μm/min vs 0.74±0.05μm/min, $p<0.0001$) (Figure 34a). Interestingly, following cQD inhalation exposure, more AMs could be lavaged from LFA-1-blocking mice than from isotype mAbs-treated mice (Figure 34b) ((74.73±10.74) $*10^4$ vs (30.27±2.5) $*10^4$, $p<0.05$). Therefore, LFA-1 blockade also impaired the ability of AMs to anchor to the alveolar wall in vivo. In addition, also the number of recruited neutrophils was notably reduced in anti-LFA-1-treated mice upon 60min after cQDs inhalation (3.31±0.43/10^4μm^2) as compared to isotype-matched control mAb pretreated mice (4.80±0.88/10^4μm^2) (Figure 34e-f).

To investigate whether CNP-induced neutrophil recruitment is mediated by LFA-1 of AMs like observed for cQDs, we blocked LFA-1 via oropharyngeal aspiration of anti-LFA-1 antibody. In anti-LFA-1-pretreated mice, CNP-evoked neutrophil recruitment (3.22±0.23/10^4μm^2 vs 5.13±0.96/10^4μm^2, $p<0.01$) as well as AM crawling velocity (0.33±0.03μm/min vs 0.57±0.04μm/min, $p<0.0001$) and interaction strength between AMs and lung epithelial cells (AMs number in BAL: (60.58±6.84)$*10^4$ vs (18.08±3.19)$*10^4$, $p<0.01$) (Figure 34c, d), was significantly diminished at 60 min as compared to mice receiving isotype-

matched control monoclonal antibodies (Figure 34g-h).

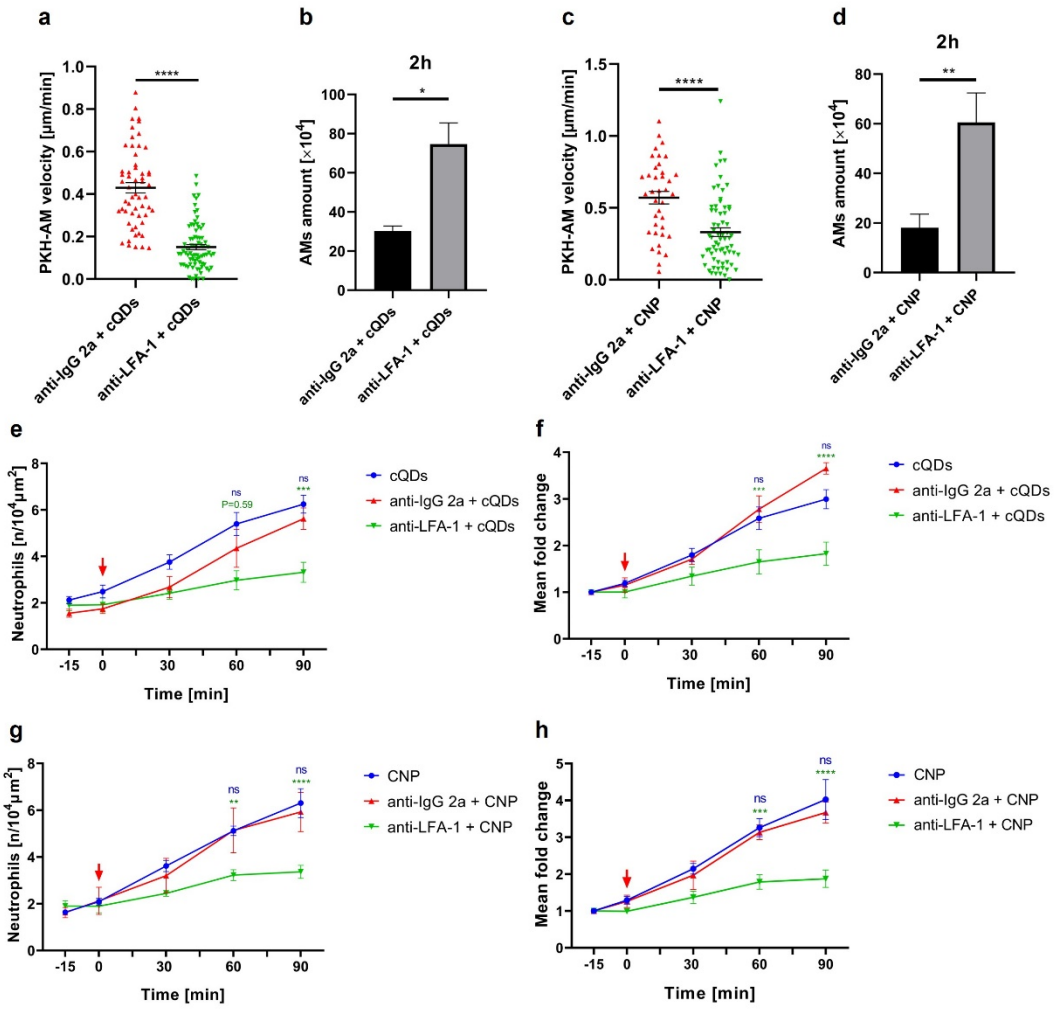

Figure 34 NPs-evoked neutrophil recruitment is mediated by LFA-1. (a) Average track velocity (µm/min) of AMs in isotype or LFA-1-blocking mAb -treated mice followed by cQDs inhalation exposure during a 1h L-IVM imaging session (Means ± SEM, n=3-6 mice/group, paired Student's t-test). (b) Quantification of AMs in BAL fluid of mice treated with anti-LFA-1 mAbs or isotype mAbs prior to inhalation of cQDs (2h), n = 3/group. (c) Average track velocity (µm/min) of AMs in isotype or LFA-1-blocking mAb-treated mice followed by CNPs inhalation exposure during a 1h L-IVM imaging session (Means ± SEM, n=3-6 mice/group, paired Student's t-test). (d) Quantification of AMs in BAL fluid of mice treated with anti-LFA-1 mAbs or isotype mAbs prior to inhalation of CNPs (2h). n = 3/group. (e) and (g) Alterations in the amounts of neutrophils over time under L-IVM were compared between mice pretreated with anti-LFA-1 mAb or isotype mAb followed by cQD (e) or CNP (g) inhalation. (NPs inhalation starting at 0 min, red arrow, Means ± SEM, n=4-6 mice/group, Two-way ANOVA test). (f) and (h) Results are presented as mean fold change from neutrophil amounts of 15 minutes prior to cQDs (f) or CNP (H) inhalation as baseline condition (NPs inhalation starting at 0 min, red arrow, Means ± SEM, n=3-6 mice/group, Two-way ANOVA test). (e) and (f): Green ⋆ anti-LFA-1 + cQDs vs anti-IgG 2a + cQDs, blue * cQDs vs anti-IgG 2a + cQDs. (g) and (h) Green ⋆ anti-LFA-1 + CNP vs anti-IgG 2a + CNP, blue * CNP vs anti-IgG 2a + CNP.

Next, we tested whether LFA-1 blocking impaired AM crawling was important for the capture of inhaled QDs by AMs. Pre-treatment with anti-LFA-1 mAb

induced a significant reduction in cQDs internalization in AMs at 60min as compared to isotype mAb-treated mice (4.54%±0.71% vs 7.95%±0.82%, p>0.05) (Figure 35a). Besides, we found that 3h pre-treatment with anti-LFA-1 mAb did not inhibit MHS phagocytosis in vitro (Figure 35b), by using pHrodo E.coli particles to analyze MHS phagocytosis capability (Zhong et al., 2021). Taken together, this data suggests, that the decreased efficiency of AMs to take up NPs upon blocking of LFA-1 is due to the effect on AMs motility rather than on AMs phagocytosis.

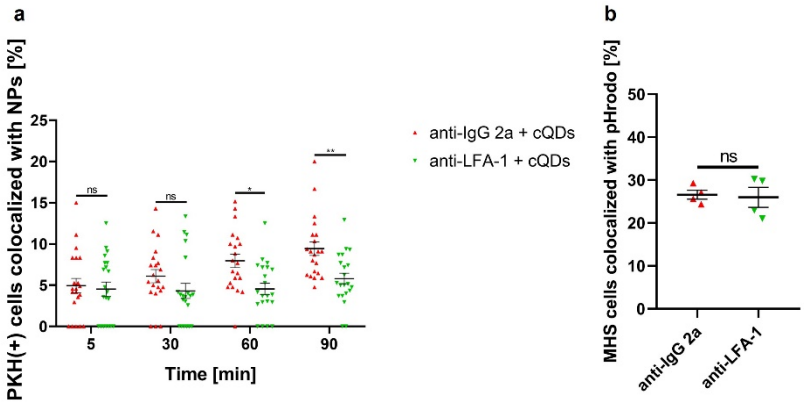

Figure 35 LFA-1 blockade reduced the NP clearance capacity of AMs but not the NP phagocytosis capacity. (a) Quantification of QDs uptake by AMs in mice pretreated via oropharyngeal application of anti-LFA-1 mAb or isotype mAb 3h before cQDs inhalation (NPs inhalation starting at 0 min, Means ± SEM, n=3 mice/group, Two-way ANOVA test). (b) Macrophage phagocytosis capacity was analyzed using pHrodo E. coli by flow cytometry of MHS cells treated with anti-LFA-1 mAb or isotype mAb control 3h prior to pHrodo E. coli (5μg/ml) application in vitro (Means ± SEM, n=4, paired Student's t-test).

In order to explore whether diminished neutrophil recruitment is caused by the penetration of antibodies across the epithelial barrier and the subsequent direct action on neutrophils (Vicente-Manzanares & Sánchez-Madrid, 2004), we administered the LFA-1-blocking antibody directly into the circulatory system at a concentration which blocked TNF-α-induced neutrophil recruitment in skeletal muscle tissue (Dunne et al., 2002) to test whether cQD-evoked neutrophilic

inflammation was directly regulated by neutrophil expressed LFA-1. Intravenous application of anti-LFA-1 blocking mAb in mice receiving cQDs by inhalation, did not alter the number of recruited neutrophils in the lungs, compared to WT mice receiving cQDs only (60 min: 4.71±0.76/10^4µm^2 vs 5.39±0.49/10^4µm^2, p=0.57) (Figure 36a, b). This indicates that LFA-1 mAb applied to the lung, did not cross the epithelial barrier and therefore did not directly affect neutrophil's response in the circulation upon NP inhalation. These results clearly support the view, that blocking LFA-1 in AMs results in the inhibition of cQD and CNP-induced neutrophil recruitment.

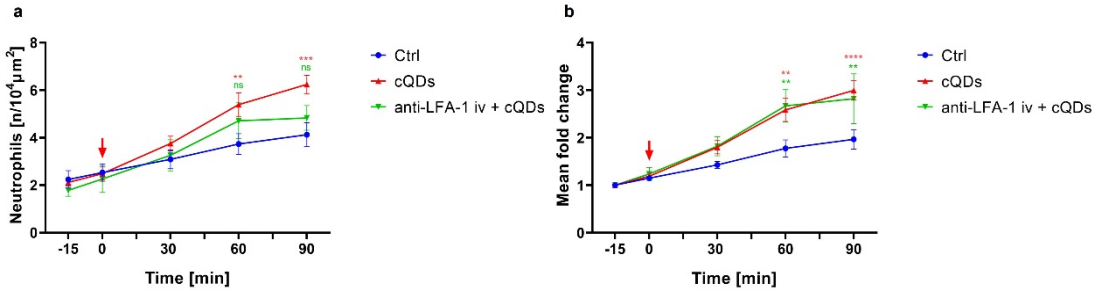

Figure 36 Blocking of intravascular LFA-1 has no effect on cQDs-evoked recruitment of neutrophils. (a) Alterations in the amounts of neutrophils over the time of 90 min were analyzed in mice receiving LFA-1 blocking antibody via intravenous injection 30 min prior to inhalation of cQDs or vehicle-control. (NPs inhalation starting at 0 min, Means ± SEM, n=3 mice/group, Two-way ANOVA test). (b) Results are presented as mean fold change from neutrophil amounts of 15 minutes prior to NP inhalation as the baseline condition. (NPs inhalation starting at 0 min, red arrow, Means ± SEM, n=3-6 mice/group, Two-way ANOVA test). Red * cQDs vs vehicle-control, green * anti-LFA-1 iv + cQDs vs vehicle-control.

3.5.6 Blocking of epithelial ICAM-1 disables AM patrolling and clearance of deposited NPs in the alveoli

As the ligand for LFA-1, ICAM-1 is highly expressed in the murine alveolar epithelium. Besides, it is implicated in leukocyte migration into the lung (Chong et al., 2021). We administered 30µg anti-ICAM-1 antibody into the airway of WT mice, 3h later followed by inhalation of cQDs. Blocking of ICAM-1 caused a

notable decrease of PKH-AMs migration in the alveolar cavity (0.31±0.02μm/min vs 0.46±0.03μm/min, $p<0.01$) (Figure 37a). Compared with isotype-treated mice ($4.89±1.20/10^4μm^2$), low numbers of neutrophils were found in the lungs 60 min after cQDs inhalation ($2.74±0.36/10^4μm^2$) (Figure 37e-f). To examine the impact of CNP, we administered Printex 90 directly into the lungs via inhalation of anesthetized mice 3h after treatment with ICAM-1 blocking mAbs. Lack of ICAM-1 significantly affected the AM crawling in the alveoli (0.42±0.04μm/min vs 0.64±0.04μm/min, $p<0.001$), suggesting AMs crawling occurred dependent on expression of ICAM-1 on lung epithelial cells or AMs (Figure 37c). At 60 min after CNP inhalation, ICAM-1 blocking resulted in a significant decrease in lung localized neutrophils compared to anti-IgG 2b isotype-treated mice ($2.33±0.21/10^4μm^2$ vs $4.41±0.37/10^4μm^2$, $p<0.0001$) (Figure37g-h). In ICAM-1 mAbs-treated mice, binding of AMs to epithelial cells weakened, since more AMs were lavaged from the lungs of 2h cQDs-exposed mice ($66.48±10.4 *10^4$ vs $19.47±8.91*10^4$, $p<0.05$) (Figure 37b) and 2h CN-exposed mice (44.14±7.69 *104 vs $33.19±8.74 *10^4$) (Figure 37d) than isotype mAbs-treated mice.

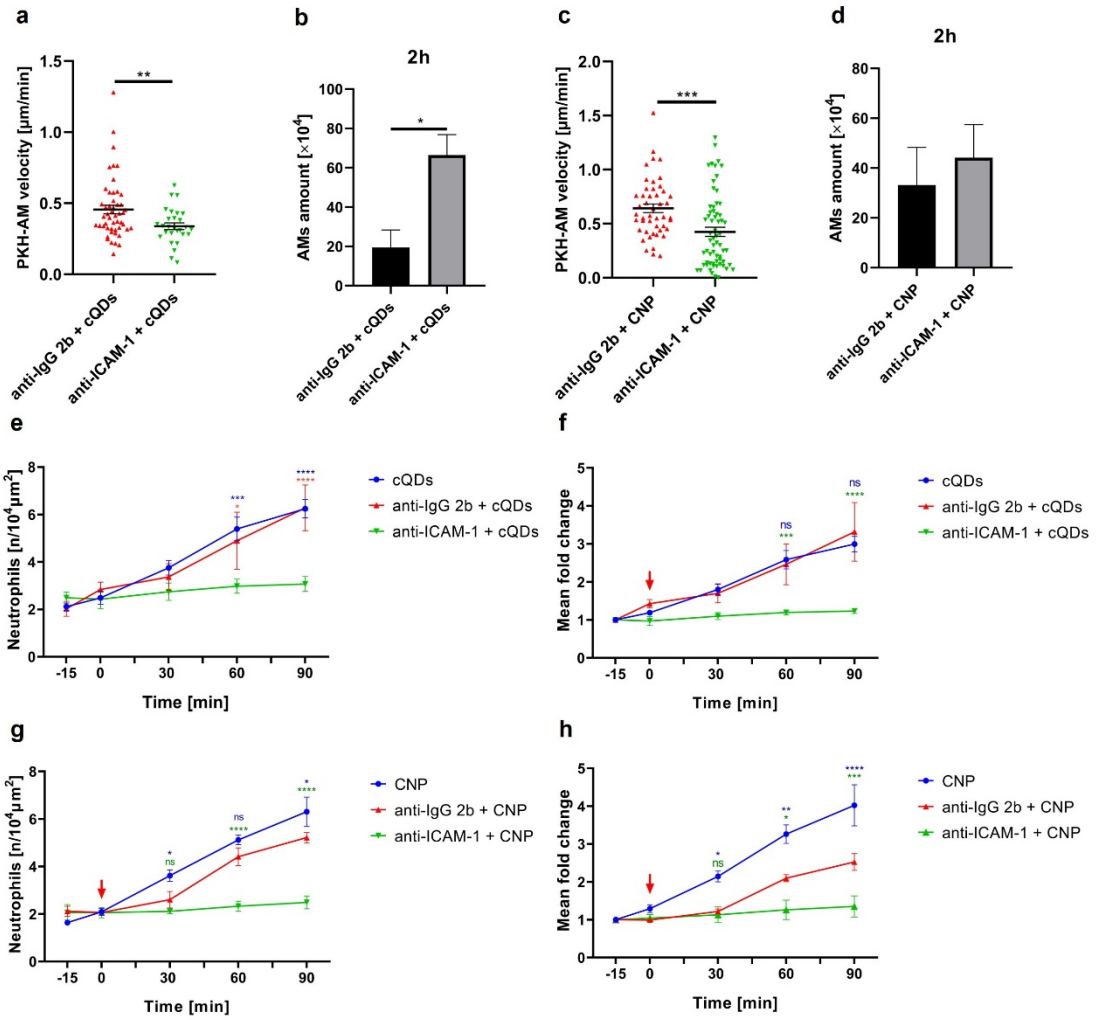

Figure 37 NPs-evoked neutrophil recruitment is mediated by ICAM-1 in the lungs. (a) Average track velocity (µm/min) of AMs in isotype or ICAM-1-blocking mAb-treated mice followed by cQDs inhalation during a 1h L-IVM imaging session (Means ± SEM, n=3-6 mice/group, paired Student's t-test). (b) Quantification of AMs in BAL fluid of mice treated with anti-ICAM-1 mAbs or isotype mAbs prior to inhalation of cQDs (2h). n = 3/group. (c) Average track velocity (µm/min) of AMs in isotype or ICAM-1-blocking mAb-treated mice followed by CNP inhalation during a 1h L-IVM imaging session (Means ± SEM, n=3-6 mice/group, paired Student's t-test). (d) Quantification of AMs in BAL fluid of mice treated with anti-ICAM-1 mAbs or isotype mAbs prior to inhalation of CNPs (2h) (Means ± SEM, n=3-6 mice/group, paired Student's t-test). € and (g) Alterations in the amounts of neutrophils over time of 90 min were analyzed in mice receiving anti-ICAM-1 mAb or isotype mAb prior to inhalation of cQ€(e) or CNP (g). (NPs inhalation starting at 0 min, red arrow, Means ± SEM, n=4-6 mice/group, Two-way ANOVA test). (f) and (h) Data are presented as mean fold change from neutrophil amounts of 15 minutes prior to cQDs (f) or CNP (h) inhalation from baseline condition (NPs inhalation starting at 0 min, red arrow, Means ± SEM, n=3-6 mice/group, Two-way ANOVA t€). (e) and (f): Green * anti-ICAM-1 + cQDs vs anti-IgG 2b + cQDs, blue * cQDs vs anti-IgG 2b + cQDs. (g) and (h) Green * anti-ICAM-1 + CNP vs anti-IgG 2b + CNP, blue * CNP vs anti-IgG 2b + CNP.

To investigate whether attenuated AM patrolling due to ICAM-1 blockade has effects on the clearance of deposited NPs by AMs, the anti-ICAM-1 and isotype-mAbs treated mice were observed with L-IVM after QDs aerosol inhalation.

ICAM-1 mAb treatment impaired the ability of AMs to collect NPs in the alveolar cavity, as compared to the isotype-treated control group (60min: 3.97±0.68% vs 10.34±1.1%, p<0.0001) (Figure 38a). However, in in-vitro experiment, MHS cells incubated with ICAM-1 mAbs (3h) displayed no significant difference in pHrodo phagocytosis at 60min compared with isotype-treated MHS cells (Figure 38b). This indirectly supports that AMs use ICAM-1 to migrate on the alveolar epithelium to clear NPs deposited in the alveoli without directly affecting the phagocytic ability of AMs.

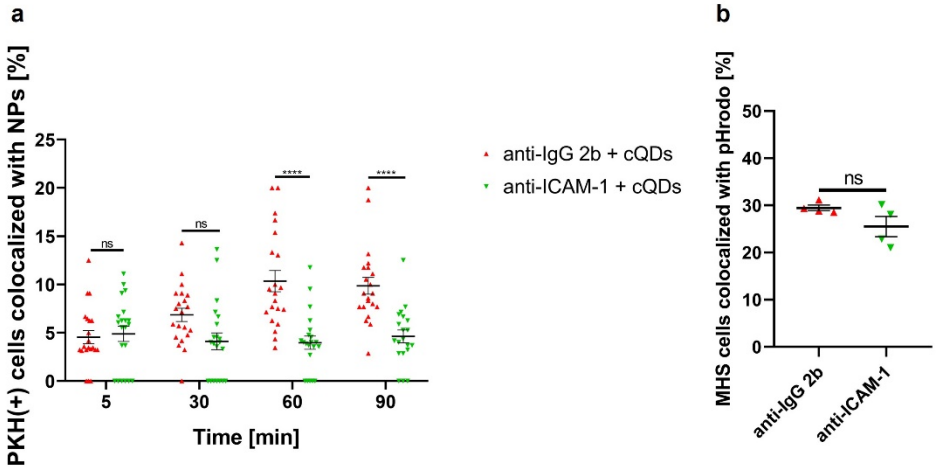

Figure 38 ICAM-1 blockade reduced the NP clearance capacity of AMs but not their NP phagocytosis capacity. (a) Quantification of QD uptake by AMs in vivo pretreated by oropharyngeal application with anti-ICAM-1 mAb or isotype mAb 3h after followed by cQDs inhalation (NP inhalation starting at 0 min, Means ± SEM, n=3 mice/group, Two-way ANOVA test). (b) AM phagocytosis was analyzed using pHrodo E. coli by flow cytometry of MHS cell treated with anti-ICAM-1 mAb or isotype mAb control 3h prior to pHrodo E. coli (5μg/ml) application for 1h in vitro (Means ± SEM, n=4, paired Student's t-test).

Similar to the LFA-1 blocking antibody, the anti-ICAM-1 antibody was applied to the blood circulation to verify if the effect on neutrophil recruitment could be due to antibody infiltration into the blood vessels. Since NP-induced neutrophil recruitment was even promoted after application(iv.) of anti-ICAM-1 mAbs (60min: 6.91/10^4μm^2 ±0.52 vs 5.39±0.49/10^4μm^2, p<0.05) (Figure 39a, b), the

data indicated that only blocking ICAM-1 of AMs results in impaired cQDs-induced neutrophil recruitment.

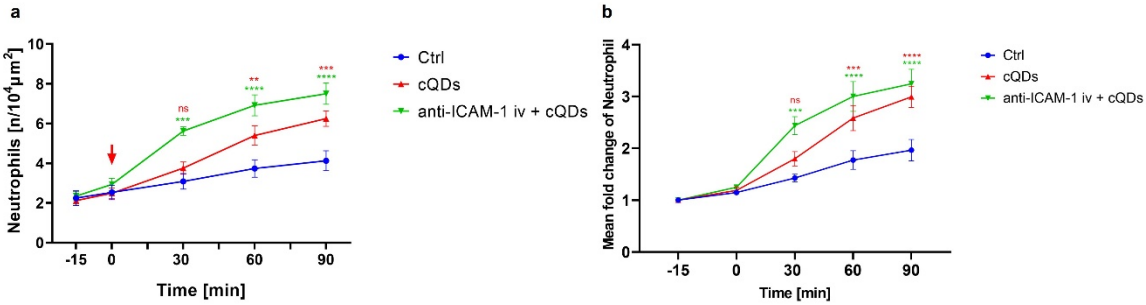

Figure 39 Blocking of intravascular ICAM-1 has no effect on cQDs-evoked recruitment of neutrophils. (a) Alterations in the amounts of neutrophils over time under L-IVM were measured in mice receiving ICAM-1 blocking antibody via intravenous injection 30 min prior to inhalation of cQDs. (NPs inhalation starting at 0 min, Means ± SEM, n=3 mice/group, Two-way ANOVA test). (b) Results are presented as mean fold change from neutrophil amounts of 15 minutes prior to NP inhalation as the baseline condition. (NPs inhalation starting at 0 min, red arrow, Means ± SEM, n=3-6 mice/group, Two-way ANOVA test). Red * cQDs vs vehicle-control, green * anti-ICAM-1 iv + cQDs vs vehicle-control.

In this regard, H. Zhong et al. found that inhibition of ROS production by using NAC suppressed the LPS-induced ICAM-1 expression and phagocytic ability of bone marrow-derived macrophages in vitro (Zhong et al., 2021). To investigate the effect of ROS generation on AMs and its effect on NP-induced neutrophil recruitment, we applied 30µg NAC into the lung of WT mice (3h), then followed by inhalation of cQDs. In the lungs of NAC-pretreated mice, the number of neutrophils decreased to the level of control mice (60min: 4.35±0.82/10^4µm^2 vs 3.74±0.44/10^4µm^2) (Figure 40a). In in vitro experiments, MHS cells incubated with NAC (3h) pHrodo phagocytosis at 60min compared with the control group were decreased (Figure 40b).

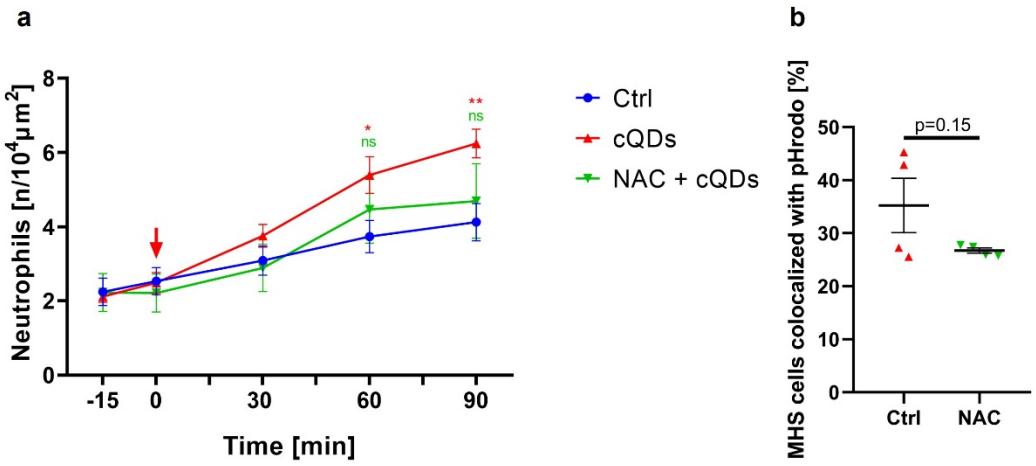

Figure 40 Inhibition of ROS generation reduced the cQD-induced rapid neutrophil recruitment but did not affect the phagocytic capacity of AMs. (a) Alterations in the amounts of neutrophils over time under L-IVM were compared between the mice receiving NAC-pretreatment prior to inhalation of cQDs or vehicle-control. (NPs inhalation starting at 0 min, Means ± SEM, n=3 mice/group, Two-way ANOVA test). Red * cQDs vs vehicle-control, green * NAC + cQDs vs vehicle-control. (b) AMs phagocytosis was analyzed using pHrodo E. coli by flow cytometry of MHS cell treated with NAC or control 3h prior to pHrodo E. coli (5µg/ml) application for 1h in vitro (Means ± SEM, n=4, paired Student's t-test).

To investigate the long-term effect (24 hours) of LFA-1/ICAM-1 blockade of AMs on NP-induced neutrophil recruitment we applied anti-LFA-1 / anti-ICAM-1 mAbs followed by cQDs inhalation exposure 0.5 hours later. After 24h, BAL analysis revealed that LFA-1 blockade of AMs seems to have a tendency to induce neutrophil infiltration into the alveoli, and ICAM-1 blockade of AMs also seems to increase neutrophil infiltration into the airways (Figure 41).

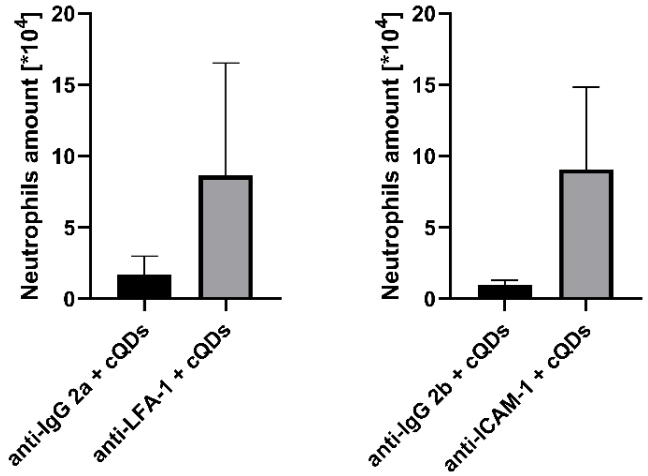

Figure 41 24-hour blocking effect of LFA-1/ICAM-1 on NP-induced neutrophil recruitment. The numbers of BAL neutrophils were determined with May Grunwald-stained BAL cells (Cytospin) of mice pretreated with anti-LFA-1 mAbs prior to inhalation of cQDs for 24h. The numbers of BAL neutrophils were determined with May Grunwald-stained BAL cells (Cytospin) of mice pretreated with anti-ICAM-1 mAbs prior to inhalation of cQDs for 24h (parametric data used paired Student's t-test and nonparametric data used Mann-Whitney rank-sum test, n=3 mice/group).

3.5.7 C5aR1 is involved in mediating NP-induced neutrophil recruitment

C5aR1(CD88) is highly expressed on AMs and AMs are stimulated by rapidly produced C5a to chemotaxis and uptake of bacteria (Neupane et al., 2020) (Figure 42a). Many studies showed that C5a is closely related to basophil or mast cell degranulation during basophilia granulocyte anaphylaxis (CBA) or skin inflammation (Golden et al., 1986; Golden et al., 1987; Swerlick et al., 1988, 1989). To assess if the C5a-C5aR1 axis was vital in neutrophil recruitment after NP inhalation, we applied C5aR1-blocking (CD88) mAbs by oropharyngeal aspiration, followed by cQD and CNP aerosol inhalation. Only baseline levels of AMs cQD uptake were detected in the intravital images of anti-C5ar1-treated mice as compared to isotype Ab-pretreated mice (60min: 4.03±0.64% vs 10.34±1.1%, $p<0.0001$) (Figure 42f). Interestingly, anti-C5ar1 mAb treatment had no effect on the patrolling status of AMs upon cQDs exposure (Figure 42d). Anti-C5ar1 treatment resulted in blocking neutrophil accumulation 60 min after cQD inhalation (60min: $2.28\pm0.21/10^4\mu m^2$ vs $4.41\pm0.37/10^4\mu m^2$, $p<0.01$) (Figure 42b), as well as after CNP-inhalation ($2.85\pm0.29/10^4\mu m^2$ vs $4.41\pm0.37/10^4\mu m^2$, $p<0.01$) (Figure 42c). In vitro, after AM-like MHS cells were incubated for 3h with anti-C5aR1 mAbs, pHrodo E-coli particle phagocytosis was decreased at 60min (24.24±1.04% vs

29.45±0.59%, p<0.01) (Figure 42e). These results suggest that blocking C5aR prevents NP-induced neutrophil recruitment due to a reduced phagocytic ability of AM without altering AMs patrolling behavior.

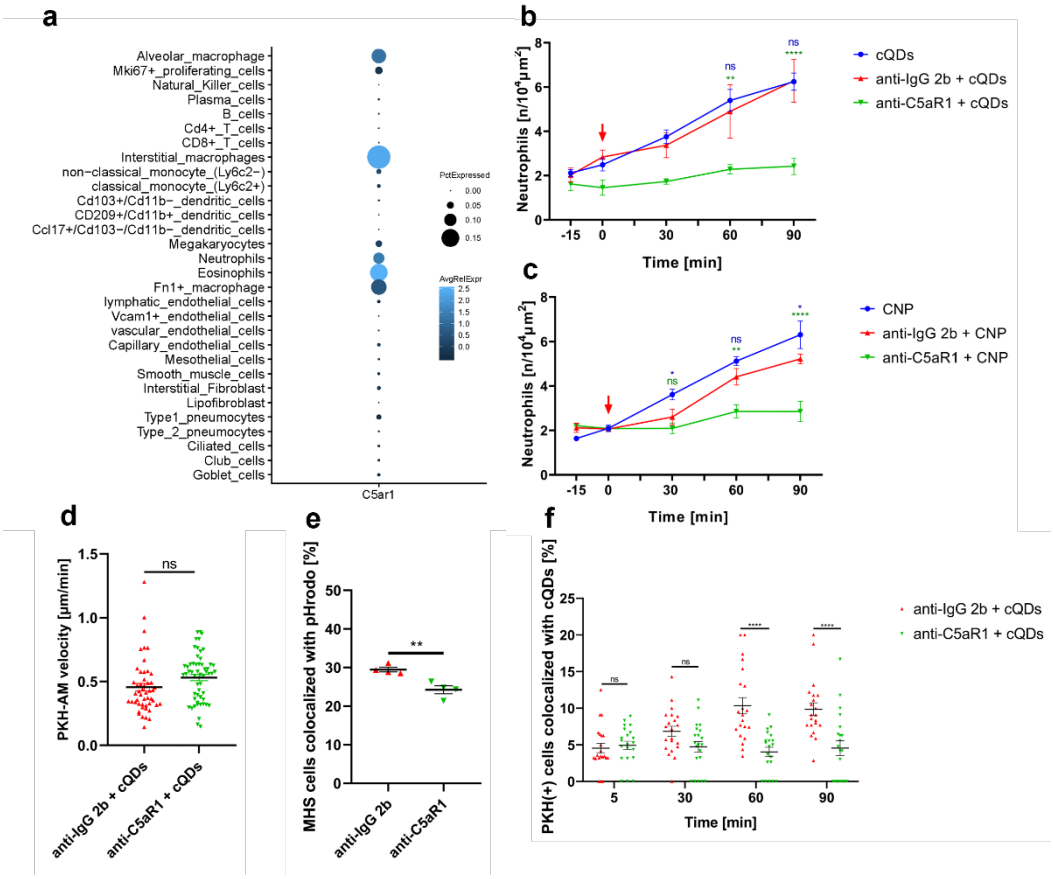

Figure 42 NPs-induced neutrophil recruitment is mediated by C5aR. (a) Healthy mice lung cell atlas. C5ar1 is highly expressed on the surface of alveolar macrophages and interstitial macrophages, from Schiller & Theis lab Atlas data (Sharma & Sharma, 2007). (b) and (c) Alterations in the amounts of neutrophils over time under L-IVM were compared between mice treated with anti-C5ar1 (anti-CD88) mAbs or isotype Abs before inhalation of cQDs (b) or CNP (c) and vehicle-control. (NPs inhalation starting at 0 min, Means ± SEM, n=3-4 mice/group, Two-way ANOVA test). (NPs inhalation starting at 0 min, Means ± SEM, n=3 mice/group, Two-way ANOVA test). (b): Green * anti-C5aR1 + cQDs vs anti-IgG 2b + cQDs, blue * cQDs vs anti-IgG 2b + cQDs. (c) Green * anti-C5aR1 + CNP vs anti-IgG 2b + CNP, blue * CNP vs anti-IgG 2b + CNP. (d) Average track velocity (µm/min) of AMs in isotype or C5aR1-blocking mAbs-treated mice followed by cQDs inhalation exposure during a 1h L-IVM imaging session (Means ± SEM, n=3-4 mice/group, paired Student's t-test). (e) Macrophage phagocytosis was analyzed using pHrodo E. coli by flow cytometry of MHS cells treated with C5aR1- blocking mAbs or isotype control mAbs 3h prior to phHodo. E. coli (5µg/ml) application for 1h. (Means ± SEM, n=3 mice/group, one-way ANOVA test). (f) Quantification of QD uptake by AMs in mice pretreated by oropharyngeal application with anti C5aR1 mAbs or isotype mAbs 3h prior to cQDs inhalation (NPs inhalation starting at 0 min, Means ± SEM, n=3 mice/group, two-way ANOVA test).

3.5.8 Anti-CD44 mAbs failed to impair cQD-induced neutrophil recruitment

Like integrins, selectins and calmodulin, CD44 is also a member of the cell adhesion molecule family (CAM)(Nascimento et al., 2016). The CD44 is a transmembrane adhesion molecule participating in hyaluronan binding and metabolism and performs an important function in inflammatory and immune responses, assisting in the uptake and elimination of granules and apoptotic cells by phagocytes (macrophages, monocytes, etc.) (Vachon et al., 2006). CD44-targeted therapy has been shown to benefit a variety of autoimmune and inflammatory disease treatments, like antibody-induced arthritis and autoimmune diabetes (Amash et al., 2016). Therefore, we investigated whether also anti-CD44 was involved in mediating NP-induced neutrophil recruitment. We applied CD44-blocking mAbs or isotype mAbs into the airway of WT mice 3h prior to cQDs inhalation. 90min after cQDs application in the CD44-treated group, there was no difference in the proportion of particles internalizing AMs compared to isotype mAbs applied mice (90min: 11.49±1.26% vs 9.86±0.87%, p=0.63) (Figure 43c). Similarly, CD44-blockade did not affect the NPs-induced neutrophil recruitment (90min: 5.13±0.90 /10^4μm^2 vs 6.28±0.96 /10^4μm^2, P=0.37) and AMs crawling in alveoli (0.42±0.03μm/min vs 0.46±0.03μm/min, p=0.42) (Figure 43a-b). In all, a CD44-blockade failed to impair cQD-induced neutrophil recruitment, AM crawling and AM phagocytosis of NPs in vivo.

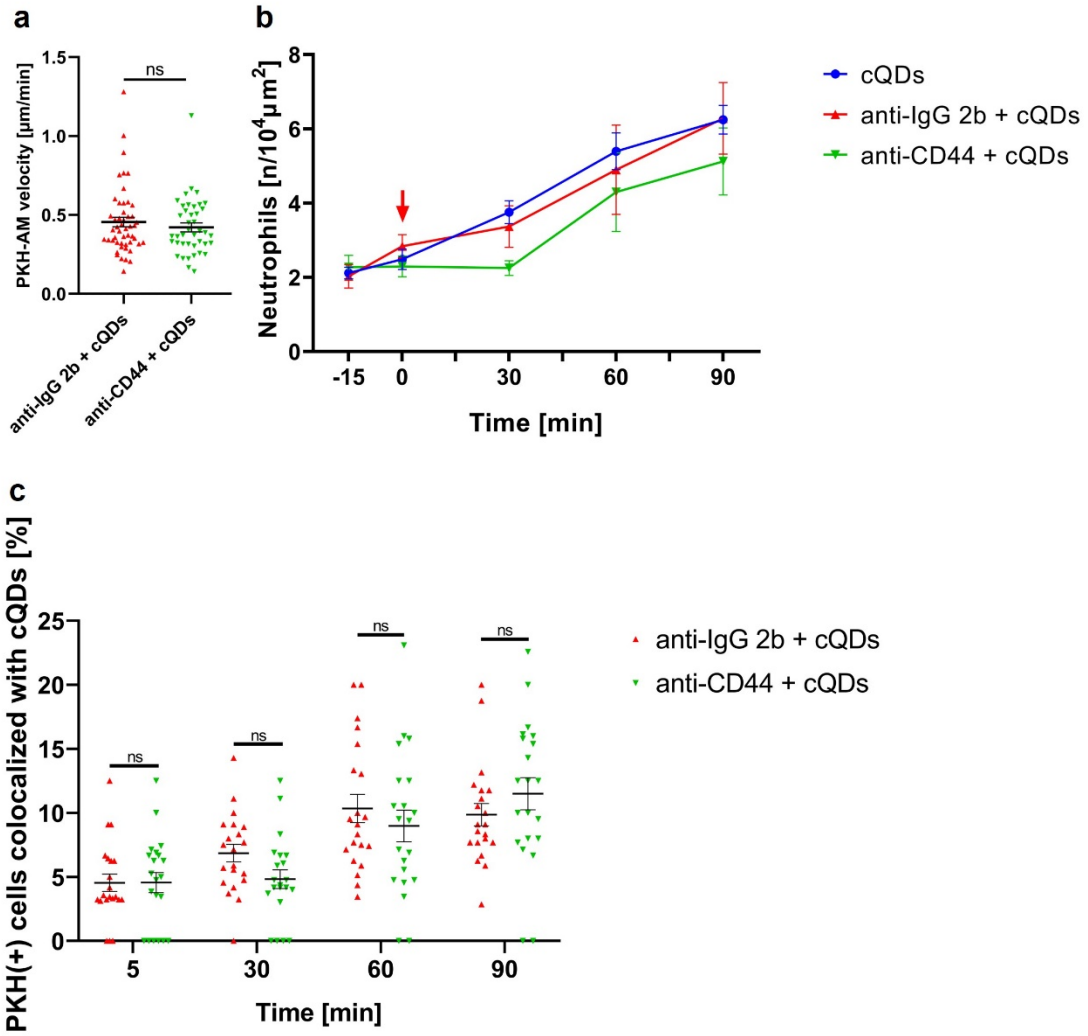

Figure 43 cQDs-induced neutrophil recruitment is not mediated by CD44. (a) Average track velocity (µm/min) of AMs in isotype or anti- CD44 mAbs-treated mice followed by cQDs inhalation exposure during a 1h L-IVM imaging session (Means ± SEM, n=3-4 mice/group, paired Student's t-test). (b) Alterations in the amounts of neutrophils over time under L-IVM were compared between isotype- and anti- CD44 mAbs-treated mice prior to inhalation of cQDs or vehicle-control. (NPs inhalation starting at 0 min, Means ± SEM, n=3-4 mice/group, Two-way ANOVA test). (c) Quantification of QDs uptake by AMs in isotype- and anti-CD44 mAbs-pretreated mice after cQDs inhalation. (NPs inhalation starting at 0 min, Means ± SEM, n=3 mice/group, Two-way ANOVA test).

3.5.9 FcγR I activation of AMs initiates rapidly neutrophil recruitment upon NPs exposure

Like F4/80 or the protein tyrosine kinase MER (MERTK), FcγR I is specifically expressed on the surface of mouse macrophages (Guilliams et al., 2014). Based on earlier studies in primary murine macrophages, FcγR knock-out

mouse models, and human monocyte-derived macrophages, FcγR-mediated phagocytosis was more efficient at inducing inflammation than CR-mediated phagocytosis (Acharya et al., 2019; Aderem et al., 1985; Wright & Silverstein, 1982). The immunotherapeutic drugs targeting FcγR I (CD64) show prominent medical potential in addressing chronic inflammation induced by M1-type dysregulated macrophages (Akinrinmade et al., 2017). FcγR is closely involved in the degranulation of many kinds of inflammatory cells, such as NK cells and mast cells (Elias et al., 2021; Fitzpatrick et al., 2020; Nimmerjahn & Ravetch, 2008; Paranjape et al., 2020; Syenina et al., 2015). To determine FcγR I function on NP-induced neutrophil recruitment, we blocked FcγR I with anti-CD64 mAbs administered into the lungs 3h before NPs inhalation. 60 minutes after cQDs inhalation ($2.39\pm0.34/10^4\mu m^2$ vs $4.89\pm1.20/10^4\mu m^2$, $P<0.01$) as well as after CNP exposure, fewer neutrophils accumulated in the lungs in the anti-CD64 treated groups than in the isotype control group ($2.54\pm0.59/10^4\mu m^2$ vs $4.41\pm0.37/10^4\mu m^2$, $P<0.01$) (Figure 44a, b). After anti-FcγR I mAbs treatment, the NPs phagocytosis of AMs was greatly reduced compared to isotype mAbs treated mice (60 min: 4.68±0.88% vs 10.34±1.1%, $p<0.0001$) (Figure 44e), while it had no effect on the patrolling movement of AMs in vivo (0.43±0.03 μm/min vs 0.46±0.03 μm/min, $p=0.63$) (Figure 44c). Flow cytometry result of pHrodo E. coli phagocytosis by MHS cells indicated, that CD64 mAbs blocking attenuated MHS cell phagocytosis in comparison to the isotype treated group (24.68±0.6% vs 29.45±0.59%, $p<0.001$) (Figure

44d). Taken together, these results indicate that FcγR I mediates NP-induced neutrophil recruitment through macrophage phagocytic ability rather than AMs crawling. In addition, FcγR I might also affect AM degranulation in vivo.

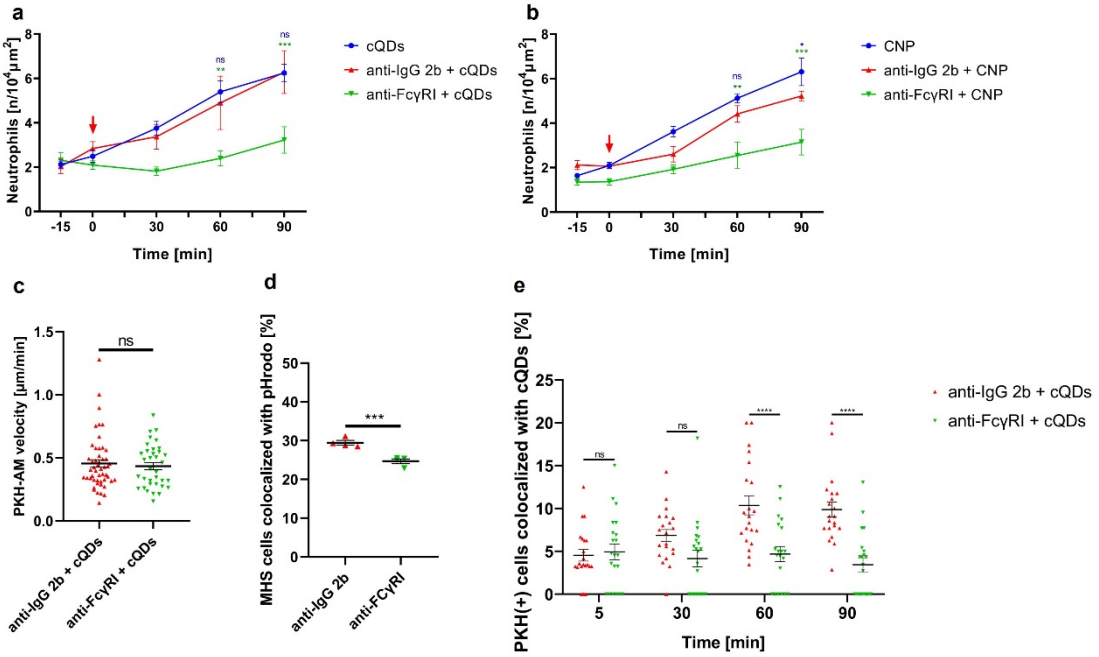

Figure 44 cQDs-induced neutrophil recruitment is mediated via FcγR I. (a) and (b) Alterations in the amounts of neutrophils over time under L-IVM were compared between the mice treated with anti-FcγRI-mAbs or isotype mAbs before cQDs(a) or CNP (b) inhalation or vehicle-control (NPs inhalation starting at 0 min, Means ± SEM, n=3-4 mice/group, Two-way ANOVA test). (a): Green ⁎ anti-FcγRI + cQDs vs anti-IgG 2b + cQDs, Blue ⁎ cQDs vs anti-IgG 2b + cQDs. (b) Green ⁎ anti-FcγRI + CNP vs anti-IgG 2b + CNP, Blue ⁎ CNP vs anti-IgG 2b + CNP. (C) Average track velocity (µm/min) of AMs in isotype or anti-FcγRI mAbs -treated mice followed by cQDs inhalation exposure during a 1h L-IVM imaging session (Means ± SEM, n=3-4 mice/group, paired Student's t-test). (d) Macrophage phagocytosis was analyzed using pHrodo E. coli by flow cytometry of MHS cell treated with anti-FcγRI mAbs or isotype mAbs control 3h before pHrodo E. coli (5µg/ml) application (1h). (Means ± SEM, n=3 mice/group, one-way ANOVA test). (e) Quantification of QD uptake by AMs in mice pretreated by oropharyngeal application of anti-FcγRI mAbs or isotype mAbs 3h before cQD inhalation (NP inhalation starting at 0 min, Means ± SEM, n=3 mice/group, two-way ANOVA test).

4. Discussion

4.1 Real-time monitoring of NP-induced immune responses using L-IVM

NPs have several characteristics of microbial preparations, such as size and orderly molecular surface patterns, presenting different surface signals, which facilitate or prevent clearance of phagocytes (such as macrophages, dendritic cells, etc.) and generate a complicated immune response (Liu et al., 2017). In real life, engineered NPs are widely used in industrial manufacturing, medical diagnosis and treatment (Gupta et al., 2014; Santos et al., 2019; Yohan & Chithrani, 2014). In addition, we are also exposed to a large number of naturally or accidentally formed NPs, such as motor fuel combustion, and weathering reaction products (Hochella et al., 2019; Kittelson, 2000). Numerous studies have shown that different inhaled NP exposures are indeed harmful to human health. Inhaled carbon nanomaterials or silica NPs can damage the tissues and cells in situ and induce pulmonary inflammation, granulomas, and fibrosis (Chou et al., 2008; Ganguly et al., 2017; Lam et al., 2004; Oberdörster et al., 2002; Warheit et al., 2007). Besides, inhaled metallic and non-metallic NPs were translocated into secondary organs, including the central nervous system and digestive system, leading to secondary damage (Oberdörster et al., 2004; Oberdörster et al., 2002; Semmler et al., 2004; Sharma & Sharma, 2007). In CNP-instilled mice, our group found that the level of neutrophils infiltrating into the alveoli peaked at 12-24 hours and returned to normal levels after 7 days of

exposure. Correspondingly, the neutrophil chemokines CXCL1, CXCL2, and CXCL5 reached their maximum values after 12h of exposure (Chen et al., 2016). However, the spatial-temporal events taking place in the early phase of NP induced neutrophil recruitment from the pulmonary microvasculature to the alveolar compartment remain largely elusive.

To visualize and measure in real-time the cellular pulmonary innate immune response simultaneously with NP dynamics, we applied in this thesis state-of-the-art intravital microscopy (IVM) on the alveolar region of the murine lung, in combination with ventilator-assisted inhalation of nebulized NP aerosols. This novel approach enabled the study of (sub-)cellular dynamic events, which were inaccessible up to now. Lung intravital microscopy has specific challenges (Headley et al., 2016; Rodriguez-Tirado et al., 2016), such as the restricted access to the lung. To solve this issue, microsurgery was performed to create an observation window in the animal's chest, allowing the lung tissue to be displayed directly under the microscope. To avoid imaging artifacts by the respiratory and cardiac motion which makes imaging of the non-stabilized lung extremely challenging, negative pressure suction was applied to stabilize or fix the observed lung tissue to the observation window.

The limited penetration depth is due to the repetitive refraction index mismatches between air and "water" and restricts the penetration depth to the first alveolar layer for widefield systems, which has been used in this thesis, as well as for advanced confocal and multiphoton systems. Future developments

in adaptive optical fluorescence microscopy might improve imaging depth.

Driven by developments in the Krummel lab, which resulted in a drastic improvement of the so far existing imaging windows, lung intravital imaging has now become the gold standard of cellular lung research in vivo (Headley et al., 2016; Rodriguez-Tirado et al., 2016). As far as we know, no previous research has applied L-IVM to directly investigate inhaled NPs-induced neutrophil recruitment in the murine lung.

4.2 Airborne NP exposure was simulated by ventilator-assisted NPs aerosol inhalation

Pulmonary nanoparticle exposure/nano-drug delivery is a relatively complex process, which aims to deliver environmentally relevant NPs or therapeutically relevant nano-drugs to the lungs. There are many delivery methods available: such as oropharyngeal aspiration, transtracheal inhalation, and transtracheal instillation (Ehrmann et al., 2020). The establishment of ventilator-assisted aerosol inhalation is difficult due to equipment requirements and experimental requirements, but it has great potential. The main advantages are acceptable dose efficiency, clinically realistic dose rate, acceptable exposure time, the realistic physiology inhalation process simulation, and homogeneous drug deposition throughout the lung (Ehrmann et al., 2020). In our exposure system, the ventilator-assisted nebulizer generated 3.5-4 μm aerosol droplets. Meanwhile, the NPs were uniformly distributed throughout the lung within a short time (1-2 min) with a stable delivery efficiency (around 0.5%).

Nanoparticle deposition on the lung surface was detected within several seconds with L-IVM. In short, mice were exposed to inhaled NPs reproducibly and efficiently by this exposure system.

4.3 Polyethylenglycolylation (PEGylation) modification inhibited NP-induced rapid recruitment of neutrophils.

Quantum-Dots (QDs, 15-20 nm diameter) have been selected as the fluorescent model NPs of this study because of their distinct optical properties such as high emission intensity, weak photobleaching, and narrow emission spectrum (Medintz et al., 2005; Nekolla et al., 2016; Rehberg et al., 2012). We selected commercially available QDs which are coated with a functional layer that consists of either PEG (PEG-QDs), PEG with an amine coating (aPEG-QDs), or carboxyl functions solely (cQDs) as model NPs. These NPs are widely used in biomedical imaging in vivo (Medintz et al., 2005). In addition, they are also applied to study the effects of nanoparticle surface modification on cellular nanotoxicology or cellular uptake (Geys et al., 2008; Rehberg et al., 2010; Uhl et al., 2018; Zhang et al., 2011; Zhang & Monteiro-Riviere, 2009). For example, the Monteiro-Riviere lab used HEK cells and monocyte-differentiated dendritic cells to investigate the cellular uptake mechanism of surface modified QDs and found that cQDs were endocytosed by cells starting at 30min, whereas aPEG-QDs were not. Cellular endocytosis of cQDs is mediated by clathrin and scavenger receptors and regulated by F-actin and phospholipase C (Zhang et al., 2011; Zhang & Monteiro-Riviere, 2009). Moreover, our group reported that

cQDs can induce neutrophil recruitment in the blood vessels of the cremaster muscle, while PEG-QDs or aPEG-QDs application did not (Rehberg et al., 2010).

Similar to these results obtained in skeletal muscle tissue after i.v. application, we found that as early as 60 min after inhalation, cQDs, but neither aPEG-QDs nor PEG-QDs application, elicited an increase in neutrophil numbers as compared to the control group, n (deposited dose: 16 cm2/g). Furthermore, the same deposited dose 24h after cQD inhalation induced approximately 10% neutrophil ratio of BAL immune cells in accordance with predictions from a previous retrospective analysis (Schmid & Stoeger, 2016).

PEG is composed of repeating ethylene glycol units. When they are connected to a polypeptide or another molecule, the condition is named “PEGylation” (Harris & Chess, 2003). PEGylation is widely applied in pharmaceuticals and has a vital function in the stabilization of NPs (Gref et al., 1994; Suk et al., 2016). The nanoparticle surface is easily recognized by opsonin (complement compounds, immunoglobulins, etc.) in the blood, and the opsonin then accumulates on the nanoparticle surface. The NPs are then cleared with opsonin by the body's natural clearance mechanism (Cai & Chen, 2019; Monopoli et al., 2012). PEGylation forms a steric barrier to reduce opsonization of NPs (Lasic et al., 1991), and it can therefore reduce NP phagocytosis by the mononuclear phagocyte system (MPS) induced by aggregation of opsonin (Suk et al., 2016). The above-mentioned characteristics make

PEGylated NPs widely used in the therapy of different illnesses by the higher drug loading efficiency of anti-cancer drugs and RNA interference therapy improvement (Almeida et al., 2019; Chen et al., 2019; Mitchell et al., 2021; Pei et al., 2020). Besides, the COVID-19 messenger ribonucleic acid (mRNA) vaccine manufactured by Pfizer/BioN-Tech delivers mRNA, which is packaged with a PEGylated lipid nanoparticle (LNP) to improve the effectiveness of the vaccine (de Vrieze, 2021; Lee et al., 2021). Dong-Han Lee et al. revealed that Au-NPs remarkably decreased skin cell viability at 500-2000 μM concentration, while the toxicity of PEGylated-Au-NMs was correspondingly reduced at the same concentration (Lee et al., 2021). Additionally, previous research of the covalent attachment of PEG to proteins demonstrated that PEGylation reduced the immunogenicity of proteins (Suk et al., 2016).

An early study demonstrated that exposing healthy mice to high doses of CNP induces acute lung inflammation (André et al., 2006). Then our group found that after CNP instillation exposure for 3 hours, around 50% AMs had CNP load, and a small amount of PMN had infiltrated into the alveoli from blood, reaching a peak at 24 hours. Meanwhile, the levels of CXCL1, CXCL2, and TNF in the BAL fluid had increased compared to the control group (Chen et al., 2016). Comparing the toxicity of inhalation and intra-arterial infusion exposures of CNP, inhalation exposure caused significant acute pulmonary and systemic inflammation, whereas infusion did not (Ganguly et al., 2017). Similarly, McConnachie et al. demonstrated that 8-hour instillation exposure of tri-n-

octylphosphine oxide, polymaleic anhydride-alt-1-tetradecene (TOPO-PMAT) CdSe/ZnS QDs induced increased CXCL1 and TNFα release and the neutrophil influx into alveoli (McConnachie et al., 2013). In vitro, Vivian Lee exposed mouse lung epithelial cells and AMs to TOPO-PMAT CdSe/ZnS QDs, which induced the release of chemokines CXCL1, CXCL-2, IL-6, IL-12, and other inflammation-related cytokines (Lee et al., 2015). Importantly, comparable increases in neutrophil numbers and AM patrolling movement were also detected upon inhalation of carbon black NPs (CNP) as well as cQDs exposure in our study. From these results, QDs and CNPs seem to have similar immune response processes (including immune cells activation and inflammatory factors release) after exposure.

4.4 Neutrophils exhibited recruitment behavior in microvessels close to deposited cQD sites and the recruitment was not mediated by intravascular ICAM-1, LFA-1, and CXCL1.

The recruitment of neutrophils from the blood to the extravascular sites of sterile or infectious tissue damage is a hallmark of the early innate immune response (Lämmermann et al., 2013). After passing through the tissue and reaching the injury site of the skin, the neutrophils often exhibit swarming behavior, many of which interact in a homotypic manner (extremely coordinated chemotaxis) to form large clusters (Lämmermann et al., 2013). Moreover, these homotypic neutrophil interactions have been shown to help to limit the spread of infection (Poplimont et al., 2020). The persistent neutrophil swarming behavior in mice

takes about 30-60 minutes from the beginning to the stable stage, depending on the number of neutrophils involved (Lämmermann et al., 2013).

LPS (i.v.) application stimulated rapid crawling of neutrophils in the pulmonary microvessels, and this behavior was CD11b, TLR4 and Myd88 dependent. At the same time, this fast crawling was beneficial to clear bacteria from the bloodstream (Yipp et al., 2017). However, influenza virus infection reduced blood flow and decreased neutrophil movement within the lung microvessels (Ueki et al., 2018). Following cecal ligation and puncture (CLP)-induced sepsis, the pulmonary microvascular flow velocity in rats was reduced by 27% to 34% compared to healthy rats (Waisman et al., 2006).

With our inhalation approach, neutrophil accumulation was induced around 30min after NP inhalation and had a significant difference from the control group in 60min. Besides, comparing cQDs-enriched and cQDs-deficient regions, it was revealed that neutrophils preferentially resided in microvessels close to deposited cQD sites from 60 min after exposure, where they exhibited probing and crawling behavior. Previous study in our lab found that as early as 15 minutes after cQDs were injected (i.v.), leukocytes had recruitment-related behaviors, such as tightly adhering to the vascular lumen, crawling on the endothelium in skeletal (cremaster) muscle vessels. This neutrophil recruitment was dependent on intravascular ICAM-1 (Rehberg et al., 2010). Similarly, after 60 minutes we observed that more neutrophils were recruited into the airway compared to the control group, and these neutrophils aggregated near the

deposited NPs. Similarly, cigarette smoke exposure increased ICAM-1 expression in the lungs and the number of alveolar-localized neutrophils (Aggarwal et al., 2013; Balamayooran et al., 2012). However, in comparison to the situation in skeletal muscle intravascular, blockade of ICAM-1 did not inhibit neutrophil recruitment induced by nanoparticle inhalation. In addition, we also blocked LFA-1, the integrin corresponding to ICAM-1, and the neutrophil chemoattractant CXCL1 in blood circulation, which also failed to prevent the occurrence of neutrophil recruitment. This seems to indicate that the process of nanoparticle-induced neutrophil recruitment with different exposure routes are mediated by different pathways.

4.5 Following NP exposure, neutrophils were rapidly recruited into the alveoli and assisted in the clearance of NPs

Neutrophils are the main anti-pathogen immune cells in organisms. The core of their function is their ability to be recruited to the site of infection, to rapidly recognize and phagocytose microorganisms, and to attack and eliminate pathogens with a combination of cytotoxic mechanisms (Klebanoff et al., 2013; Mayadas et al., 2014; Nauseef & Borregaard, 2014). Catherine A. Fromen indicated that the phagocytic capability of neutrophils was related to the elimination of intravenous particles, and the neutrophils that have phagocyted the NPs were transferred to the liver (Fromen et al., 2017). The elimination of NPs in the blood is mainly completed by the mononuclear phagocytic system (Chrishtop et al., 2021; Poupot et al., 2018), but neutrophils also obviously

undertake a certain amount of removal of NPs. We found that a large number of NPs (cQDs) were internalized in localized neutrophils in alveoli by L-IVM and could be recovered in BAL. Therefore, alveolar localized neutrophils (15.35% ±6.63%) seem to contribute to the clearance of alveolar deposited NPs in the lungs. To our knowledge, no studies have reported that neutrophils can scavenge inhaled NPs, while most studies mainly revealed that neutrophils clear pathogens in lung microbe-infection models (Hashimoto et al., 2007; Neupane et al., 2020; Newton et al., 2016; Tsai et al., 2000). Neutrophils recognize microorganisms by binding to pattern recognition receptors (PRR) present on their surface (Kobayashi et al., 2018). In addition, soluble proteins, such as antibodies or complements, can opsonize microorganisms, allowing neutrophils to effectively recognize and uptake or degranulate (Bardoel et al., 2014; Németh et al., 2020). When NPs particles are deposited in the alveoli, they seem to only have interaction with two types of epithelial cells: ATI and AT II cells (Chen et al., 2016) or AMs (Takenaka et al., 2012), which constitute or colonize the alveoli. It is ignored that the recruited cells, like neutrophils, lymphocytes, et al., infiltrate into the alveoli and interact with the NPs. This interaction may assist in nanoparticle clearance or further trigger the inflammatory cascade. But the molecular and functional details of nanoparticle internalization by neutrophils in the airway remain unclear and should be further characterized.

4.6 NP-induced accumulation of neutrophils in the pulmonary circulation reduces pulmonary blood flow velocity

Dan Waisman and his colleague observed in patients with influenza virus infection, that inflammation reduced the blood flow of subpleural microvessels and led to hypoxemia (Waisman et al., 2006). Hiroshi Ueki et al. revealed that from the second day after infection, the blood flow velocity of MA-Venus-H5N1 infected mice was reduced, compared with control mice, which stayed at the same low level as the infection progressed (Ueki et al., 2018). Blood flow velocity is mainly affected by the diameter of the vessel (Feletou et al., 2008; Granger et al., 2010). In our study, cQDs and CNP inhalation induced neutrophil recruitment in the lung, leading to leukocyte stasis in the alveolar capillaries, which might result in or contribute to the decrease in blood perfusion velocity in the similar size vessel. In cromolyn or blocking antibodies pretreated mice, NPs-evoked neutrophil recruitment was prevented, and the blood flow velocity was also preserved at normal levels as in healthy mice, indicating that blood flow velocity decreasing in the microcirculation may be one of the hallmarks of nanoparticle-induced inflammation. Besides, intratracheal instillation of diesel exhaust particulates (DEP, 50 μg) in hamsters (24h) induced acute pulmonary inflammation, increased histamine release and promoted peripheral venous thrombosis. Pretreatment with cromolyn reduced BAL neutrophil and histamine release levels and inhibited platelet activation. We will further investigate the mechanism of inhaled nanomaterials and platelet activation/pulmonary micro

thrombosis (Nemmar et al., 2004).

4.7 cQDs-exposure, as well as CNP-exposure, stimulated AM patrolling in alveoli, whereas aPEG-QDs-exposure did not

AMs, as resident phagocytes in the alveoli, are essential for the elimination of pathogens via non-specific phagocytosis. Macrophages have a variety of surface receptors for the recognition and internalization of pathogenic agents (viruses, NPs, etc.) (Ishikawa et al., 2017; Taylor et al., 2005). Class A scavenger receptors such as SR-A1 and MARCO bind to silica and titanium NPs and stimulate macrophages to cause an inflammatory response (Arredouani et al., 2004; Thakur et al., 2009; Thakur et al., 2008). Besides, the class B scavenger receptor CD36 (Tsugita et al., 2017), expressed on the surface of AMs, also binds to silica particles and induces silica-induced chronic lung inflammation (Lagassé et al., 2016). Macrophages can also recognize particles through other cell surface receptors, such as mannose receptors (MRs), toll-like receptors (TLRs), Fc receptors, and complement receptors (CRs) (Aderem & Underhill, 1999; Lorenzo S, 2013).

Anti-F4/80 antibodies can specifically label Kupffer cells in vivo (Deppermann et al., 2020; Surewaard et al., 2016; Wong et al., 2013; Zeng et al., 2016). However, there are no previous research using fluorescent indicator antibodies to directly label the surface of AMs (such as CD11c, Siglec-F) in vivo. Besides, there are also no AM-specific reporter mice established. Recently, Neupane and colleagues achieved specific labeling of AMs by oropharyngeal aspiration

application of the dye PKH-26PCL (Merck KGaA, Darmstadt, Germany). With this approach more than 90% of PKH (+) cells were AMs (Neupane et al., 2020). We used the same method to visualize AMs and found that a single AM could maintain the environmental homeostasis of every 3 alveoli, which is also consistent with some previous studies (Neupane et al., 2020; Westphalen et al., 2014). Meanwhile, we also confirmed that more than 90% of PKH-labeled cells are cells with high Siglec-F expression by FACS analysis. AM motility has been demonstrated by this approach (Neupane et al., 2020), which contradicted the long-standing belief that AMs are sessile immune cells without any movement in the alveoli (Westphalen et al., 2014). In order to explain the mismatch between the number of AMs and the number of alveoli, it is necessary to rush pathogens or cell debris toward AMs with alveolar fluid flow assistance (Sakuma et al., 1993; Westphalen et al., 2014). Neupane et al. observed that AMs had a patrolling movement through channels (pores of Kohn) with a median velocity of around 0.8 μm/min. Besides, these AMs sensed, chemotaxis towards and efficiently phagocytosed inhaled bacterial pathogens, like Pseudomonas aeruginosa and Staphylococcus aureus (Neupane et al., 2020). In this regard, we observed the crawling movement of AMs to collect and carry deposited NPs on alveolar walls. We even observed the exchange of cQDs from one PKH-labeled AM to another. More intriguingly, cQDs-exposure, as well as CNP-exposure increased the migration velocity of AMs in the alveoli of the respective mice, as compared to the control group, whereas aPEG-QDs

exposure decreased AM crawling velocity. Viral infection (influenza) can reduce the crawling ability of AMs in the alveoli, and blockade of IFNγ restored the patrol crawling ability of AMs. At the same time, influenza infection led to the upregulation of alphaE:beta7 (CD103) expression of AMs, an integrin in mucosal tissues, immobilizing AMs on the alveolar surface (Neupane et al., 2020). Sinbad Sweeney et al. observed that AM migratory capacity was markedly reduced at 1 and 5 days after MWCNT (20μm) application in vitro, which was related to markedly increased expression of MARCO scavenger receptor and AMs activity (Sweeney et al., 2015). This seems to imply that the exposed nanoparticle shape affects patrolling movements. In addition, our in-vivo model with ventilator-assisted nanoparticle inhalation is closer to the real exposure situation compared to the in-vitro model. Finally, these NP-internalizing AMs stimulated neutrophils to gather within their surrounding capillaries comparing blank AMs. In contrast, alveolar epithelial cells that directly contacted or internalized NPs did not cause neutrophils to aggregate around them. In conclusion, AMs, but not alveolar epithelial cells, are the driver effector cells of nanoparticle-induced neutrophil recruitment.

4.8 Compared with aPEG-QDs, cQDs are more easily internalized and cleared by AMs

Klibanov et al. demonstrated that PEGylation can prolong the half-life in the blood circulation of systemically administered liposomes from <30 minutes to 5 hours (Klibanov et al., 1990). Because of the lack of PEGylation protection,

cQDs bound rapidly to proteins in the blood and were cleared by phagocytes due to opsonization (Rehberg et al., 2010). Interestingly, we co-incubated the immortalized alveolar macrophage (MHS) cell line with cQDs and aPEG-QDs for one hour, and we found that cQDs are more easily internalized by MHS cells than aPEG-QDs. We found that PEG packaging had a significant effect on the uptake of QDs by AMs, and this PEG packaging also determined whether it caused short-term recruitment of neutrophils after QDs exposure. This seems to imply that uptake by AMs is a prerequisite of cQDs-induced neutrophil recruitment. Most of the nanomaterial-mediated lung immune cell response in the alveoli, including the effects on cell uptake, cell viability, and inflammation induction, were performed by AMs (de Vrieze, 2021; Dong et al., 2015; Frank et al., 2015). Based on L-IVM imaging, we verified that cQDs-positive AMs were correlated with a higher number of neutrophils in their close vicinity, whereas cQD-negative AMs as well as “cell-free” cQDs had no local effect on neutrophil recruitment. This implied that the spatial/locally restricted recruitment of neutrophils in response to NPs was indeed mediated by AMs. The data further indicated that immune response can thereby be tuned at the individual alveolar level, thus ensuring rapid clearance of local insults and maintenance of tissue homeostasis, at low levels of NP challenge.

AMs and neutrophils, as the first immune cells to respond, have a close relationship in nanomaterial-induced “chronic” immune response. MWCNT (5 to 40 μg) administered through pharyngeal aspiration promoted rapid and

significant fibrosis formation close to particle deposition in the lungs. In parallel with the fibrosis, the obvious infiltration of neutrophils and macrophages and TGF-β1 and PDGF-A secretion significantly increased in the lungs (Dong et al., 2015). Jagjit S Yadav Lab indicated that AMs functioned as the major effector cells in CNT-triggered pulmonary inflammation through the MyD88 pathway. The depletion of AMs by treatment via orotracheal administration of liposomal clodronate decreased CNT-induced neutrophilic inflammation (Frank et al., 2015). AMs depletion (clodronate liposomes i.v.) prevented the inflammatory response which was induced by Residual Oil Fly Ash (ROFA) (1 mg/kg body weight), as PM surrogate, such as inflammatory cytokines (TNFα and IL-6) release, leukocyte recruitment (rolling and adhesion on vessel walls) in mesenteric venules (Marchini et al., 2016). Similarly, repeated exposure to dust extract (DE) resulted in a significant increase in CD11b+ / CD11c+ macrophages in the lung. Meanwhile, the phagocytic ability of macrophages was enhanced, and inflammatory factors release (IL-6, CXCL1, and CXCL2) increased. Macrophage depletion inhibited neutrophil infiltration and TNFα and IL-6 release during the first DE exposure (Poole et al., 2012). Similarly, our study also revealed that AMs are effector cells for nanoparticle-induced neutrophil recruitment. Restricting the patrolling ability of AMs abolished neutrophil recruitment at the early stage (1h) of NPs exposure but prolonging this restriction time (24h) instead promoted neutrophil recruitment induced by NPs exposure.

4.9 NP-induced enhanced macrophage patrolling and rapid neutrophil recruitment are mediated by ICAM-1/LFA-1

Regarding the elimination of inhaled NPs by AMs as a dynamic process, AM migration velocity should be an indeed critical factor in NPs elimination efficiency of AMs. The PEG shells contained in aPEG-QDs could reduce opsonin aggregation-induced phagocytosis of NPs by phagocytes (Suk et al., 2016), since more AMs were observed to take up cQDs in a short time, compared to aPEG-QDs exposure in our study. Besides, aPEG-QDs may directly bind to LFA-1/ICAM-1 to impair AMs patrol crawling, which requires further mechanistic studies. Similar to cQDs, CNP exposure also caused marked enhancement of alveolar macrophage migration. Compared with isotype-treated mice, the displacement ability of AMs in LFA-1/ICAM-1-blocking antibody-treated mice was impaired. It has recently been shown that the displacement ability of AMs in the lung is mediated by LFA-1 integrin on AMs, since blocking of the LFA-1 site has resulted in the loss of patrolling movement of AMs in the alveoli of healthy mice (Neupane et al., 2020). We investigated the LFA-1/ICAM-1 function of AMs in NPs-exposed lungs with L-IVM. Anti-LFA-1 and anti-ICAM-1 pre-treatment both alleviated the increase in AMs patrol speed caused by cQDs inhalation. Subsequently, the proportion of cQDs(+) AMs did not increase over time. Besides, we found that LFA-1 or ICAM-1 blockade did not affect the phagocytic ability of AMs in in-vitro experiments. In all, the effect of anti-LFA-1 and anti-ICAM-1 on the clearance of cQDs by AMs

was due to a reduction in the migration of AMs in the alveoli, rather than an alteration in the phagocytic capacity of AMs. In addition, the short-term (1h) recruitment of neutrophils caused by cQDs was completely eliminated in the lung of Anti-LFA-1 and anti-ICAM-1 pre-treatment mice. The long-term effects of LFA-1 and ICAM-1 blockade on NP-induced neutrophil recruitment for 24 hours appeared to be minimal, even pro-inflammatory. The blocking mAbs might be recognized as “foreign” by scavenger receptors and trigger neutrophil recruitment on a longer time scale. Because AMs patrolling in the alveoli was only recently proposed, there was no research on the function of LFA-1/ICAM-1 in AMs migration upon NP exposure in vivo. It is well documented that LFA-1 and ICAM-1 played a vital role in the activation and migration of other immune cells (such as T cells, leukocytes, platelets, etc.). LFA-1/ICAM-1 mediated adhesion was critical for the extravasation of naive and activated T cells into lymph nodes and tissues (Krummel et al., 2016; Park et al., 2010; Shimaoka et al., 2002; Shulman et al., 2009). In addition, the activation of LFA-1 and the expression of ICAM-1 were also necessary for effective T cell activation (Petruzzelli et al., 1998; Verma et al., 2016; Wabnitz et al., 2010).

4.10 The production of ROS stimulated the rapid recruitment of neutrophils induced by NPs.

On the one hand, the patrol speed of AMs seems to be a key factor of AM nanoparticle clearance efficiency. On the other hand, the phagocytic ability of AMs could constitute another important factor for AMs to clear deposited

nanomaterials. In addition to the fact that the blockade of ICAM-1/LFA-1 could affect the patrolling migration ability of AMs, it has been shown that ICAM-1 is directly involved in macrophage phagocytosis. ICAM-1 on macrophage regulating phagocytosis depended on the production of ROS mediated by TLR4 (Zhong et al., 2021). The production of ROS was involved in the degranulation of various immune cells, such as neutrophils (Alsaleh et al., 2019; George et al., 2021; Grimes et al., 2020; Tackenberg et al., 2020), mast cells (Soria-Castro et al., 2021; Żelechowska et al., 2021), and NK cells (Najar et al., 2018a, 2018b). In our study, inhibition of ROS with NAC decreased the neutrophils recruitment after cQDs exposure compared to the cQDs-inhalation group.

4.11 Alveolar surfactant protein coronas formed on the surface of cQDs increased phagocytosis by AMs

Surfactants are present on the alveolar surface and are mainly composed of lipids (90%; phospholipids and some neutral lipids such as cholesterol) and surfactant proteins (10%; SP-A, SP-B, SP-C, and SP-D) (Milad & Morissette, 2021). The main phospholipid component is phosphatidylcholine (PC) (Milad & Morissette, 2021). It is primarily a complex secreted by alveolar type II epithelial (ATII) cells. Its recycling and clearance are completed by the cooperation of ATII and AMs, and the clearance activity of AMs is also regulated by the granulocyte-monocyte colony-stimulating factor (GM-CSF) (Quintero & Wright, 2002). As already explained, PEGylation of NPs largely prevents protein binding to increase its half-life in circulation (Peracchia et al., 1999; Schipper et

al., 2009). In our earlier study, cQDs (i.v. injection) were easily taken up by perivascular macrophages. Due to PEGylation, QDs avoided protein binding and made them invisible to phagocytes (Rehberg et al., 2010). Without the protection of PEGylation, proteins preferred to aggregate around cQDs to form protein coronas, which increased the possibility of its uptake by phagocytes (Nekolla et al., 2016; Rehberg et al., 2010). From our results, the lack of PEGylation in cQDs was more likely to aggregate within alveolar surfactants.it may be that cQDs were more likely to bind surfactant components, and the PEG structure prevented this binding. AMs phagocytosed alveolar surfactants containing a large number of cQDs, and induced corresponding immune responses, such as neutrophil recruitment. Besides, this phagocytic process was mediated by C5ar1 of AMs. Further elucidation of how the NPs with “surfactant protein” corona was formed and how the NPs are phagocytosed by AMs needs to be clarified.

4.12 NP uptake triggers cellular degranulation and initiates neutrophil recruitment.

Various immune cells (NK cells, eosinophils, mast cells, etc.) have vesicles that can bind to the intracellular membrane and these vesicles store substances that are immediately available for host immune defense (Mok et al., 2021). These substances are products of the trans-Golgi network, mainly including cytokines (IFN-γ, TNF-α, GM-CSF, interleukin family, etc.) (Bernard et al., 2017; Legrand et al., 2010); oxidative agents (MPO, EPO) (Borelli et al., 2003) or cytolytic, cell

membrane pore-forming proteins (perforin, granulysin, defensins, LL-37, etc.) (Borregaard et al., 2007). Pathogens directly stimulate immune cells to degranulate to release antipathogenic compounds onto the pathogen directly. Alternatively, immune cells can bind to another host cell invaded by the pathogens (Mok et al., 2021). Previously, our group has demonstrated that preventing cellular degranulation with cromolyn completely eliminated the cQDs-evoked leukocyte recruitment in cremaster muscle vessels (Rehberg et al., 2010). Anne Dudeck revealed that the release of TNF from vascular-colonizing mast cells caused spatially restricted extravasation of neutrophils to the site of inflammation in inflamed skin (Dudeck et al., 2021). BesB. V. Lê et al. compared the levels of inflammation-related cytokines in BAL from LPS-treated mice with or without cromolyn pretreatment, and they found TNF-α and IL-1β levels and lung MPO activity significantly reduced in the cromolyn-pretreated mice group (Huber-Lang et al., 2002), which is in line with our own findings. Pneumology mast cells are predominantly located in the central airways rather than the small airways of mice (Fuchs et al., 2012). It has been shown that AMs and epithelial cells rapidly released MVs into the alveoli after LPS treatment, and these MVs carried large amounts of TNF which induced ICAM-1 and keratinocyte-derived cytokine (KC) expression on lung epithelial cells (4h) (Soni et al., 2016). In addition to acting as a mast cell stabilizer, cromolyn also affected AM-mediated immune responses. Sodium cromoglycate inhibited the generation of reactive oxygen species (ROS) by the activation of

guinea pig AMs and prevented ROS-induced lung damage in vitro (Sadeghi-Hashjin et al., 2002). Mechanistic studies revealed that sodium cromoglycate (0.5-4 mM) reversibly blocks superoxide anion production from primary AMs stimulation by formyl peptide and leukotriene B4, thereby modulating pulmonary inflammatory responses which may contribute to asthma (Holian et al., 1991). The protective effect of disodium cromoglycate (DSCG) on rabbit primary AMs in phagocytosis of fibrotic silica have been demonstrated. Lower acid phosphatase production and AMs death rate after silica application were measured in the DSCG treatment group compared to the control group (Vlcková et al., 1976). Meanwhile, in the silica-exposed lungs of rats, disodium cromoglycate application could prevent cell destruction and lung tissue fibrosis (Vlcková et al., 1976). We have verified that the pretreatment of mice exposed to NPs with sodium cromoglycate conferred similar protection. In our study, blocking cellular degranulation, which most likely affected immune cell degranulation, not only prevented the NPs (cQDs or CNP) induced neutrophil recruitment in a short time (60 min) as inhibition of ROS production did, but it also blocked neutrophil recruitment upon long-term NPs exposure (24h). This might provide a new direction for reducing the harm of nanoparticle exposure in the future.

Furthermore, our data demonstrated that AMs were effector cells for nanoparticle-induced neutrophil recruitment which was mediated through rapid TNFα release. Whether AMs drive the “long-term” inflammatory response after

nanoparticle exposure is controversial. Chen et al. revealed that AMs isolated from the lungs of mice after 3 to 12 hours upon CNP instillation exposure did not show any pro-inflammatory features at the genetic level (Chen et al., 2016). Conversely, van Eeden SF and his colleagues found that AM, but not alveolar epithelial cells, was the driver of lung pro-inflammatory response after inhalation of PM via IL-1β, IL-6, and TNF-α release, and that AMs could further induce systemic inflammation (Mukae et al., 2001; Terashima et al., 1997). Combining our results seems to imply that, following NPs exposure, AMs rapidly degranulated and released TNFα stored in micro vesicles to mediate neutrophil recruitment into alveoli to possibly to assist AMs to clear NPs.

4.13 Activation of alveolar macrophage CRs and FcγR I by NPs triggers neutrophil recruitment

A variety of opsonizing receptors (such as Fcγ receptors and complement receptors) on the surface of phagocytes are closely related to effectively identifying target particles and initiating phagocytosis. Classic FcγRs are cellular membrane-associated proteins expressed on many kinds of immune cells, like macrophages, DCs, natural killer (NK) cells, neutrophils, and B cells (Fitzpatrick et al., 2020). They mediate cellular immune-related activities such as the degranulation of NK cells, mast cells, and basophils (Elias et al., 2021; Fitzpatrick et al., 2020; Nimmerjahn & Ravetch, 2008; Paranjape et al., 2020; Syenina et al., 2015), phagocytosis of phagocytes (Hawley et al., 2017), antigen presentation of dendritic cells (van Montfoort et al., 2012; Yada et al., 2003),

activation of B cells (Grunst et al., 2020). Shlomo Elias and colleagues demonstrated that NK cell degranulation was mediated by the binding of the Fc fragment of an anti-RhD antibody to CD16, the major Fcγ receptor (FcγR) expressed on NK cells, depending on the glycosylation by anti-RhD antibodies (Elias et al., 2021). Like F4/80 or the protein tyrosine kinase MER (MERTK), FcγR I was specifically expressed on the surface of mouse macrophages (Guilliams et al., 2014). The Randolph laboratory (Guilliams et al., 2014). The Randolph laboratory (Gautier et al., 2012), using their examination of macrophage core transcripts at the protein level in lung tissue (Immunological Genome Consortium), gated forMerTK+ FCγR I+ cells revealing that the vast majority of these cells were SiglecF+ lung macrophages (AMs). Blocking of Fc γR I (anti-CD64 mAbs) significantly reduced bacteria (spirochetal) uptake and the secretion of pro-inflammatory cytokines by IFNγ-stimulated macrophages (Hawley et al., 2017). In our experiments, when the mice were pre-treated by anti-CD64 (anti-FcγR I) mAbs in the airway via oropharyngeal aspiration, cQDs-induced neutrophil recruitment was abolished. All in all, FcγR I-mediated neutrophil recruitment upon NPs exposure has a complex mechanism. FcγR I blocking with anti-CD64 mAbs reduced the NPs phagocytic capacity of AMs as well as the cellular degranulation process upon NPs exposure, thus inhibiting the nanoparticle-induced neutrophil recruitment process.

C5a and C3a, as members of the complement family, are strongly associated with the recruitment of immune cells, such as neutrophils, eosinophils,

monocytes, and T lymphocytes, during inflammation (Guo & Ward, 2005; Mollah & Tam, 2022; Shivshankar et al., 2020). C5aR is ubiquitously expressed in many kinds of cells, especially on the surface of immune cells like macrophages, neutrophils, and T cells (Monk et al., 2007). On the surface of AMs in healthy mice, C5aR, but not C3aR, is highly expressed. Besides, both C5aR and C3aR are expressed at low levels in the alveolar epithelium (Schiller & Theis lab Atlas data, http://146.107.176.18:3838/MLAA_backup/). IL-6 stimulated the upregulation of C5aR in numerous organs (lung, liver, kidney, and heart) in septic rats (Riedemann et al., 2003). Mechanistic research revealed that C5 produced by epithelial cells was cleaved into C5a by AM-derived serine proteases. When C5a was bound to the corresponding receptor C5aR, it initiated an inflammatory signal cascade (Chiba et al., 2015). C5a and its degradation product, C5a des-Arg, caused skin inflammatory responses, such as neutrophil-rich leukocyte infiltration, edema, and mast cell degranulation, immediately after intradermal injection (Swerlick et al., 1988, 1989). In hamsters, intravenously administered disodium cromoglycate (DSCG) (3.0-30 mg/kg) inhibits vascular permeability and basophil degranulation, thereby alleviating C5a-induced cutaneous basophilia granulocyte anaphylaxis (CBA) (Golden et al., 1986; Golden et al., 1987). We revealed that blockade of C5aR by anti-CD88 mAbs eliminated NPs-induced neutrophil recruitment without the alteration of the patrolling status of AMs, a result consistent with the possible inhibition of nanoparticle-induced immune cell degranulation by

intravascular injection of cromolyn. Our data indicated that deposited NPs in the lung induced cellular degranulation and stimulated neutrophil recruitment. The usage of CD88/CD64 blocking antibody could inhibit not only the degranulation process like cromolyn application but also decrease the uptake capacity of NPs by AMs, thereby preventing rapid neutrophil recruitment. Investigations if there is direct evidence of the release of granules from AMs are underway.

Numerous studies have confirmed the importance of CD44 in the recruitment of leukocytes in various organs of the body (Mikecz et al., 1995; Nascimento et al., 2016; Sarraj et al., 2006; Vachon et al., 2006). The interaction of CD44 and HA plays an important role in the leukocyte recruitment cascade. During neutrophil rolling, the engagement between CD44 on neutrophils and E-selectin on the endothelium is required for slow rolling (Katayama et al., 2005). In models of peritonitis, T cells utilize CD44-HA interactions into the inflamed peritoneal cavity (DeGrendele et al., 1997). In in vivo microscopy experiments, it was found that the adhesion of neutrophils (Khan et al., 2004) and T cells (Bonder et al., 2006) on the endothelium is closely related to the interaction between CD44 and HA. In addition to this, CD44 has also an essential impact on the phagocytosis of macrophages (Vachon et al., 2006), and this process may induce the activation of the HA receptor (Rios de la Rosa et al., 2017) and complement receptor-3 (CR3) (Amash et al., 2016; Vachon et al., 2007).

Overall, our data indicated a close relation between AM activity (phagocytosis,

migration, and degranulation) and the rapid and site-specific recruitment of neutrophils during the early phase of particle inhalation, suggesting a specific role of AMs in triggering the immune response by different NPs.

5. Conclusion

1. NP-induced neutrophil recruitment is initiated by AMs and related to NP internalization/uptake by AMs.
2. The particle uptake efficacy depends on three factors: (1) NP surface modification; (2) the speed of macrophage patrolling movement in the alveoli; (3) AMs phagocytic/internalizing capability.

(1) PEGylation modification of NPs which are deposited in the alveoli renders the NPs invisible to AMs via avoiding protein corona formation and impairs subsequent NP-induced neutrophil recruitment.

(2) AM patrolling mainly involves ICAM-1 and LFA-1 interaction in the alveoli and can be blocked by respective antibodies applied to the airway side but not to the vascular side. Blocking ICAM-1 and LFA-1 also effectively impaired particle-triggered neutrophil recruitment.

(3) The macrophage receptors C5aR1 and FcγRI mediate AM phagocytic ability to internalize particles. Blocking C5aR1 or FcγRI also completely blocked neutrophile recruitment.

3. Particle-triggered neutrophil recruitment to the airspace requires degranulation and can be inhibited by cromolyn treatment.
4. Recruitment of neutrophils further requires TNFα as anti-TNFα blocking treatment in the airway can reduce the neutrophilic inflammatory response.
5. Scavenging ROS via NAC also decreased cQDs-induced neutrophil

recruitment to some extent but was less effective than ICAM-1/LFA-1 blocking.

6. Reference

Acharya, D., Li, X. R. L., Heineman, R. E., & Harrison, R. E. (2019). Complement Receptor-Mediated Phagocytosis Induces Proinflammatory Cytokine Production in Murine Macrophages. *Front Immunol*, *10*, 3049. https://doi.org/10.3389/fimmu.2019.03049

Aderem, A., & Underhill, D. M. (1999). Mechanisms of phagocytosis in macrophages. *Annu Rev Immunol*, *17*, 593-623. https://doi.org/10.1146/annurev.immunol.17.1.593

Aderem, A. A., Wright, S. D., Silverstein, S. C., & Cohn, Z. A. (1985). Ligated complement receptors do not activate the arachidonic acid cascade in resident peritoneal macrophages. *J Exp Med*, *161*(3), 617-622. https://doi.org/10.1084/jem.161.3.617

Adivitiya, Kaushik, M. S., Chakraborty, S., Veleri, S., & Kateriya, S. (2021). Mucociliary Respiratory Epithelium Integrity in Molecular Defense and Susceptibility to Pulmonary Viral Infections. *Biology (Basel)*, *10*(2). https://doi.org/10.3390/biology10020095

Aggarwal, N. R., Chau, E., Garibaldi, B. T., Mock, J. R., Sussan, T., Rao, K., Rao, K., Menon, A. G., D'Alessio, F. R., Damarla, M., Biswal, S., King, L. S., & Sidhaye, V. K. (2013). Aquaporin 5 regulates cigarette smoke induced emphysema by modulating barrier and immune properties of the epithelium. *Tissue Barriers*, *1*(4), e25248. https://doi.org/10.4161/tisb.25248

Aggarwal, P., Hall, J. B., McLeland, C. B., Dobrovolskaia, M. A., & McNeil, S. E. (2009). Nanoparticle interaction with plasma proteins as it relates to particle biodistribution, biocompatibility and therapeutic efficacy. *Adv Drug Deliv Rev*, *61*(6), 428-437. https://doi.org/10.1016/j.addr.2009.03.009

Akinrinmade, O. A., Chetty, S., Daramola, A. K., Islam, M. U., Thepen, T., & Barth, S. (2017). CD64: An Attractive Immunotherapeutic Target for M1-type Macrophage Mediated Chronic Inflammatory Diseases. *Biomedicines*, *5*(3). https://doi.org/10.3390/biomedicines5030056

Aleman, K., Noordzij, J. G., de Groot, R., van Dongen, J. J., & Hartwig, N. G. (2001). Reviewing Omenn syndrome. *Eur J Pediatr*, *160*(12), 718-725. https://doi.org/10.1007/s004310100816

Alexis, N. E., Lay, J. C., Zeman, K. L., Geiser, M., Kapp, N., & Bennett, W. D. (2006). In vivo particle uptake by airway macrophages in healthy volunteers. *Am J Respir Cell Mol Biol*, *34*(3), 305-313. https://doi.org/10.1165/rcmb.2005-0373OC

Alflen, A., Prüfer, S., Ebner, K., Reuter, S., Aranda Lopez, P., Scharrer, I., Banno, F., Stassen, M., Schild, H., Jurk, K., Bosmann, M., Beckert, H., & Radsak, M. P. (2017). ADAMTS-13 regulates neutrophil recruitment in a mouse model of invasive pulmonary aspergillosis. *Sci Rep*, *7*(1), 7184. https://doi.org/10.1038/s41598-017-07340-3

Alizadeh-Tabrizi, N., Hall, S., & Lehmann, C. (2020). Intravital Imaging of Pulmonary Immune Response in Inflammation and Infection. *Front Cell Dev Biol*, *8*, 620471. https://doi.org/10.3389/fcell.2020.620471

Almeida, A. P. B., Damaceno, G. B. R., Carneiro, A. F., Bohr, A., Gonçalves, H. R., Valadares, M. C., Nascimento, T. L., & Lima, E. M. (2019). Mucopenetrating lipoplexes modified with PEG and hyaluronic acid for CD44-targeted local siRNA delivery to the lungs. *J Biomater Appl*, *34*(5), 617-630. https://doi.org/10.1177/0885328219863291

Alsaleh, N. B., Mendoza, R. P., & Brown, J. M. (2019). Exposure to silver nanoparticles primes mast

cells for enhanced activation through the high-affinity IgE receptor. *Toxicol Appl Pharmacol*, *382*, 114746. https://doi.org/10.1016/j.taap.2019.114746

Amash, A., Wang, L., Wang, Y., Bhakta, V., Fairn, G. D., Hou, M., Peng, J., Sheffield, W. P., & Lazarus, A. H. (2016). CD44 Antibody Inhibition of Macrophage Phagocytosis Targets Fcγ Receptor- and Complement Receptor 3-Dependent Mechanisms. *J Immunol*, *196*(8), 3331-3340. https://doi.org/10.4049/jimmunol.1502198

André, E., Stoeger, T., Takenaka, S., Bahnweg, M., Ritter, B., Karg, E., Lentner, B., Reinhard, C., Schulz, H., & Wjst, M. (2006). Inhalation of ultrafine carbon particles triggers biphasic pro-inflammatory response in the mouse lung. *Eur Respir J*, *28*(2), 275-285. https://doi.org/10.1183/09031936.06.00071205

Angelillo-Scherrer, A. (2012). Leukocyte-derived microparticles in vascular homeostasis. *Circ Res*, *110*(2), 356-369. https://doi.org/10.1161/circresaha.110.233403

Armand, L., Tarantini, A., Beal, D., Biola-Clier, M., Bobyk, L., Sorieul, S., Pernet-Gallay, K., Marie-Desvergne, C., Lynch, I., Herlin-Boime, N., & Carriere, M. (2016). Long-term exposure of A549 cells to titanium dioxide nanoparticles induces DNA damage and sensitizes cells towards genotoxic agents. *Nanotoxicology*, *10*(7), 913-923. https://doi.org/10.3109/17435390.2016.1141338

Arredouani, M., Yang, Z., Ning, Y., Qin, G., Soininen, R., Tryggvason, K., & Kobzik, L. (2004). The scavenger receptor MARCO is required for lung defense against pneumococcal pneumonia and inhaled particles. *J Exp Med*, *200*(2), 267-272. https://doi.org/10.1084/jem.20040731

AS., N. (2021). *Understanding the function and behaviour of alveolar macrophages.* University of Calgary]. Calgary, AB.

Baan, R., Straif, K., Grosse, Y., Secretan, B., El Ghissassi, F., & Cogliano, V. (2006). Carcinogenicity of carbon black, titanium dioxide, and talc. *Lancet Oncol*, *7*(4), 295-296. https://doi.org/10.1016/s1470-2045(06)70651-9

Balamayooran, G., Batra, S., Cai, S., Mei, J., Worthen, G. S., Penn, A. L., & Jeyaseelan, S. (2012). Role of CXCL5 in leukocyte recruitment to the lungs during secondhand smoke exposure. *Am J Respir Cell Mol Biol*, *47*(1), 104-111. https://doi.org/10.1165/rcmb.2011-0260OC

Bardoel, B. W., Kenny, E. F., Sollberger, G., & Zychlinsky, A. (2014). The balancing act of neutrophils. *Cell Host Microbe*, *15*(5), 526-536. https://doi.org/10.1016/j.chom.2014.04.011

Barletta, K. E., Cagnina, R. E., Wallace, K. L., Ramos, S. I., Mehrad, B., & Linden, J. (2012). Leukocyte compartments in the mouse lung: distinguishing between marginated, interstitial, and alveolar cells in response to injury. *J Immunol Methods*, *375*(1-2), 100-110. https://doi.org/10.1016/j.jim.2011.09.013

Bartneck, M., Keul, H. A., Zwadlo-Klarwasser, G., & Groll, J. (2010). Phagocytosis independent extracellular nanoparticle clearance by human immune cells. *Nano Lett*, *10*(1), 59-63. https://doi.org/10.1021/nl902830x

Baseler, L. J., Falzarano, D., Scott, D. P., Rosenke, R., Thomas, T., Munster, V. J., Feldmann, H., & de Wit, E. (2016). An Acute Immune Response to Middle East Respiratory Syndrome Coronavirus Replication Contributes to Viral Pathogenicity. *Am J Pathol*, *186*(3), 630-638. https://doi.org/10.1016/j.ajpath.2015.10.025

Bernard, N. F., Kiani, Z., Tremblay-McLean, A., Kant, S. A., Leeks, C. E., & Dupuy, F. P. (2017). Natural Killer (NK) Cell Education Differentially Influences HIV Antibody-Dependent NK Cell

Activation and Antibody-Dependent Cellular Cytotoxicity. *Front Immunol*, *8*, 1033. https://doi.org/10.3389/fimmu.2017.01033

Bigert, C., Gustavsson, P., Hallqvist, J., Hogstedt, C., Lewné, M., Plato, N., Reuterwall, C., & Schéele, P. (2003). Myocardial infarction among professional drivers. *Epidemiology*, *14*(3), 333-339.

Boeck, S., Wittwer, C., Heinemann, V., Haas, M., Kern, C., Stieber, P., Nagel, D., & Holdenrieder, S. (2013). Cytokeratin 19-fragments (CYFRA 21-1) as a novel serum biomarker for response and survival in patients with advanced pancreatic cancer. *Br J Cancer*, *108*(8), 1684-1694. https://doi.org/10.1038/bjc.2013.158

Bonder, C. S., Clark, S. R., Norman, M. U., Johnson, P., & Kubes, P. (2006). Use of CD44 by CD4+ Th1 and Th2 lymphocytes to roll and adhere. *Blood*, *107*(12), 4798-4806. https://doi.org/10.1182/blood-2005-09-3581

Boraschi, D., & Tagliabue, A. (2013). The interleukin-1 receptor family. *Semin Immunol*, *25*(6), 394-407. https://doi.org/10.1016/j.smim.2013.10.023

Borelli, V., Vita, F., Shankar, S., Soranzo, M. R., Banfi, E., Scialino, G., Brochetta, C., & Zabucchi, G. (2003). Human eosinophil peroxidase induces surface alteration, killing, and lysis of Mycobacterium tuberculosis. *Infect Immun*, *71*(2), 605-613. https://doi.org/10.1128/iai.71.2.605-613.2003

Borregaard, N., Sørensen, O. E., & Theilgaard-Mönch, K. (2007). Neutrophil granules: a library of innate immunity proteins. *Trends Immunol*, *28*(8), 340-345. https://doi.org/10.1016/j.it.2007.06.002

Brinkmann, V., Reichard, U., Goosmann, C., Fauler, B., Uhlemann, Y., Weiss, D. S., Weinrauch, Y., & Zychlinsky, A. (2004). Neutrophil extracellular traps kill bacteria. *Science*, *303*(5663), 1532-1535. https://doi.org/10.1126/science.1092385

Brown, D. M., Donaldson, K., Borm, P. J., Schins, R. P., Dehnhardt, M., Gilmour, P., Jimenez, L. A., & Stone, V. (2004). Calcium and ROS-mediated activation of transcription factors and TNF-alpha cytokine gene expression in macrophages exposed to ultrafine particles. *Am J Physiol Lung Cell Mol Physiol*, *286*(2), L344-353. https://doi.org/10.1152/ajplung.00139.2003

Brunck, M. E., Andersen, S. B., Timmins, N. E., Osborne, G. W., & Nielsen, L. K. (2014). Absolute counting of neutrophils in whole blood using flow cytometry. *Cytometry A*, *85*(12), 1057-1064. https://doi.org/10.1002/cyto.a.22503

Burn, G. L., Foti, A., Marsman, G., Patel, D. F., & Zychlinsky, A. (2021). The Neutrophil. *Immunity*, *54*(7), 1377-1391. https://doi.org/10.1016/j.immuni.2021.06.006

Cai, R., & Chen, C. (2019). The Crown and the Scepter: Roles of the Protein Corona in Nanomedicine. *Adv Mater*, *31*(45), e1805740. https://doi.org/10.1002/adma.201805740

Chen, D., Parayath, N., Ganesh, S., Wang, W., & Amiji, M. (2019). The role of apolipoprotein- and vitronectin-enriched protein corona on lipid nanoparticles for in vivo targeted delivery and transfection of oligonucleotides in murine tumor models. *Nanoscale*, *11*(40), 18806-18824. https://doi.org/10.1039/c9nr05788a

Chen, J., & Hoek, G. (2020). Long-term exposure to PM and all-cause and cause-specific mortality: A systematic review and meta-analysis. *Environ Int*, *143*, 105974. https://doi.org/10.1016/j.envint.2020.105974

Chen, S., Yin, R., Mutze, K., Yu, Y., Takenaka, S., Königshoff, M., & Stoeger, T. (2016). No involvement of alveolar macrophages in the initiation of carbon nanoparticle induced acute lung

inflammation in mice. *Part Fibre Toxicol*, *13*(1), 33. https://doi.org/10.1186/s12989-016-0144-6

Chiba, N., Shimada, K., Chen, S., Jones, H. D., Alsabeh, R., Slepenkin, A. V., Peterson, E., Crother, T. R., & Arditi, M. (2015). Mast cells play an important role in chlamydia pneumoniae lung infection by facilitating immune cell recruitment into the airway. *J Immunol*, *194*(8), 3840-3851. https://doi.org/10.4049/jimmunol.1402685

Choi, H. S., Ashitate, Y., Lee, J. H., Kim, S. H., Matsui, A., Insin, N., Bawendi, M. G., Semmler-Behnke, M., Frangioni, J. V., & Tsuda, A. (2010). Rapid translocation of nanoparticles from the lung airspaces to the body. *Nat Biotechnol*, *28*(12), 1300-1303. https://doi.org/10.1038/nbt.1696

Chong, D. L. W., Rebeyrol, C., José, R. J., Williams, A. E., Brown, J. S., Scotton, C. J., & Porter, J. C. (2021). ICAM-1 and ICAM-2 Are Differentially Expressed and Up-Regulated on Inflamed Pulmonary Epithelium, but Neither ICAM-2 nor LFA-1: ICAM-1 Are Required for Neutrophil Migration Into the Airways In Vivo. *Front Immunol*, *12*, 691957. https://doi.org/10.3389/fimmu.2021.691957

Chou, C. C., Hsiao, H. Y., Hong, Q. S., Chen, C. H., Peng, Y. W., Chen, H. W., & Yang, P. C. (2008). Single-walled carbon nanotubes can induce pulmonary injury in mouse model. *Nano Lett*, *8*(2), 437-445. https://doi.org/10.1021/nl0723634

Chrishtop, V. V., Prilepskii, A. Y., Nikonorova, V. G., & Mironov, V. A. (2021). Nanosafety vs. nanotoxicology: adequate animal models for testing in vivo toxicity of nanoparticles. *Toxicology*, *462*, 152952. https://doi.org/10.1016/j.tox.2021.152952

Cronin, J. G., Jones, N., Thornton, C. A., Jenkins, G. J. S., Doak, S. H., & Clift, M. J. D. (2020). Nanomaterials and Innate Immunity: A Perspective of the Current Status in Nanosafety. *Chem Res Toxicol*, *33*(5), 1061-1073. https://doi.org/10.1021/acs.chemrestox.0c00051

Cryan, S. A., Sivadas, N., & Garcia-Contreras, L. (2007). In vivo animal models for drug delivery across the lung mucosal barrier. *Adv Drug Deliv Rev*, *59*(11), 1133-1151. https://doi.org/10.1016/j.addr.2007.08.023

Crystal, R. G., Randell, S. H., Engelhardt, J. F., Voynow, J., & Sunday, M. E. (2008). Airway epithelial cells: current concepts and challenges. *Proc Am Thorac Soc*, *5*(7), 772-777. https://doi.org/10.1513/pats.200805-041HR

Current Strategies for Engineering Controls in Nanomaterial Production and Downstream Handling Processes. (2013). *U.S. National Institute for Occupational Safety and Health*, 1–3. https://doi.org/10.26616/NIOSHPUB2014102. (Retrieved 2017-03-05.)

Davis, J. D., & Wypych, T. P. (2021). Cellular and functional heterogeneity of the airway epithelium. *Mucosal Immunol*, *14*(5), 978-990. https://doi.org/10.1038/s41385-020-00370-7

de Vrieze, J. (2021). Pfizer's vaccine raises allergy concerns. *Science*, *371*(6524), 10-11. https://doi.org/10.1126/science.371.6524.10

DeGrendele, H. C., Estess, P., & Siegelman, M. H. (1997). Requirement for CD44 in activated T cell extravasation into an inflammatory site. *Science*, *278*(5338), 672-675. https://doi.org/10.1126/science.278.5338.672

Demento, S. L., Eisenbarth, S. C., Foellmer, H. G., Platt, C., Caplan, M. J., Mark Saltzman, W., Mellman, I., Ledizet, M., Fikrig, E., Flavell, R. A., & Fahmy, T. M. (2009). Inflammasome-activating nanoparticles as modular systems for optimizing vaccine efficacy. *Vaccine*, *27*(23), 3013-3021. https://doi.org/10.1016/j.vaccine.2009.03.034

Deppermann, C., Kratofil, R. M., Peiseler, M., David, B. A., Zindel, J., Castanheira, F., van der Wal, F., Carestia, A., Jenne, C. N., Marth, J. D., & Kubes, P. (2020). Macrophage galactose lectin is critical for Kupffer cells to clear aged platelets. *J Exp Med*, *217*(4). https://doi.org/10.1084/jem.20190723

Deshpande, R., & Zou, C. (2020). Pseudomonas Aeruginosa Induced Cell Death in Acute Lung Injury and Acute Respiratory Distress Syndrome. *Int J Mol Sci*, *21*(15). https://doi.org/10.3390/ijms21155356

Doerschuk, C. M. (2000). Leukocyte trafficking in alveoli and airway passages. *Respir Res*, *1*(3), 136-140. https://doi.org/10.1186/rr24

Doerschuk, C. M., Beyers, N., Coxson, H. O., Wiggs, B., & Hogg, J. C. (1993). Comparison of neutrophil and capillary diameters and their relation to neutrophil sequestration in the lung. *J Appl Physiol (1985)*, *74*(6), 3040-3045. https://doi.org/10.1152/jappl.1993.74.6.3040

Donaldson, K., Murphy, F. A., Duffin, R., & Poland, C. A. (2010). Asbestos, carbon nanotubes and the pleural mesothelium: a review of the hypothesis regarding the role of long fibre retention in the parietal pleura, inflammation and mesothelioma. *Part Fibre Toxicol*, *7*, 5. https://doi.org/10.1186/1743-8977-7-5

Dong, J., Porter, D. W., Batteli, L. A., Wolfarth, M. G., Richardson, D. L., & Ma, Q. (2015). Pathologic and molecular profiling of rapid-onset fibrosis and inflammation induced by multi-walled carbon nanotubes. *Arch Toxicol*, *89*(4), 621-633. https://doi.org/10.1007/s00204-014-1428-y

Dostert, C., Pétrilli, V., Van Bruggen, R., Steele, C., Mossman, B. T., & Tschopp, J. (2008). Innate immune activation through Nalp3 inflammasome sensing of asbestos and silica. *Science*, *320*(5876), 674-677. https://doi.org/10.1126/science.1156995

Dudeck, J., Kotrba, J., Immler, R., Hoffmann, A., Voss, M., Alexaki, V. I., Morton, L., Jahn, S. R., Katsoulis-Dimitriou, K., Winzer, S., Kollias, G., Fischer, T., Nedospasov, S. A., Dunay, I. R., Chavakis, T., Müller, A. J., Schraven, B., Sperandio, M., & Dudeck, A. (2021). Directional mast cell degranulation of tumor necrosis factor into blood vessels primes neutrophil extravasation. *Immunity*, *54*(3), 468-483.e465. https://doi.org/10.1016/j.immuni.2020.12.017

Duman, F. D., Akkoc, Y., Demirci, G., Bavili, N., Kiraz, A., Gozuacik, D., & Acar, H. Y. (2019). Bypassing pro-survival and resistance mechanisms of autophagy in EGFR-positive lung cancer cells by targeted delivery of 5FU using theranostic Ag(2)S quantum dots. *J Mater Chem B*, *7*(46), 7363-7376. https://doi.org/10.1039/c9tb01602c

Dunne, J. L., Ballantyne, C. M., Beaudet, A. L., & Ley, K. (2002). Control of leukocyte rolling velocity in TNF-alpha-induced inflammation by LFA-1 and Mac-1. *Blood*, *99*(1), 336-341. https://doi.org/10.1182/blood.v99.1.336

Dykman, L., & Khlebtsov, N. (2012). Gold nanoparticles in biomedical applications: recent advances and perspectives. *Chem Soc Rev*, *41*(6), 2256-2282. https://doi.org/10.1039/c1cs15166e

Dykman, L. A., & Khlebtsov, N. G. (2011). Gold nanoparticles in biology and medicine: recent advances and prospects. *Acta Naturae*, *3*(2), 34-55.

Ehrmann, S., Schmid, O., Darquenne, C., Rothen-Rutishauser, B., Sznitman, J., Yang, L., Barosova, H., Vecellio, L., Mitchell, J., & Heuze-Vourc'h, N. (2020). Innovative preclinical models for pulmonary drug delivery research. *Expert Opin Drug Deliv*, *17*(4), 463-478.

https://doi.org/10.1080/17425247.2020.1730807

Eken, C., Sadallah, S., Martin, P. J., Treves, S., & Schifferli, J. A. (2013). Ectosomes of polymorphonuclear neutrophils activate multiple signaling pathways in macrophages. *Immunobiology*, *218*(3), 382-392. https://doi.org/10.1016/j.imbio.2012.05.021

Elias, S., Kol, I., Kahlon, S., Amore, R., Zeibak, M., Mevorach, D., Elchalal, U., Zelig, O., & Mandelboim, O. (2021). Anti-RhD antibody therapy modulates human natural killer cell function. *Haematologica*, *106*(7), 1846-1856. https://doi.org/10.3324/haematol.2019.238097

Fehrenbach, H., Brasch, F., Uhlig, S., Weisser, M., Stamme, C., Wendel, A., & Richter, J. (1998). Early alterations in intracellular and alveolar surfactant of the rat lung in response to endotoxin. *Am J Respir Crit Care Med*, *157*(5 Pt 1), 1630-1639. https://doi.org/10.1164/ajrccm.157.5.9611070

Feletou, M., Tang, E. H., & Vanhoutte, P. M. (2008). Nitric oxide the gatekeeper of endothelial vasomotor control. *Front Biosci*, *13*, 4198-4217. https://doi.org/10.2741/3000

Fitzpatrick, E. A., Wang, J., & Strome, S. E. (2020). Engineering of Fc Multimers as a Protein Therapy for Autoimmune Disease. *Front Immunol*, *11*, 496. https://doi.org/10.3389/fimmu.2020.00496

Frampton, M. W., Stewart, J. C., Oberdörster, G., Morrow, P. E., Chalupa, D., Pietropaoli, A. P., Frasier, L. M., Speers, D. M., Cox, C., Huang, L. S., & Utell, M. J. (2006). Inhalation of ultrafine particles alters blood leukocyte expression of adhesion molecules in humans. *Environ Health Perspect*, *114*(1), 51-58. https://doi.org/10.1289/ehp.7962

Frank, E. A., Birch, M. E., & Yadav, J. S. (2015). MyD88 mediates in vivo effector functions of alveolar macrophages in acute lung inflammatory responses to carbon nanotube exposure. *Toxicol Appl Pharmacol*, *288*(3), 322-329. https://doi.org/10.1016/j.taap.2015.08.004

Fromen, C. A., Kelley, W. J., Fish, M. B., Adili, R., Noble, J., Hoenerhoff, M. J., Holinstat, M., & Eniola-Adefeso, O. (2017). Neutrophil-Particle Interactions in Blood Circulation Drive Particle Clearance and Alter Neutrophil Responses in Acute Inflammation. *ACS Nano*, *11*(11), 10797-10807. https://doi.org/10.1021/acsnano.7b03190

Fuchs, B., Sjöberg, L., Möller Westerberg, C., Ekoff, M., Swedin, L., Dahlén, S. E., Adner, M., & Nilsson, G. P. (2012). Mast cell engraftment of the peripheral lung enhances airway hyperresponsiveness in a mouse asthma model. *Am J Physiol Lung Cell Mol Physiol*, *303*(12), L1027-1036. https://doi.org/10.1152/ajplung.00227.2012

Fuchs, T. A., Abed, U., Goosmann, C., Hurwitz, R., Schulze, I., Wahn, V., Weinrauch, Y., Brinkmann, V., & Zychlinsky, A. (2007). Novel cell death program leads to neutrophil extracellular traps. *J Cell Biol*, *176*(2), 231-241. https://doi.org/10.1083/jcb.200606027

Futosi, K., Fodor, S., & Mócsai, A. (2013). Neutrophil cell surface receptors and their intracellular signal transduction pathways. *Int Immunopharmacol*, *17*(3), 638-650. https://doi.org/10.1016/j.intimp.2013.06.034

Ganguly, K., Ettehadieh, D., Upadhyay, S., Takenaka, S., Adler, T., Karg, E., Krombach, F., Kreyling, W. G., Schulz, H., Schmid, O., & Stoeger, T. (2017). Early pulmonary response is critical for extra-pulmonary carbon nanoparticle mediated effects: comparison of inhalation versus intra-arterial infusion exposures in mice. *Part Fibre Toxicol*, *14*(1), 19. https://doi.org/10.1186/s12989-017-0200-x

Ganguly, K., Upadhyay, S., Irmler, M., Takenaka, S., Pukelsheim, K., Beckers, J., Hamelmann, E., Schulz, H., & Stoeger, T. (2009). Pathway focused protein profiling indicates differential

function for IL-1B, -18 and VEGF during initiation and resolution of lung inflammation evoked by carbon nanoparticle exposure in mice. *Part Fibre Toxicol*, *6*, 31. https://doi.org/10.1186/1743-8977-6-31

Gautier, E. L., Shay, T., Miller, J., Greter, M., Jakubzick, C., Ivanov, S., Helft, J., Chow, A., Elpek, K. G., Gordonov, S., Mazloom, A. R., Ma'ayan, A., Chua, W. J., Hansen, T. H., Turley, S. J., Merad, M., & Randolph, G. J. (2012). Gene-expression profiles and transcriptional regulatory pathways that underlie the identity and diversity of mouse tissue macrophages. *Nat Immunol*, *13*(11), 1118-1128. https://doi.org/10.1038/ni.2419

Gazendam, R. P., van de Geer, A., Roos, D., van den Berg, T. K., & Kuijpers, T. W. (2016). How neutrophils kill fungi. *Immunol Rev*, *273*(1), 299-311. https://doi.org/10.1111/imr.12454

Ge, J., Lan, M., Zhou, B., Liu, W., Guo, L., Wang, H., Jia, Q., Niu, G., Huang, X., Zhou, H., Meng, X., Wang, P., Lee, C. S., Zhang, W., & Han, X. (2014). A graphene quantum dot photodynamic therapy agent with high singlet oxygen generation. *Nat Commun*, *5*, 4596. https://doi.org/10.1038/ncomms5596

Geerdink, R. J., Pillay, J., Meyaard, L., & Bont, L. (2015). Neutrophils in respiratory syncytial virus infection: A target for asthma prevention. *J Allergy Clin Immunol*, *136*(4), 838-847. https://doi.org/10.1016/j.jaci.2015.06.034

Geiser, M. (2002). Morphological aspects of particle uptake by lung phagocytes. *Microsc Res Tech*, *57*(6), 512-522. https://doi.org/10.1002/jemt.10105

Geissler, K., Gunzer, M., & Ostermann, H. (2018). How Safe Is the Administration of Long-Acting Granulocyte Colony-Stimulating Factor in Cancer Patients? *Oncol Res Treat*, *41*(5), 316-326. https://doi.org/10.1159/000486681

George, S. T., Lai, J., Ma, J., Stacey, H. D., Miller, M. S., & Mullarkey, C. E. (2021). Neutrophils and Influenza: A Thin Line between Helpful and Harmful. *Vaccines (Basel)*, *9*(6). https://doi.org/10.3390/vaccines9060597

Getts, D. R., Shea, L. D., Miller, S. D., & King, N. J. (2015). Harnessing nanoparticles for immune modulation. *Trends Immunol*, *36*(7), 419-427. https://doi.org/10.1016/j.it.2015.05.007

Geys, J., Nemmar, A., Verbeken, E., Smolders, E., Ratoi, M., Hoylaerts, M. F., Nemery, B., & Hoet, P. H. (2008). Acute toxicity and prothrombotic effects of quantum dots: impact of surface charge. *Environ Health Perspect*, *116*(12), 1607-1613. https://doi.org/10.1289/ehp.11566

Global, regional, and national comparative risk assessment of 79 behavioural, environmental and occupational, and metabolic risks or clusters of risks, 1990-2015: a systematic analysis for the Global Burden of Disease Study 2015. (2016). *Lancet*, *388*(10053), 1659-1724. https://doi.org/10.1016/s0140-6736(16)31679-8

Golden, H. W., Crean, G. L., Iacuzio, D. A., & Otterness, I. G. (1986). Effect of disodium cromoglycate on cutaneous basophil anaphylaxis. *J Immunol*, *137*(5), 1495-1503.

Golden, H. W., Iacuzio, D. A., & Otterness, I. G. (1987). Inhibition of C5a-induced basophil degranulation by disodium cromoglycate. *Agents Actions*, *21*(3-4), 371-374. https://doi.org/10.1007/bf01966519

Gordon, S. B., Bruce, N. G., Grigg, J., Hibberd, P. L., Kurmi, O. P., Lam, K. B., Mortimer, K., Asante, K. P., Balakrishnan, K., Balmes, J., Bar-Zeev, N., Bates, M. N., Breysse, P. N., Buist, S., Chen, Z., Havens, D., Jack, D., Jindal, S., Kan, H., . . . Martin, W. J., 2nd. (2014). Respiratory risks from household air pollution in low and middle income countries. *Lancet Respir Med*, *2*(10), 823-860. https://doi.org/10.1016/s2213-2600(14)70168-7

Granger, D. N., Rodrigues, S. F., Yildirim, A., & Senchenkova, E. Y. (2010). Microvascular responses to cardiovascular risk factors. *Microcirculation*, *17*(3), 192-205. https://doi.org/10.1111/j.1549-8719.2009.00015.x

Gref, R., Minamitake, Y., Peracchia, M. T., Trubetskoy, V., Torchilin, V., & Langer, R. (1994). Biodegradable long-circulating polymeric nanospheres. *Science*, *263*(5153), 1600-1603. https://doi.org/10.1126/science.8128245

Grimes, D., Johnson, R., Pashos, M., Cummings, C., Kang, C., Sampedro, G. R., Tycksen, E., McBride, H. J., Sah, R., Lowell, C. A., & Clemens, R. A. (2020). ORAI1 and ORAI2 modulate murine neutrophil calcium signaling, cellular activation, and host defense. *Proc Natl Acad Sci U S A*, *117*(39), 24403-24414. https://doi.org/10.1073/pnas.2008032117

Grunst, M. W., Grandea, A. G., 3rd, Janaka, S. K., Hammad, I., Grimes, P., Karl, J. A., Wiseman, R., O'Connor, D. H., & Evans, D. T. (2020). Functional Interactions of Common Allotypes of Rhesus Macaque FcγR2A and FcγR3A with Human and Macaque IgG Subclasses. *J Immunol*, *205*(12), 3319-3332. https://doi.org/10.4049/jimmunol.2000501

Guilliams, M., Bruhns, P., Saeys, Y., Hammad, H., & Lambrecht, B. N. (2014). The function of Fcγ receptors in dendritic cells and macrophages. *Nat Rev Immunol*, *14*(2), 94-108. https://doi.org/10.1038/nri3582

Guilliams, M., De Kleer, I., Henri, S., Post, S., Vanhoutte, L., De Prijck, S., Deswarte, K., Malissen, B., Hammad, H., & Lambrecht, B. N. (2013). Alveolar macrophages develop from fetal monocytes that differentiate into long-lived cells in the first week of life via GM-CSF. *J Exp Med*, *210*(10), 1977-1992. https://doi.org/10.1084/jem.20131199

Gunaydin, G., Gedik, M. E., & Ayan, S. (2021). Photodynamic Therapy for the Treatment and Diagnosis of Cancer-A Review of the Current Clinical Status. *Front Chem*, *9*, 686303. https://doi.org/10.3389/fchem.2021.686303

Guo, G., Liu, W., Liang, J., He, Z., Xu, H., & Yang, X. (2007). Probing the cytotoxicity of CdSe quantum dots with surface modification. *Materials Letters*, *61*, 1641-1644. https://doi.org/10.1016/j.matlet.2006.07.105

Guo, R. F., & Ward, P. A. (2005). Role of C5a in inflammatory responses. *Annu Rev Immunol*, *23*, 821-852. https://doi.org/10.1146/annurev.immunol.23.021704.115835

Gupta, R., Mehra, N. K., & Jain, N. K. (2014). Fucosylated multiwalled carbon nanotubes for Kupffer cells targeting for the treatment of cytokine-induced liver damage. *Pharm Res*, *31*(2), 322-334. https://doi.org/10.1007/s11095-013-1162-9

Hadrup, N., Zhernovkov, V., Jacobsen, N. R., Voss, C., Strunz, M., Ansari, M., Schiller, H. B., Halappanavar, S., Poulsen, S. S., Kholodenko, B., Stoeger, T., Saber, A. T., & Vogel, U. (2020). Acute Phase Response as a Biological Mechanism-of-Action of (Nano)particle-Induced Cardiovascular Disease. *Small*, *16*(21), e1907476. https://doi.org/10.1002/smll.201907476

Hardman, R. (2006). A toxicologic review of quantum dots: toxicity depends on physicochemical and environmental factors. *Environ Health Perspect*, *114*(2), 165-172. https://doi.org/10.1289/ehp.8284

Harris, J. M., & Chess, R. B. (2003). Effect of pegylation on pharmaceuticals. *Nat Rev Drug Discov*, *2*(3), 214-221. https://doi.org/10.1038/nrd1033

Hashimoto, Y., Moki, T., Takizawa, T., Shiratsuchi, A., & Nakanishi, Y. (2007). Evidence for phagocytosis of influenza virus-infected, apoptotic cells by neutrophils and macrophages in mice. *J Immunol*, *178*(4), 2448-2457. https://doi.org/10.4049/jimmunol.178.4.2448

Hawley, K. L., Cruz, A. R., Benjamin, S. J., La Vake, C. J., Cervantes, J. L., LeDoyt, M., Ramirez, L. G., Mandich, D., Fiel-Gan, M., Caimano, M. J., Radolf, J. D., & Salazar, J. C. (2017). IFNγ Enhances CD64-Potentiated Phagocytosis of Treponema pallidum Opsonized with Human Syphilitic Serum by Human Macrophages. *Front Immunol*, *8*, 1227. https://doi.org/10.3389/fimmu.2017.01227

Headley, M. B., Bins, A., Nip, A., Roberts, E. W., Looney, M. R., Gerard, A., & Krummel, M. F. (2016). Visualization of immediate immune responses to pioneer metastatic cells in the lung. *Nature*, *531*(7595), 513-517. https://doi.org/10.1038/nature16985

Hellstrand, E., Lynch, I., Andersson, A., Drakenberg, T., Dahlbäck, B., Dawson, K. A., Linse, S., & Cedervall, T. (2009). Complete high-density lipoproteins in nanoparticle corona. *Febs j*, *276*(12), 3372-3381. https://doi.org/10.1111/j.1742-4658.2009.07062.x

Hermann, D. M., & Gunzer, M. (2019). Polymorphonuclear Neutrophils Play a Decisive Role for Brain Injury and Neurological Recovery Poststroke. *Stroke*, *50*(3), e40-e41. https://doi.org/10.1161/strokeaha.118.021564

Hochella, M. F., Jr., Mogk, D. W., Ranville, J., Allen, I. C., Luther, G. W., Marr, L. C., McGrail, B. P., Murayama, M., Qafoku, N. P., Rosso, K. M., Sahai, N., Schroeder, P. A., Vikesland, P., Westerhoff, P., & Yang, Y. (2019). Natural, incidental, and engineered nanomaterials and their impacts on the Earth system. *Science*, *363*(6434). https://doi.org/10.1126/science.aau8299

Hogg, J. C., & Doerschuk, C. M. (1995). Leukocyte traffic in the lung. *Annu Rev Physiol*, *57*, 97-114. https://doi.org/10.1146/annurev.ph.57.030195.000525

Holian, A., Hamilton, R., & Scheule, R. K. (1991). Mechanistic aspects of cromolyn sodium action on the alveolar macrophage: inhibition of stimulation by soluble agonists. *Agents Actions*, *33*(3-4), 318-325. https://doi.org/10.1007/bf01986580

Hu, Z., Cano, I., & D'Amore, P. A. (2021). Update on the Role of the Endothelial Glycocalyx in Angiogenesis and Vascular Inflammation. *Front Cell Dev Biol*, *9*, 734276. https://doi.org/10.3389/fcell.2021.734276

Huang, J., Wang, L., Lin, R., Wang, A. Y., Yang, L., Kuang, M., Qian, W., & Mao, H. (2013). Casein-coated iron oxide nanoparticles for high MRI contrast enhancement and efficient cell targeting. *ACS Appl Mater Interfaces*, *5*(11), 4632-4639. https://doi.org/10.1021/am400713j

Huang, X., Teng, X., Chen, D., Tang, F., & He, J. (2010). The effect of the shape of mesoporous silica nanoparticles on cellular uptake and cell function. *Biomaterials*, *31*(3), 438-448. https://doi.org/10.1016/j.biomaterials.2009.09.060

Huber-Lang, M., Younkin, E. M., Sarma, J. V., Riedemann, N., McGuire, S. R., Lu, K. T., Kunkel, R., Younger, J. G., Zetoune, F. S., & Ward, P. A. (2002). Generation of C5a by phagocytic cells. *Am J Pathol*, *161*(5), 1849-1859. https://doi.org/10.1016/s0002-9440(10)64461-6

Hussell, T., & Bell, T. J. (2014). Alveolar macrophages: plasticity in a tissue-specific context. *Nat Rev Immunol*, *14*(2), 81-93. https://doi.org/10.1038/nri3600

Hwang, T. L., Aljuffali, I. A., Hung, C. F., Chen, C. H., & Fang, J. Y. (2015). The impact of cationic solid lipid nanoparticles on human neutrophil activation and formation of neutrophil extracellular traps (NETs). *Chem Biol Interact*, *235*, 106-114. https://doi.org/10.1016/j.cbi.2015.04.011

Ichinose, M., Sugiura, H., Yamagata, S., Koarai, A., & Shirato, K. (2000). Increase in reactive nitrogen

species production in chronic obstructive pulmonary disease airways. *Am J Respir Crit Care Med*, *162*(2 Pt 1), 701-706. https://doi.org/10.1164/ajrccm.162.2.9908132

International Organization for Standardization. (2008). Technical Specification: Nanotechnologies—terminology and Definitions for Nano-objects—Nanoparticle, Nanofibre and Nanoplate.

Ishikawa, E., Mori, D., & Yamasaki, S. (2017). Recognition of Mycobacterial Lipids by Immune Receptors. *Trends Immunol*, *38*(1), 66-76. https://doi.org/10.1016/j.it.2016.10.009

Islam, M. N., Das, S. R., Emin, M. T., Wei, M., Sun, L., Westphalen, K., Rowlands, D. J., Quadri, S. K., Bhattacharya, S., & Bhattacharya, J. (2012). Mitochondrial transfer from bone-marrow-derived stromal cells to pulmonary alveoli protects against acute lung injury. *Nat Med*, *18*(5), 759-765. https://doi.org/10.1038/nm.2736

Jamalipour Soufi, G., & Iravani, S. (2020). Eco-friendly and sustainable synthesis of biocompatible nanomaterials for diagnostic imaging: current challenges and future perspectives [10.1039/D0GC00734J]. *Green Chemistry*, *22*(9), 2662-2687. https://doi.org/10.1039/D0GC00734J

Jeevanandam, J., Barhoum, A., Chan, Y. S., Dufresne, A., & Danquah, M. K. (2018). Review on nanoparticles and nanostructured materials: history, sources, toxicity and regulations. *Beilstein J Nanotechnol*, *9*, 1050-1074. https://doi.org/10.3762/bjnano.9.98

Jorch, S. K., & Kubes, P. (2017). An emerging role for neutrophil extracellular traps in noninfectious disease. *Nat Med*, *23*(3), 279-287. https://doi.org/10.1038/nm.4294

Kagawa, J. (2002). Health effects of diesel exhaust emissions--a mixture of air pollutants of worldwide concern. *Toxicology*, *181-182*, 349-353. https://doi.org/10.1016/s0300-483x(02)00461-4

Katayama, Y., Hidalgo, A., Chang, J., Peired, A., & Frenette, P. S. (2005). CD44 is a physiological E-selectin ligand on neutrophils. *J Exp Med*, *201*(8), 1183-1189. https://doi.org/10.1084/jem.20042014

Khan, A. I., Kerfoot, S. M., Heit, B., Liu, L., Andonegui, G., Ruffell, B., Johnson, P., & Kubes, P. (2004). Role of CD44 and hyaluronan in neutrophil recruitment. *J Immunol*, *173*(12), 7594-7601. https://doi.org/10.4049/jimmunol.173.12.7594

Khan, Z., Shen, X. Z., Bernstein, E. A., Giani, J. F., Eriguchi, M., Zhao, T. V., Gonzalez-Villalobos, R. A., Fuchs, S., Liu, G. Y., & Bernstein, K. E. (2017). Angiotensin-converting enzyme enhances the oxidative response and bactericidal activity of neutrophils. *Blood*, *130*(3), 328-339. https://doi.org/10.1182/blood-2016-11-752006

Khandoga, A., Kessler, J. S., Meissner, H., Hanschen, M., Corada, M., Motoike, T., Enders, G., Dejana, E., & Krombach, F. (2005). Junctional adhesion molecule-A deficiency increases hepatic ischemia-reperfusion injury despite reduction of neutrophil transendothelial migration. *Blood*, *106*(2), 725-733. https://doi.org/10.1182/blood-2004-11-4416

Khandoga, A., Stoeger, T., Khandoga, A. G., Bihari, P., Karg, E., Ettehadieh, D., Lakatos, S., Fent, J., Schulz, H., & Krombach, F. (2010). Platelet adhesion and fibrinogen deposition in murine microvessels upon inhalation of nanosized carbon particles. *J Thromb Haemost*, *8*(7), 1632-1640. https://doi.org/10.1111/j.1538-7836.2010.03904.x

Khreis, H., Kelly, C., Tate, J., Parslow, R., Lucas, K., & Nieuwenhuijsen, M. (2017). Exposure to traffic-related air pollution and risk of development of childhood asthma: A systematic review and meta-analysis. *Environ Int*, *100*, 1-31. https://doi.org/10.1016/j.envint.2016.11.012

Kienle, K., Glaser, K. M., Eickhoff, S., Mihlan, M., Knöpper, K., Reátegui, E., Epple, M. W., Gunzer, M., Baumeister, R., Tarrant, T. K., Germain, R. N., Irimia, D., Kastenmüller, W., & Lämmermann, T. (2021). Neutrophils self-limit swarming to contain bacterial growth in vivo. *Science*, *372*(6548). https://doi.org/10.1126/science.abe7729

Kim, N. D., & Luster, A. D. (2015). The role of tissue resident cells in neutrophil recruitment. *Trends Immunol*, *36*(9), 547-555. https://doi.org/10.1016/j.it.2015.07.007

Kittelson, D. B. (2000). RECENT MEASUREMENTS OF NANOPARTICLE EMISSIONS FROM ENGINES.

Kittelson, D. B. (2001). Recent measurements of nanoparticle emissions from engines. *Current Research on Diesel Exhaust Particles*, *9*, 451-457.

Klebanoff, S. J., Kettle, A. J., Rosen, H., Winterbourn, C. C., & Nauseef, W. M. (2013). Myeloperoxidase: a front-line defender against phagocytosed microorganisms. *J Leukoc Biol*, *93*(2), 185-198. https://doi.org/10.1189/jlb.0712349

Klibanov, A. L., Maruyama, K., Torchilin, V. P., & Huang, L. (1990). Amphipathic polyethyleneglycols effectively prolong the circulation time of liposomes. *FEBS Lett*, *268*(1), 235-237. https://doi.org/10.1016/0014-5793(90)81016-h

Knox, E. G. (2005). Oil combustion and childhood cancers. *J Epidemiol Community Health*, *59*(9), 755-760. https://doi.org/10.1136/jech.2004.031674

Knudsen, L., & Ochs, M. (2018). The micromechanics of lung alveoli: structure and function of surfactant and tissue components. *Histochem Cell Biol*, *150*(6), 661-676. https://doi.org/10.1007/s00418-018-1747-9

Kobayashi, S. D., Malachowa, N., & DeLeo, F. R. (2018). Neutrophils and Bacterial Immune Evasion. *J Innate Immun*, *10*(5-6), 432-441. https://doi.org/10.1159/000487756

Kolaczkowska, E., & Kubes, P. (2013). Neutrophil recruitment and function in health and inflammation. *Nat Rev Immunol*, *13*(3), 159-175. https://doi.org/10.1038/nri3399

Kopf, M., Schneider, C., & Nobs, S. P. (2015). The development and function of lung-resident macrophages and dendritic cells. *Nat Immunol*, *16*(1), 36-44. https://doi.org/10.1038/ni.3052

Kramer, K., Voss, H. P., Grimbergen, J. A., Mills, P. A., Huetteman, D., Zwiers, L., & Brockway, B. (2000). Telemetric monitoring of blood pressure in freely moving mice: a preliminary study. *Lab Anim*, *34*(3), 272-280. https://doi.org/10.1258/002367700780384663

Kreyling, W. G., Hirn, S., & Schleh, C. (2010). Nanoparticles in the lung. *Nat Biotechnol*, *28*(12), 1275-1276. https://doi.org/10.1038/nbt.1735

Krummel, M. F., Bartumeus, F., & Gérard, A. (2016). T cell migration, search strategies and mechanisms. *Nat Rev Immunol*, *16*(3), 193-201. https://doi.org/10.1038/nri.2015.16

Kuhnle, G. E., Leipfinger, F. H., & Goetz, A. E. (1993). Measurement of microhemodynamics in the ventilated rabbit lung by intravital fluorescence microscopy. *J Appl Physiol (1985)*, *74*(3), 1462-1471. https://doi.org/10.1152/jappl.1993.74.3.1462

Kuroda, E., Ozasa, K., Temizoz, B., Ohata, K., Koo, C. X., Kanuma, T., Kusakabe, T., Kobari, S., Horie, M., Morimoto, Y., Nakajima, S., Kabashima, K., Ziegler, S. F., Iwakura, Y., Ise, W., Kurosaki, T., Nagatake, T., Kunisawa, J., Takemura, N., . . . Ishii, K. J. (2016). Inhaled Fine Particles Induce Alveolar Macrophage Death and Interleukin-1α Release to Promote Inducible Bronchus-Associated Lymphoid Tissue Formation. *Immunity*, *45*(6), 1299-1310. https://doi.org/10.1016/j.immuni.2016.11.010

Lagassé, H. A., Anidi, I. U., Craig, J. M., Limjunyawong, N., Poupore, A. K., Mitzner, W., & Scott, A.

L. (2016). Recruited monocytes modulate malaria-induced lung injury through CD36-mediated clearance of sequestered infected erythrocytes. *J Leukoc Biol*, *99*(5), 659-671. https://doi.org/10.1189/jlb.4HI0315-130RRR

Lai, Y. C., Potoka, K. C., Champion, H. C., Mora, A. L., & Gladwin, M. T. (2014). Pulmonary arterial hypertension: the clinical syndrome. *Circ Res*, *115*(1), 115-130. https://doi.org/10.1161/circresaha.115.301146

Lam, C. W., James, J. T., McCluskey, R., & Hunter, R. L. (2004). Pulmonary toxicity of single-wall carbon nanotubes in mice 7 and 90 days after intratracheal instillation. *Toxicol Sci*, *77*(1), 126-134. https://doi.org/10.1093/toxsci/kfg243

Lämmermann, T., Afonso, P. V., Angermann, B. R., Wang, J. M., Kastenmüller, W., Parent, C. A., & Germain, R. N. (2013). Neutrophil swarms require LTB4 and integrins at sites of cell death in vivo. *Nature*, *498*(7454), 371-375. https://doi.org/10.1038/nature12175

Lasic, D. D., Martin, F. J., Gabizon, A., Huang, S. K., & Papahadjopoulos, D. (1991). Sterically stabilized liposomes: a hypothesis on the molecular origin of the extended circulation times. *Biochim Biophys Acta*, *1070*(1), 187-192. https://doi.org/10.1016/0005-2736(91)90162-2

Lee, D. H., Choi, S. Y., Jung, K. K., Yang, J. Y., Jeong, J. Y., Oh, J. H., Kim, S. H., & Lee, J. H. (2021). The Research of Toxicity and Sensitization Potential of PEGylated Silver and Gold Nanomaterials. *Toxics*, *9*(12). https://doi.org/10.3390/toxics9120355

Lee, V., McMahan, R. S., Hu, X., Gao, X., Faustman, E. M., Griffith, W. C., Kavanagh, T. J., Eaton, D. L., McGuire, J. K., & Parks, W. C. (2015). Amphiphilic polymer-coated CdSe/ZnS quantum dots induce pro-inflammatory cytokine expression in mouse lung epithelial cells and macrophages. *Nanotoxicology*, *9*(3), 336-343. https://doi.org/10.3109/17435390.2014.930532

Legrand, F., Driss, V., Delbeke, M., Loiseau, S., Hermann, E., Dombrowicz, D., & Capron, M. (2010). Human eosinophils exert TNF-α and granzyme A-mediated tumoricidal activity toward colon carcinoma cells. *J Immunol*, *185*(12), 7443-7451. https://doi.org/10.4049/jimmunol.1000446

Leiva-Juárez, M. M., Kolls, J. K., & Evans, S. E. (2018). Lung epithelial cells: therapeutically inducible effectors of antimicrobial defense. *Mucosal Immunol*, *11*(1), 21-34. https://doi.org/10.1038/mi.2017.71

Ley, K., Laudanna, C., Cybulsky, M. I., & Nourshargh, S. (2007). Getting to the site of inflammation: the leukocyte adhesion cascade updated. *Nat Rev Immunol*, *7*(9), 678-689. https://doi.org/10.1038/nri2156

Li, Z., Luo, G., Hu, W. P., Hua, J. L., Geng, S., Chu, P. K., Zhang, J., Wang, H., & Yu, X. F. (2020). Mediated Drug Release from Nanovehicles by Black Phosphorus Quantum Dots for Efficient Therapy of Chronic Obstructive Pulmonary Disease. *Angew Chem Int Ed Engl*, *59*(46), 20568-20576. https://doi.org/10.1002/anie.202008379

Lim, C. S., Porter, D. W., Orandle, M. S., Green, B. J., Barnes, M. A., Croston, T. L., Wolfarth, M. G., Battelli, L. A., Andrew, M. E., Beezhold, D. H., Siegel, P. D., & Ma, Q. (2020). Resolution of Pulmonary Inflammation Induced by Carbon Nanotubes and Fullerenes in Mice: Role of Macrophage Polarization. *Front Immunol*, *11*, 1186. https://doi.org/10.3389/fimmu.2020.01186

Liu, F., Cheng, X., Wu, S., Hu, B., Yang, C., Deng, S., & Shi, Q. (2022). Nickel oxide nanoparticles

induce apoptosis and ferroptosis in airway epithelial cells via ATF3. *Environ Toxicol*. https://doi.org/10.1002/tox.23467

Liu, J., Li, R., & Yang, B. (2020). Carbon Dots: A New Type of Carbon-Based Nanomaterial with Wide Applications. *ACS Central Science*, *6*(12), 2179-2195. https://doi.org/10.1021/acscentsci.0c01306

Liu, S., Jørgensen, J. T., Ljungman, P., Pershagen, G., Bellander, T., Leander, K., Magnusson, P. K. E., Rizzuto, D., Hvidtfeldt, U. A., Raaschou-Nielsen, O., Wolf, K., Hoffmann, B., Brunekreef, B., Strak, M., Chen, J., Mehta, A., Atkinson, R. W., Bauwelinck, M., Varraso, R., . . . Andersen, Z. J. (2021). Long-term exposure to low-level air pollution and incidence of asthma: the ELAPSE project. *Eur Respir J*, *57*(6). https://doi.org/10.1183/13993003.03099-2020

Liu, S., Lim, Y. H., Pedersen, M., Jørgensen, J. T., Amini, H., Cole-Hunter, T., Mehta, A. J., So, R., Mortensen, L. H., Westendorp, R. G. J., Loft, S., Bräuner, E. V., Ketzel, M., Hertel, O., Brandt, J., Jensen, S. S., Christensen, J. H., Sigsgaard, T., Geels, C., . . . Andersen, Z. J. (2021). Long-term air pollution and road traffic noise exposure and COPD: the Danish Nurse Cohort. *Eur Respir J*, *58*(6). https://doi.org/10.1183/13993003.04594-2020

Liu, Y., Hardie, J., Zhang, X., & Rotello, V. M. (2017). Effects of engineered nanoparticles on the innate immune system. *Semin Immunol*, *34*, 25-32. https://doi.org/10.1016/j.smim.2017.09.011

Liz, R., Simard, J. C., Leonardi, L. B., & Girard, D. (2015). Silver nanoparticles rapidly induce atypical human neutrophil cell death by a process involving inflammatory caspases and reactive oxygen species and induce neutrophil extracellular traps release upon cell adhesion. *Int Immunopharmacol*, *28*(1), 616-625. https://doi.org/10.1016/j.intimp.2015.06.030

Looney, M. R., & Headley, M. B. (2020). Live imaging of the pulmonary immune environment. *Cell Immunol*, *350*, 103862. https://doi.org/10.1016/j.cellimm.2018.09.007

Looney, M. R., Thornton, E. E., Sen, D., Lamm, W. J., Glenny, R. W., & Krummel, M. F. (2011). Stabilized imaging of immune surveillance in the mouse lung. *Nat Methods*, *8*(1), 91-96. https://doi.org/10.1038/nmeth.1543

Lorenzo S, G.-F. A. (2013). *Handbook of Immunological properties of Engineered nanomaterials*. Singapore: World scientific.

Ma, Y., Bai, Y., Mao, H., Hong, Q., Yang, D., Zhang, H., Liu, F., Wu, Z., Jin, Q., Zhou, H., Cao, J., Zhao, J., Zhong, X., & Mao, H. (2016). A panel of promoter methylation markers for invasive and noninvasive early detection of NSCLC using a quantum dots-based FRET approach. *Biosens Bioelectron*, *85*, 641-648. https://doi.org/10.1016/j.bios.2016.05.067

Madani, S. Y., Mandel, A., & Seifalian, A. M. (2013). A concise review of carbon nanotube's toxicology. *Nano Rev*, *4*. https://doi.org/10.3402/nano.v4i0.21521

Marchiando, A. M., Graham, W. V., & Turner, J. R. (2010). Epithelial barriers in homeostasis and disease. *Annu Rev Pathol*, *5*, 119-144. https://doi.org/10.1146/annurev.pathol.4.110807.092135

Marchini, T., Wolf, D., Michel, N. A., Mauler, M., Dufner, B., Hoppe, N., Beckert, J., Jäckel, M., Magnani, N., Duerschmied, D., Tasat, D., Alvarez, S., Reinöhl, J., von Zur Muhlen, C., Idzko, M., Bode, C., Hilgendorf, I., Evelson, P., & Zirlik, A. (2016). Acute exposure to air pollution particulate matter aggravates experimental myocardial infarction in mice by potentiating cytokine secretion from lung macrophages. *Basic Res Cardiol*, *111*(4), 44. https://doi.org/10.1007/s00395-016-0562-5

Marki, A., Esko, J. D., Pries, A. R., & Ley, K. (2015). Role of the endothelial surface layer in neutrophil recruitment. *J Leukoc Biol*, *98*(4), 503-515. https://doi.org/10.1189/jlb.3MR0115-011R

Matysiak-Brynda, E., Bujak, P., Augustin, E., Kowalczyk, A., Mazerska, Z., Pron, A., & Nowicka, A. M. (2018). Stable nanoconjugates of transferrin with alloyed quaternary nanocrystals Ag-In-Zn-S as a biological entity for tumor recognition. *Nanoscale*, *10*(3), 1286-1296. https://doi.org/10.1039/c7nr07819f

Mayadas, T. N., Cullere, X., & Lowell, C. A. (2014). The multifaceted functions of neutrophils. *Annu Rev Pathol*, *9*, 181-218. https://doi.org/10.1146/annurev-pathol-020712-164023

McConnachie, L. A., Botta, D., White, C. C., Weldy, C. S., Wilkerson, H. W., Yu, J., Dills, R., Yu, X., Griffith, W. C., Faustman, E. M., Farin, F. M., Gill, S. E., Parks, W. C., Hu, X., Gao, X., Eaton, D. L., & Kavanagh, T. J. (2013). The glutathione synthesis gene Gclm modulates amphiphilic polymer-coated CdSe/ZnS quantum dot-induced lung inflammation in mice. *PLoS One*, *8*(5), e64165. https://doi.org/10.1371/journal.pone.0064165

Medintz, I. L., Uyeda, H. T., Goldman, E. R., & Mattoussi, H. (2005). Quantum dot bioconjugates for imaging, labelling and sensing. *Nat Mater*, *4*(6), 435-446. https://doi.org/10.1038/nmat1390

Melnicoff, M. J., Morahan, P. S., Jensen, B. D., Breslin, E. W., & Horan, P. K. (1988). In vivo labeling of resident peritoneal macrophages. *J Leukoc Biol*, *43*(5), 387-397. https://doi.org/10.1002/jlb.43.5.387

Mikecz, K., Brennan, F. R., Kim, J. H., & Glant, T. T. (1995). Anti-CD44 treatment abrogates tissue oedema and leukocyte infiltration in murine arthritis. *Nat Med*, *1*(6), 558-563. https://doi.org/10.1038/nm0695-558

Milad, N., & Morissette, M. C. (2021). Revisiting the role of pulmonary surfactant in chronic inflammatory lung diseases and environmental exposure. *Eur Respir Rev*, *30*(162). https://doi.org/10.1183/16000617.0077-2021

Misharin, A. V., Morales-Nebreda, L., Reyfman, P. A., Cuda, C. M., Walter, J. M., McQuattie-Pimentel, A. C., Chen, C. I., Anekalla, K. R., Joshi, N., Williams, K. J. N., Abdala-Valencia, H., Yacoub, T. J., Chi, M., Chiu, S., Gonzalez-Gonzalez, F. J., Gates, K., Lam, A. P., Nicholson, T. T., Homan, P. J., . . . Perlman, H. (2017). Monocyte-derived alveolar macrophages drive lung fibrosis and persist in the lung over the life span. *J Exp Med*, *214*(8), 2387-2404. https://doi.org/10.1084/jem.20162152

Mitchell, M. J., Billingsley, M. M., Haley, R. M., Wechsler, M. E., Peppas, N. A., & Langer, R. (2021). Engineering precision nanoparticles for drug delivery. *Nat Rev Drug Discov*, *20*(2), 101-124. https://doi.org/10.1038/s41573-020-0090-8

Miyata, R., & van Eeden, S. F. (2011). The innate and adaptive immune response induced by alveolar macrophages exposed to ambient particulate matter. *Toxicol Appl Pharmacol*, *257*(2), 209-226. https://doi.org/10.1016/j.taap.2011.09.007

Mok, A. C., Mody, C. H., & Li, S. S. (2021). Immune Cell Degranulation in Fungal Host Defence. *J Fungi (Basel)*, *7*(6). https://doi.org/10.3390/jof7060484

Mollah, F., & Tam, S. (2022). Complement Deficiency. In *StatPearls*. StatPearls Publishing

Copyright © 2022, StatPearls Publishing LLC.

Monk, P. N., Scola, A. M., Madala, P., & Fairlie, D. P. (2007). Function, structure and therapeutic potential of complement C5a receptors. *Br J Pharmacol*, *152*(4), 429-448. https://doi.org/10.1038/sj.bjp.0707332

Monopoli, M. P., Aberg, C., Salvati, A., & Dawson, K. A. (2012). Biomolecular coronas provide the biological identity of nanosized materials. *Nat Nanotechnol*, *7*(12), 779-786. https://doi.org/10.1038/nnano.2012.207

Morán, G., Uberti, B., Ortloff, A., & Folch, H. (2018). Aspergillus fumigatus-sensitive IgE is associated with bronchial hypersensitivity in a murine model of neutrophilic airway inflammation. *J Mycol Med*, *28*(1), 128-136. https://doi.org/10.1016/j.mycmed.2017.11.005

Morawska, L., Bofinger, N. D., Kocis, L., & Nwankwoala, A. (1998). Submicrometer and Supermicrometer Particles from Diesel Vehicle Emissions. *Environmental Science & Technology*, *32*(14), 2033-2042. https://doi.org/10.1021/es970826+

Mould, K. J., Moore, C. M., McManus, S. A., McCubbrey, A. L., McClendon, J. D., Griesmer, C. L., Henson, P. M., & Janssen, W. J. (2021). Airspace Macrophages and Monocytes Exist in Transcriptionally Distinct Subsets in Healthy Adults. *Am J Respir Crit Care Med*, *203*(8), 946-956. https://doi.org/10.1164/rccm.202005-1989OC

Moyano, D. F., Liu, Y., Peer, D., & Rotello, V. M. (2016). Modulation of Immune Response Using Engineered Nanoparticle Surfaces. *Small*, *12*(1), 76-82. https://doi.org/10.1002/smll.201502273

Mukae, H., Vincent, R., Quinlan, K., English, D., Hards, J., Hogg, J. C., & van Eeden, S. F. (2001). The effect of repeated exposure to particulate air pollution (PM10) on the bone marrow. *Am J Respir Crit Care Med*, *163*(1), 201-209. https://doi.org/10.1164/ajrccm.163.1.2002039

Muñoz, L. E., Bilyy, R., Biermann, M. H., Kienhöfer, D., Maueröder, C., Hahn, J., Brauner, J. M., Weidner, D., Chen, J., Scharin-Mehlmann, M., Janko, C., Friedrich, R. P., Mielenz, D., Dumych, T., Lootsik, M. D., Schauer, C., Schett, G., Hoffmann, M., Zhao, Y., & Herrmann, M. (2016). Nanoparticles size-dependently initiate self-limiting NETosis-driven inflammation. *Proc Natl Acad Sci U S A*, *113*(40), E5856-e5865. https://doi.org/10.1073/pnas.1602230113

Najafi-Hajivar, S., Zakeri-Milani, P., Mohammadi, H., Niazi, M., Soleymani-Goloujeh, M., Baradaran, B., & Valizadeh, H. (2016). Overview on experimental models of interactions between nanoparticles and the immune system. *Biomed Pharmacother*, *83*, 1365-1378. https://doi.org/10.1016/j.biopha.2016.08.060

Najar, M., Fayyad-Kazan, M., Meuleman, N., Bron, D., Fayyad-Kazan, H., & Lagneaux, L. (2018a). Immunomodulatory effects of foreskin mesenchymal stromal cells on natural killer cells. *J Cell Physiol*, *233*(7), 5243-5254. https://doi.org/10.1002/jcp.26305

Najar, M., Fayyad-Kazan, M., Meuleman, N., Bron, D., Fayyad-Kazan, H., & Lagneaux, L. (2018b). Mesenchymal stromal cells of the bone marrow and natural killer cells: cell interactions and cross modulation. *J Cell Commun Signal*, *12*(4), 673-688. https://doi.org/10.1007/s12079-018-0448-4

Narasaraju, T., Yang, E., Samy, R. P., Ng, H. H., Poh, W. P., Liew, A. A., Phoon, M. C., van Rooijen, N., & Chow, V. T. (2011). Excessive neutrophils and neutrophil extracellular traps contribute to acute lung injury of influenza pneumonitis. *Am J Pathol*, *179*(1), 199-210. https://doi.org/10.1016/j.ajpath.2011.03.013

Nascimento, T. L., Hillaireau, H., Vergnaud, J., & Fattal, E. (2016). Lipid-based nanosystems for CD44 targeting in cancer treatment: recent significant advances, ongoing challenges and unmet needs. *Nanomedicine (Lond)*, *11*(14), 1865-1887. https://doi.org/10.2217/nnm-2016-5000

Naumenko, V., Turk, M., Jenne, C. N., & Kim, S. J. (2018). Neutrophils in viral infection. *Cell Tissue Res*, *371*(3), 505-516. https://doi.org/10.1007/s00441-017-2763-0

Nauseef, W. M., & Borregaard, N. (2014). Neutrophils at work. *Nat Immunol*, *15*(7), 602-611. https://doi.org/10.1038/ni.2921

Nekolla, K., Kick, K., Sellner, S., Mildner, K., Zahler, S., Zeuschner, D., Krombach, F., & Rehberg, M. (2016). Influence of Surface Modifications on the Spatiotemporal Microdistribution of Quantum Dots In Vivo. *Small*, *12*(19), 2641-2651. https://doi.org/10.1002/smll.201600071

Németh, T., Sperandio, M., & Mócsai, A. (2020). Neutrophils as emerging therapeutic targets. *Nat Rev Drug Discov*, *19*(4), 253-275. https://doi.org/10.1038/s41573-019-0054-z

Nemmar, A., Hoet, P. H., Vermylen, J., Nemery, B., & Hoylaerts, M. F. (2004). Pharmacological stabilization of mast cells abrogates late thrombotic events induced by diesel exhaust particles in hamsters. *Circulation*, *110*(12), 1670-1677. https://doi.org/10.1161/01.Cir.0000142053.13921.21

Neupane, A. S., Willson, M., Chojnacki, A. K., Vargas, E. S. C. F., Morehouse, C., Carestia, A., Keller, A. E., Peiseler, M., DiGiandomenico, A., Kelly, M. M., Amrein, M., Jenne, C., Thanabalasuriar, A., & Kubes, P. (2020). Patrolling Alveolar Macrophages Conceal Bacteria from the Immune System to Maintain Homeostasis. *Cell*, *183*(1), 110-125.e111. https://doi.org/10.1016/j.cell.2020.08.020

Newton, A. H., Cardani, A., & Braciale, T. J. (2016). The host immune response in respiratory virus infection: balancing virus clearance and immunopathology. *Semin Immunopathol*, *38*(4), 471-482. https://doi.org/10.1007/s00281-016-0558-0

Nguyen, K. C., Rippstein, P., Tayabali, A. F., & Willmore, W. G. (2015). Mitochondrial Toxicity of Cadmium Telluride Quantum Dot Nanoparticles in Mammalian Hepatocytes. *Toxicol Sci*, *146*(1), 31-42. https://doi.org/10.1093/toxsci/kfv068

Nimmerjahn, F., & Ravetch, J. V. (2008). Fcgamma receptors as regulators of immune responses. *Nat Rev Immunol*, *8*(1), 34-47. https://doi.org/10.1038/nri2206

Oberdörster, G., Sharp, Z., Atudorei, V., Elder, A., Gelein, R., Kreyling, W., & Cox, C. (2004). Translocation of inhaled ultrafine particles to the brain. *Inhal Toxicol*, *16*(6-7), 437-445. https://doi.org/10.1080/08958370490439597

Oberdörster, G., Sharp, Z., Atudorei, V., Elder, A., Gelein, R., Lunts, A., Kreyling, W., & Cox, C. (2002). Extrapulmonary translocation of ultrafine carbon particles following whole-body inhalation exposure of rats. *J Toxicol Environ Health A*, *65*(20), 1531-1543. https://doi.org/10.1080/00984100290071658

Ochi, H., Iijima, T., & Ushiyama, A. (2019). Intra-vital Observation of Lung Water Retention Following Intravenous Injection of Anti-MHC-class I (H-2K) Monoclonal Antibody in Mice. *In Vivo*, *33*(5), 1477-1484. https://doi.org/10.21873/invivo.11627

Ochs, M., Nenadic, I., Fehrenbach, A., Albes, J. M., Wahlers, T., Richter, J., & Fehrenbach, H. (1999). Ultrastructural alterations in intraalveolar surfactant subtypes after experimental ischemia and reperfusion. *Am J Respir Crit Care Med*, *160*(2), 718-724. https://doi.org/10.1164/ajrccm.160.2.9809060

Olajuyin, A. M., Zhang, X., & Ji, H. L. (2019). Alveolar type 2 progenitor cells for lung injury repair. *Cell Death Discov*, *5*, 63. https://doi.org/10.1038/s41420-019-0147-9

Organization, W. H. (2016). Ambient air pollution: A global assessment of exposure and burden of disease.

Owens, D. E., 3rd, & Peppas, N. A. (2006). Opsonization, biodistribution, and pharmacokinetics of polymeric nanoparticles. *Int J Pharm*, *307*(1), 93-102. https://doi.org/10.1016/j.ijpharm.2005.10.010

Papayannopoulos, V. (2018). Neutrophil extracellular traps in immunity and disease. *Nat Rev Immunol*, *18*(2), 134-147. https://doi.org/10.1038/nri.2017.105

Paranjape, A., Haque, T. T., Kiwanuka, K. N., Qayum, A. A., Barnstein, B. O., Finkelman, F. D., Nigrovic, P. A., & Ryan, J. J. (2020). The Fyn-Stat5 cascade is required for Fcγ receptor-mediated mast cell function. *Cell Immunol*, *356*, 104134. https://doi.org/10.1016/j.cellimm.2020.104134

Park, E. J., Peixoto, A., Imai, Y., Goodarzi, A., Cheng, G., Carman, C. V., von Andrian, U. H., & Shimaoka, M. (2010). Distinct roles for LFA-1 affinity regulation during T-cell adhesion, diapedesis, and interstitial migration in lymph nodes. *Blood*, *115*(8), 1572-1581. https://doi.org/10.1182/blood-2009-08-237917

Pei, X., Zhu, Z., Gan, Z., Chen, J., Zhang, X., Cheng, X., Wan, Q., & Wang, J. (2020). PEGylated nano-graphene oxide as a nanocarrier for delivering mixed anticancer drugs to improve anticancer activity. *Sci Rep*, *10*(1), 2717. https://doi.org/10.1038/s41598-020-59624-w

Peng, L., He, M., Chen, B., Wu, Q., Zhang, Z., Pang, D., Zhu, Y., & Hu, B. (2013). Cellular uptake, elimination and toxicity of CdSe/ZnS quantum dots in HepG2 cells. *Biomaterials*, *34*(37), 9545-9558. https://doi.org/10.1016/j.biomaterials.2013.08.038

Peracchia, M. T., Harnisch, S., Pinto-Alphandary, H., Gulik, A., Dedieu, J. C., Desmaële, D., d'Angelo, J., Müller, R. H., & Couvreur, P. (1999). Visualization of in vitro protein-rejecting properties of PEGylated stealth polycyanoacrylate nanoparticles. *Biomaterials*, *20*(14), 1269-1275. https://doi.org/10.1016/s0142-9612(99)00021-6

Petrarca, C., Clemente, E., Amato, V., Pedata, P., Sabbioni, E., Bernardini, G., Iavicoli, I., Cortese, S., Niu, Q., Otsuki, T., Paganelli, R., & Di Gioacchino, M. (2015). Engineered metal based nanoparticles and innate immunity. *Clin Mol Allergy*, *13*(1), 13. https://doi.org/10.1186/s12948-015-0020-1

Petruzzelli, L., Maduzia, L., & Springer, T. A. (1998). Differential requirements for LFA-1 binding to ICAM-1 and LFA-1-mediated cell aggregation. *J Immunol*, *160*(9), 4208-4216.

Pillay, J., den Braber, I., Vrisekoop, N., Kwast, L. M., de Boer, R. J., Borghans, J. A., Tesselaar, K., & Koenderman, L. (2010). In vivo labeling with 2H2O reveals a human neutrophil lifespan of 5.4 days. *Blood*, *116*(4), 625-627. https://doi.org/10.1182/blood-2010-01-259028

Pinkerton, K. E., Green, F. H., Saiki, C., Vallyathan, V., Plopper, C. G., Gopal, V., Hung, D., Bahne, E. B., Lin, S. S., Ménache, M. G., & Schenker, M. B. (2000). Distribution of particulate matter and tissue remodeling in the human lung. *Environ Health Perspect*, *108*(11), 1063-1069. https://doi.org/10.1289/ehp.001081063

Planagumà, A., Domènech, T., Pont, M., Calama, E., García-González, V., López, R., Aulí, M., López, M., Fonquerna, S., Ramos, I., de Alba, J., Nueda, A., Prats, N., Segarra, V., Miralpeix, M., & Lehner, M. D. (2015). Combined anti CXC receptors 1 and 2 therapy is a promising anti-inflammatory treatment for respiratory diseases by reducing neutrophil migration and activation. *Pulm Pharmacol Ther*, *34*, 37-45. https://doi.org/10.1016/j.pupt.2015.08.002

Poole, J. A., Gleason, A. M., Bauer, C., West, W. W., Alexis, N., van Rooijen, N., Reynolds, S. J., Romberger, D. J., & Kielian, T. L. (2012). CD11c(+)/CD11b(+) cells are critical for organic dust-elicited murine lung inflammation. *Am J Respir Cell Mol Biol*, *47*(5), 652-659.

https://doi.org/10.1165/rcmb.2012-0095OC

Poplimont, H., Georgantzoglou, A., Boulch, M., Walker, H. A., Coombs, C., Papaleonidopoulou, F., & Sarris, M. (2020). Neutrophil Swarming in Damaged Tissue Is Orchestrated by Connexins and Cooperative Calcium Alarm Signals. *Curr Biol*, *30*(14), 2761-2776.e2767. https://doi.org/10.1016/j.cub.2020.05.030

Poupot, R., Goursat, C., & Fruchon, S. (2018). Multivalent nanosystems: targeting monocytes/macrophages. *Int J Nanomedicine*, *13*, 5511-5521. https://doi.org/10.2147/ijn.S146192

Praetner, M., Rehberg, M., Bihari, P., Lerchenberger, M., Uhl, B., Holzer, M., Eichhorn, M. E., Fürst, R., Perisic, T., Reichel, C. A., Welsch, U., & Krombach, F. (2010). The contribution of the capillary endothelium to blood clearance and tissue deposition of anionic quantum dots in vivo. *Biomaterials*, *31*(26), 6692-6700. https://doi.org/10.1016/j.biomaterials.2010.05.051

Quintero, O. A., & Wright, J. R. (2002). Clearance of surfactant lipids by neutrophils and macrophages isolated from the acutely inflamed lung. *Am J Physiol Lung Cell Mol Physiol*, *282*(2), L330-339. https://doi.org/10.1152/ajplung.00190.2001

Rabolli, V., Badissi, A. A., Devosse, R., Uwambayinema, F., Yakoub, Y., Palmai-Pallag, M., Lebrun, A., De Gussem, V., Couillin, I., Ryffel, B., Marbaix, E., Lison, D., & Huaux, F. (2014). The alarmin IL-1α is a master cytokine in acute lung inflammation induced by silica micro- and nanoparticles. *Part Fibre Toxicol*, *11*, 69. https://doi.org/10.1186/s12989-014-0069-x

Rehberg, M., Leite, C. F., Mildner, K., Horstkotte, J., Zeuschner, D., & Krombach, F. (2012). Surface chemistry of quantum dots determines their behavior in postischemic tissue. *ACS Nano*, *6*(2), 1370-1379. https://doi.org/10.1021/nn204187c

Rehberg, M., Nekolla, K., Sellner, S., Praetner, M., Mildner, K., Zeuschner, D., & Krombach, F. (2016). Intercellular Transport of Nanomaterials is Mediated by Membrane Nanotubes In Vivo. *Small*, *12*(14), 1882-1890. https://doi.org/10.1002/smll.201503606

Rehberg, M., Praetner, M., Leite, C. F., Reichel, C. A., Bihari, P., Mildner, K., Duhr, S., Zeuschner, D., & Krombach, F. (2010). Quantum dots modulate leukocyte adhesion and transmigration depending on their surface modification. *Nano Lett*, *10*(9), 3656-3664. https://doi.org/10.1021/nl102100m

Ren, L., Wang, L., Rehberg, M., Stoeger, T., Zhang, J., & Chen, S. (2021). Applications and Immunological Effects of Quantum Dots on Respiratory System. *Front Immunol*, *12*, 795232. https://doi.org/10.3389/fimmu.2021.795232

Riedemann, N. C., Guo, R. F., Bernacki, K. D., Reuben, J. S., Laudes, I. J., Neff, T. A., Gao, H., Speyer, C., Sarma, V. J., Zetoune, F. S., & Ward, P. A. (2003). Regulation by C5a of neutrophil activation during sepsis. *Immunity*, *19*(2), 193-202. https://doi.org/10.1016/s1074-7613(03)00206-1

Riediker, M., Devlin, R. B., Griggs, T. R., Herbst, M. C., Bromberg, P. A., Williams, R. W., & Cascio, W. E. (2004). Cardiovascular effects in patrol officers are associated with fine particulate matter from brake wear and engine emissions. *Part Fibre Toxicol*, *1*(1), 2. https://doi.org/10.1186/1743-8977-1-2

Riehemann, K., Schneider, S. W., Luger, T. A., Godin, B., Ferrari, M., & Fuchs, H. (2009). Nanomedicine--challenge and perspectives. *Angew Chem Int Ed Engl*, *48*(5), 872-897. https://doi.org/10.1002/anie.200802585

Rimal, B., Greenberg, A. K., & Rom, W. N. (2005). Basic pathogenetic mechanisms in silicosis: current understanding. *Curr Opin Pulm Med*, *11*(2), 169-173. https://doi.org/10.1097/01.mcp.0000152998.11335.24

Rios de la Rosa, J. M., Tirella, A., Gennari, A., Stratford, I. J., & Tirelli, N. (2017). The CD44-Mediated Uptake of Hyaluronic Acid-Based Carriers in Macrophages. *Adv Healthc Mater*, *6*(4). https://doi.org/10.1002/adhm.201601012

Ristovski, Z. D., Morawska, L., Bofinger, N. D., & Hitchins, J. (1998). Submicrometer and Supermicrometer Particulate Emission from Spark Ignition Vehicles. *Environmental Science & Technology*, *32*(24), 3845-3852. https://doi.org/10.1021/es980102d

Robe, A., Pic, E., Lassalle, H. P., Bezdetnaya, L., Guillemin, F., & Marchal, F. (2008). Quantum dots in axillary lymph node mapping: biodistribution study in healthy mice. *BMC Cancer*, *8*, 111. https://doi.org/10.1186/1471-2407-8-111

Robichaud, A., Fereydoonzad, L., & Schuessler, T. F. (2015). Delivered dose estimate to standardize airway hyperresponsiveness assessment in mice. *Am J Physiol Lung Cell Mol Physiol*, *308*(8), L837-846. https://doi.org/10.1152/ajplung.00343.2014

Röcker, C., Pötzl, M., Zhang, F., Parak, W. J., & Nienhaus, G. U. (2009). A quantitative fluorescence study of protein monolayer formation on colloidal nanoparticles. *Nat Nanotechnol*, *4*(9), 577-580. https://doi.org/10.1038/nnano.2009.195

Rodriguez-Tirado, C., Kitamura, T., Kato, Y., Pollard, J. W., Condeelis, J. S., & Entenberg, D. (2016). Long-term High-Resolution Intravital Microscopy in the Lung with a Vacuum Stabilized Imaging Window. *J Vis Exp*(116). https://doi.org/10.3791/54603

Rosales, C. (2018). Neutrophil: A Cell with Many Roles in Inflammation or Several Cell Types? *Front Physiol*, *9*, 113. https://doi.org/10.3389/fphys.2018.00113

Sadeghi-Hashjin, G., Nijkamp, F. P., Henricks, P. A., & Folkerts, G. (2002). Sodium cromoglycate and doxantrazole are oxygen radical scavengers. *Eur Respir J*, *20*(4), 867-872. https://doi.org/10.1183/09031936.02.00382002

Saitoh, Y., Terada, N., Saitoh, S., Ohno, N., Jin, T., & Ohno, S. (2012). Histochemical analyses and quantum dot imaging of microvascular blood flow with pulmonary edema in living mouse lungs by "in vivo cryotechnique". *Histochem Cell Biol*, *137*(2), 137-151. https://doi.org/10.1007/s00418-011-0892-1

Sakuma, T., Pittet, J. F., Jayr, C., & Matthay, M. A. (1993). Alveolar liquid and protein clearance in the absence of blood flow or ventilation in sheep. *J Appl Physiol (1985)*, *74*(1), 176-185. https://doi.org/10.1152/jappl.1993.74.1.176

Santos, A. C., Morais, F., Simões, A., Pereira, I., Sequeira, J. A. D., Pereira-Silva, M., Veiga, F., & Ribeiro, A. (2019). Nanotechnology for the development of new cosmetic formulations. *Expert Opin Drug Deliv*, *16*(4), 313-330. https://doi.org/10.1080/17425247.2019.1585426

Sarraj, B., Ludányi, K., Glant, T. T., Finnegan, A., & Mikecz, K. (2006). Expression of CD44 and L-selectin in the innate immune system is required for severe joint inflammation in the proteoglycan-induced murine model of rheumatoid arthritis. *J Immunol*, *177*(3), 1932-1940. https://doi.org/10.4049/jimmunol.177.3.1932

Schimmel, M., Nur, E., Biemond, B. J., van Mierlo, G. J., Solati, S., Brandjes, D. P., Otten, H. M., Schnog, J. J., & Zeerleder, S. (2013). Nucleosomes and neutrophil activation in sickle cell disease painful crisis. *Haematologica*, *98*(11), 1797-1803. https://doi.org/10.3324/haematol.2013.088021

Schipper, M. L., Iyer, G., Koh, A. L., Cheng, Z., Ebenstein, Y., Aharoni, A., Keren, S., Bentolila, L. A., Li, J., Rao, J., Chen, X., Banin, U., Wu, A. M., Sinclair, R., Weiss, S., & Gambhir, S. S. (2009). Particle size, surface coating, and PEGylation influence the biodistribution of quantum dots in living mice. *Small*, *5*(1), 126-134. https://doi.org/10.1002/smll.200800003

Schmid, O., & Stoeger, T. (2016). Surface area is the biologically most effective dose metric for acute nanoparticle toxicity in the lung. *Journal of Aerosol Science*, *99*, 133-143. https://doi.org/https://doi.org/10.1016/j.jaerosci.2015.12.006

Segal, A. W. (2005). How neutrophils kill microbes. *Annu Rev Immunol*, *23*, 197-223. https://doi.org/10.1146/annurev.immunol.23.021704.115653

Semmler-Behnke, M., Kreyling, W. G., Lipka, J., Fertsch, S., Wenk, A., Takenaka, S., Schmid, G., & Brandau, W. (2008). Biodistribution of 1.4- and 18-nm gold particles in rats. *Small*, *4*(12), 2108-2111. https://doi.org/10.1002/smll.200800922

Semmler, M., Seitz, J., Erbe, F., Mayer, P., Heyder, J., Oberdörster, G., & Kreyling, W. G. (2004). Long-term clearance kinetics of inhaled ultrafine insoluble iridium particles from the rat lung, including transient translocation into secondary organs. *Inhal Toxicol*, *16*(6-7), 453-459. https://doi.org/10.1080/08958370490439650

Shaddick, G., Thomas, M. L., Amini, H., Broday, D., Cohen, A., Frostad, J., Green, A., Gumy, S., Liu, Y., Martin, R. V., Pruss-Ustun, A., Simpson, D., van Donkelaar, A., & Brauer, M. (2018). Data Integration for the Assessment of Population Exposure to Ambient Air Pollution for Global Burden of Disease Assessment. *Environ Sci Technol*, *52*(16), 9069-9078. https://doi.org/10.1021/acs.est.8b02864

Sharma, H. S., & Sharma, A. (2007). Nanoparticles aggravate heat stress induced cognitive deficits, blood-brain barrier disruption, edema formation and brain pathology. *Prog Brain Res*, *162*, 245-273. https://doi.org/10.1016/s0079-6123(06)62013-x

Shimaoka, M., Takagi, J., & Springer, T. A. (2002). Conformational regulation of integrin structure and function. *Annu Rev Biophys Biomol Struct*, *31*, 485-516. https://doi.org/10.1146/annurev.biophys.31.101101.140922

Shivshankar, P., Fekry, B., Eckel-Mahan, K., & Wetsel, R. A. (2020). Circadian Clock and Complement Immune System-Complementary Control of Physiology and Pathology? *Front Cell Infect Microbiol*, *10*, 418. https://doi.org/10.3389/fcimb.2020.00418

Shulman, Z., Shinder, V., Klein, E., Grabovsky, V., Yeger, O., Geron, E., Montresor, A., Bolomini-Vittori, M., Feigelson, S. W., Kirchhausen, T., Laudanna, C., Shakhar, G., & Alon, R. (2009). Lymphocyte crawling and transendothelial migration require chemokine triggering of high-affinity LFA-1 integrin. *Immunity*, *30*(3), 384-396. https://doi.org/10.1016/j.immuni.2008.12.020

Sibi, R., & Dhruv, K. (2020). Biochemical Toxicology: Heavy Metals and Nanomaterials. In I. Muharrem, I. Olcay Kaplan, & O. Gabrijel (Eds.), *Biochemical Toxicology*. IntechOpen. https://doi.org/10.5772/intechopen.90928

Smith, B. R., Ghosn, E. E., Rallapalli, H., Prescher, J. A., Larson, T., Herzenberg, L. A., & Gambhir, S. S. (2014). Selective uptake of single-walled carbon nanotubes by circulating monocytes for enhanced tumour delivery. *Nat Nanotechnol*, *9*(6), 481-487. https://doi.org/10.1038/nnano.2014.62

Soni, S., Wilson, M. R., O'Dea, K. P., Yoshida, M., Katbeh, U., Woods, S. J., & Takata, M. (2016). Alveolar macrophage-derived microvesicles mediate acute lung injury. *Thorax*, *71*(11),

1020-1029. https://doi.org/10.1136/thoraxjnl-2015-208032

Soria-Castro, R., Alfaro-Doblado Á, R., Rodríguez-López, G., Campillo-Navarro, M., Meneses-Preza, Y. G., Galán-Salinas, A., Alvarez-Jimenez, V., Yam-Puc, J. C., Munguía-Fuentes, R., Domínguez-Flores, A., Estrada-Parra, S., Pérez-Tapia, S. M., Chávez-Blanco, A. D., & Chacón-Salinas, R. (2021). TLR2 Regulates Mast Cell IL-6 and IL-13 Production During Listeria monocytogenes Infection. *Front Immunol*, *12*, 650779. https://doi.org/10.3389/fimmu.2021.650779

Srivastava, K. D., Rom, W. N., Jagirdar, J., Yie, T. A., Gordon, T., & Tchou-Wong, K. M. (2002). Crucial role of interleukin-1beta and nitric oxide synthase in silica-induced inflammation and apoptosis in mice. *Am J Respir Crit Care Med*, *165*(4), 527-533. https://doi.org/10.1164/ajrccm.165.4.2106009

Stoeger, T., Reinhard, C., Takenaka, S., Schroeppel, A., Karg, E., Ritter, B., Heyder, J., & Schulz, H. (2006). Instillation of six different ultrafine carbon particles indicates a surface area threshold dose for acute lung inflammation in mice. *Environ Health Perspect*, *114*(3), 328-333. https://doi.org/10.1289/ehp.8266

Stoeger, T., Takenaka, S., Frankenberger, B., Ritter, B., Karg, E., Maier, K., Schulz, H., & Schmid, O. (2009). Deducing in vivo toxicity of combustion-derived nanoparticles from a cell-free oxidative potency assay and metabolic activation of organic compounds. *Environ Health Perspect*, *117*(1), 54-60. https://doi.org/10.1289/ehp.11370

Subramaniam, R., Barnes, P. F., Fletcher, K., Boggaram, V., Hillberry, Z., Neuenschwander, P., & Shams, H. (2014). Protecting against post-influenza bacterial pneumonia by increasing phagocyte recruitment and ROS production. *J Infect Dis*, *209*(11), 1827-1836. https://doi.org/10.1093/infdis/jit830

Suk, J. S., Xu, Q., Kim, N., Hanes, J., & Ensign, L. M. (2016). PEGylation as a strategy for improving nanoparticle-based drug and gene delivery. *Adv Drug Deliv Rev*, *99*(Pt A), 28-51. https://doi.org/10.1016/j.addr.2015.09.012

Sukhanova, A., Bozrova, S., Sokolov, P., Berestovoy, M., Karaulov, A., & Nabiev, I. (2018). Dependence of Nanoparticle Toxicity on Their Physical and Chemical Properties. *Nanoscale Res Lett*, *13*(1), 44. https://doi.org/10.1186/s11671-018-2457-x

Surewaard, B. G., Deniset, J. F., Zemp, F. J., Amrein, M., Otto, M., Conly, J., Omri, A., Yates, R. M., & Kubes, P. (2016). Identification and treatment of the Staphylococcus aureus reservoir in vivo. *J Exp Med*, *213*(7), 1141-1151. https://doi.org/10.1084/jem.20160334

Sweeney, S., Grandolfo, D., Ruenraroengsak, P., & Tetley, T. D. (2015). Functional consequences for primary human alveolar macrophages following treatment with long, but not short, multiwalled carbon nanotubes. *Int J Nanomedicine*, *10*, 3115-3129. https://doi.org/10.2147/ijn.S77867

Swerlick, R. A., Yancey, K. B., & Lawley, T. J. (1988). A direct in vivo comparison of the inflammatory properties of human C5a and C5a des Arg in human skin. *J Immunol*, *140*(7), 2376-2381.

Swerlick, R. A., Yancey, K. B., & Lawley, T. J. (1989). Inflammatory properties of human C5a and C5a des Arg/ in mast cell-depleted human skin. *J Invest Dermatol*, *93*(3), 417-422.

Syenina, A., Jagaraj, C. J., Aman, S. A., Sridharan, A., & St John, A. L. (2015). Dengue vascular leakage is augmented by mast cell degranulation mediated by immunoglobulin Fcγ receptors. *Elife*, *4*. https://doi.org/10.7554/eLife.05291

Tabuchi, A., Mertens, M., Kuppe, H., Pries, A. R., & Kuebler, W. M. (2008). Intravital microscopy of

the murine pulmonary microcirculation. *J Appl Physiol (1985)*, *104*(2), 338-346. https://doi.org/10.1152/japplphysiol.00348.2007

Tackenberg, H., Möller, S., Filippi, M. D., & Laskay, T. (2020). The Small GTPase Cdc42 Is a Major Regulator of Neutrophil Effector Functions. *Front Immunol*, *11*, 1197. https://doi.org/10.3389/fimmu.2020.01197

Takenaka, S., Möller, W., Semmler-Behnke, M., Karg, E., Wenk, A., Schmid, O., Stoeger, T., Jennen, L., Aichler, M., Walch, A., Pokhrel, S., Mädler, L., Eickelberg, O., & Kreyling, W. G. (2012). Efficient internalization and intracellular translocation of inhaled gold nanoparticles in rat alveolar macrophages. *Nanomedicine (Lond)*, *7*(6), 855-865. https://doi.org/10.2217/nnm.11.152

Tam, A., Wadsworth, S., Dorscheid, D., Man, S. F., & Sin, D. D. (2011). The airway epithelium: more than just a structural barrier. *Ther Adv Respir Dis*, *5*(4), 255-273. https://doi.org/10.1177/1753465810396539

Tarbell, J. M., & Cancel, L. M. (2016). The glycocalyx and its significance in human medicine. *J Intern Med*, *280*(1), 97-113. https://doi.org/10.1111/joim.12465

Tasaka, S., Qin, L., Saijo, A., Albelda, S. M., DeLisser, H. M., & Doerschuk, C. M. (2003). Platelet endothelial cell adhesion molecule-1 in neutrophil emigration during acute bacterial pneumonia in mice and rats. *Am J Respir Crit Care Med*, *167*(2), 164-170. https://doi.org/10.1164/rccm.2202011

Taylor, P. R., Martinez-Pomares, L., Stacey, M., Lin, H. H., Brown, G. D., & Gordon, S. (2005). Macrophage receptors and immune recognition. *Annu Rev Immunol*, *23*, 901-944. https://doi.org/10.1146/annurev.immunol.23.021704.115816

Terashima, T., Wiggs, B., English, D., Hogg, J. C., & van Eeden, S. F. (1997). Phagocytosis of small carbon particles (PM10) by alveolar macrophages stimulates the release of polymorphonuclear leukocytes from bone marrow. *Am J Respir Crit Care Med*, *155*(4), 1441-1447. https://doi.org/10.1164/ajrccm.155.4.9105091

Terry, R. J. (1939). A THORACIC WINDOW FOR OBSERVATION OF THE LUNG IN A LIVING ANIMAL. *Science*, *90*(2324), 43-44. https://doi.org/10.1126/science.90.2324.43

Thakur, S. A., Beamer, C. A., Migliaccio, C. T., & Holian, A. (2009). Critical role of MARCO in crystalline silica-induced pulmonary inflammation. *Toxicol Sci*, *108*(2), 462-471. https://doi.org/10.1093/toxsci/kfp011

Thakur, S. A., Hamilton, R. F., Jr., & Holian, A. (2008). Role of scavenger receptor a family in lung inflammation from exposure to environmental particles. *J Immunotoxicol*, *5*(2), 151-157. https://doi.org/10.1080/15476910802085863

Tian, F., Habel, N. C., Yin, R., Hirn, S., Banerjee, A., Ercal, N., Takenaka, S., Estrada, G., Kostarelos, K., Kreyling, W., & Stoeger, T. (2013). Pulmonary DWCNT exposure causes sustained local and low-level systemic inflammatory changes in mice. *Eur J Pharm Biopharm*, *84*(2), 412-420. https://doi.org/10.1016/j.ejpb.2013.03.008

Trapnell, B. C., & Whitsett, J. A. (2002). Gm-CSF regulates pulmonary surfactant homeostasis and alveolar macrophage-mediated innate host defense. *Annu Rev Physiol*, *64*, 775-802. https://doi.org/10.1146/annurev.physiol.64.090601.113847

Tsai, W. C., Strieter, R. M., Mehrad, B., Newstead, M. W., Zeng, X., & Standiford, T. J. (2000). CXC chemokine receptor CXCR2 is essential for protective innate host response in murine Pseudomonas aeruginosa pneumonia. *Infect Immun*, *68*(7), 4289-4296.

https://doi.org/10.1128/iai.68.7.4289-4296.2000

Tsugita, M., Morimoto, N., Tashiro, M., Kinoshita, K., & Nakayama, M. (2017). SR-B1 Is a Silica Receptor that Mediates Canonical Inflammasome Activation. *Cell Rep*, *18*(5), 1298-1311. https://doi.org/10.1016/j.celrep.2017.01.004

Ueki, H., Wang, I. H., Fukuyama, S., Katsura, H., da Silva Lopes, T. J., Neumann, G., & Kawaoka, Y. (2018). In vivo imaging of the pathophysiological changes and neutrophil dynamics in influenza virus-infected mouse lungs. *Proc Natl Acad Sci U S A*, *115*(28), E6622-e6629. https://doi.org/10.1073/pnas.1806265115

Uhl, B., Hirn, S., Mildner, K., Coletti, R., Massberg, S., Reichel, C. A., Rehberg, M., Zeuschner, D., & Krombach, F. (2018). The surface chemistry determines the spatio-temporal interaction dynamics of quantum dots in atherosclerotic lesions. *Nanomedicine (Lond)*, *13*(6), 623-638. https://doi.org/10.2217/nnm-2017-0350

Ursini, C. L., Cavallo, D., Fresegna, A. M., Ciervo, A., Maiello, R., Tassone, P., Buresti, G., Casciardi, S., & Iavicoli, S. (2014). Evaluation of cytotoxic, genotoxic and inflammatory response in human alveolar and bronchial epithelial cells exposed to titanium dioxide nanoparticles. *J Appl Toxicol*, *34*(11), 1209-1219. https://doi.org/10.1002/jat.3038

Vachon, E., Martin, R., Kwok, V., Cherepanov, V., Chow, C. W., Doerschuk, C. M., Plumb, J., Grinstein, S., & Downey, G. P. (2007). CD44-mediated phagocytosis induces inside-out activation of complement receptor-3 in murine macrophages. *Blood*, *110*(13), 4492-4502. https://doi.org/10.1182/blood-2007-02-076539

Vachon, E., Martin, R., Plumb, J., Kwok, V., Vandivier, R. W., Glogauer, M., Kapus, A., Wang, X., Chow, C. W., Grinstein, S., & Downey, G. P. (2006). CD44 is a phagocytic receptor. *Blood*, *107*(10), 4149-4158. https://doi.org/10.1182/blood-2005-09-3808

van de Laar, L., Saelens, W., De Prijck, S., Martens, L., Scott, C. L., Van Isterdael, G., Hoffmann, E., Beyaert, R., Saeys, Y., Lambrecht, B. N., & Guilliams, M. (2016). Yolk Sac Macrophages, Fetal Liver, and Adult Monocytes Can Colonize an Empty Niche and Develop into Functional Tissue-Resident Macrophages. *Immunity*, *44*(4), 755-768. https://doi.org/10.1016/j.immuni.2016.02.017

van Montfoort, N., t Hoen, P. A., Mangsbo, S. M., Camps, M. G., Boross, P., Melief, C. J., Ossendorp, F., & Verbeek, J. S. (2012). Fcγ receptor IIb strongly regulates Fcγ receptor-facilitated T cell activation by dendritic cells. *J Immunol*, *189*(1), 92-101. https://doi.org/10.4049/jimmunol.1103703

Verma, N. K., Fazil, M. H., Ong, S. T., Chalasani, M. L., Low, J. H., Kottaiswamy, A., P, P., Kizhakeyil, A., Kumar, S., Panda, A. K., Freeley, M., Smith, S. M., Boehm, B. O., & Kelleher, D. (2016). LFA-1/ICAM-1 Ligation in Human T Cells Promotes Th1 Polarization through a GSK3β Signaling-Dependent Notch Pathway. *J Immunol*, *197*(1), 108-118. https://doi.org/10.4049/jimmunol.1501264

Vermylen, J., Nemmar, A., Nemery, B., & Hoylaerts, M. F. (2005). Ambient air pollution and acute myocardial infarction. *J Thromb Haemost*, *3*(9), 1955-1961. https://doi.org/10.1111/j.1538-7836.2005.01471.x

Vicente-Manzanares, M., & Sánchez-Madrid, F. (2004). Role of the cytoskeleton during leukocyte responses. *Nat Rev Immunol*, *4*(2), 110-122. https://doi.org/10.1038/nri1268

Vivier, E., & Malissen, B. (2005). Innate and adaptive immunity: specificities and signaling hierarchies revisited. *Nat Immunol*, *6*(1), 17-21. https://doi.org/10.1038/ni1153

Vlcková, A., Ulrich, L., & Babinská, M. (1976). The protective action of disodium cromoglycate on alveolar macrophages in phagocytosis of fibrogenic silica. *Life Sci*, *19*(11), 1727-1735. https://doi.org/10.1016/0024-3205(76)90080-1

Volkov, Y. (2015). Quantum dots in nanomedicine: recent trends, advances and unresolved issues. *Biochem Biophys Res Commun*, *468*(3), 419-427. https://doi.org/10.1016/j.bbrc.2015.07.039

Wabnitz, G. H., Lohneis, P., Kirchgessner, H., Jahraus, B., Gottwald, S., Konstandin, M., Klemke, M., & Samstag, Y. (2010). Sustained LFA-1 cluster formation in the immune synapse requires the combined activities of L-plastin and calmodulin. *Eur J Immunol*, *40*(9), 2437-2449. https://doi.org/10.1002/eji.201040345

Waisman, D., Abramovich, A., Brod, V., Lavon, O., Nurkin, S., Popovski, F., Rotschild, A., & Bitterman, H. (2006). Subpleural microvascular flow velocities and shear rates in normal and septic mechanically ventilated rats. *Shock*, *26*(1), 87-94. https://doi.org/10.1097/01.shk.0000215317.22113.b2

Wang, Y., Tang, Z., Huang, H., Li, J., Wang, Z., Yu, Y., Zhang, C., Li, J., Dai, H., Wang, F., Cai, T., & Tang, N. (2018). Pulmonary alveolar type I cell population consists of two distinct subtypes that differ in cell fate. *Proc Natl Acad Sci U S A*, *115*(10), 2407-2412. https://doi.org/10.1073/pnas.1719474115

Warheit, D. B. (2008). How meaningful are the results of nanotoxicity studies in the absence of adequate material characterization? *Toxicol Sci*, *101*(2), 183-185. https://doi.org/10.1093/toxsci/kfm279

Warheit, D. B., Webb, T. R., Colvin, V. L., Reed, K. L., & Sayes, C. M. (2007). Pulmonary bioassay studies with nanoscale and fine-quartz particles in rats: toxicity is not dependent upon particle size but on surface characteristics. *Toxicol Sci*, *95*(1), 270-280. https://doi.org/10.1093/toxsci/kfl128

Wells, W. A., Thrall, M., Sorokina, A., Fine, J., Krishnamurthy, S., Haroon, A., Rao, B., Shevchuk, M. M., Wolfsen, H. C., Tearney, G. J., & Hariri, L. P. (2019). In Vivo and Ex Vivo Microscopy: Moving Toward the Integration of Optical Imaging Technologies Into Pathology Practice. *Arch Pathol Lab Med*, *143*(3), 288-298. https://doi.org/10.5858/arpa.2018-0298-RA

Westphalen, K., Gusarova, G. A., Islam, M. N., Subramanian, M., Cohen, T. S., Prince, A. S., & Bhattacharya, J. (2014). Sessile alveolar macrophages communicate with alveolar epithelium to modulate immunity. *Nature*, *506*(7489), 503-506. https://doi.org/10.1038/nature12902

Whitsett, J. A., & Alenghat, T. (2015). Respiratory epithelial cells orchestrate pulmonary innate immunity. *Nat Immunol*, *16*(1), 27-35. https://doi.org/10.1038/ni.3045

Wong, C. H., Jenne, C. N., Petri, B., Chrobok, N. L., & Kubes, P. (2013). Nucleation of platelets with blood-borne pathogens on Kupffer cells precedes other innate immunity and contributes to bacterial clearance. *Nat Immunol*, *14*(8), 785-792. https://doi.org/10.1038/ni.2631

Wright, C. D., Mülsch, A., Busse, R., & Osswald, H. (1989). Generation of nitric oxide by human neutrophils. *Biochem Biophys Res Commun*, *160*(2), 813-819. https://doi.org/10.1016/0006-291x(89)92506-0

Wright, S. D., & Silverstein, S. C. (1982). Tumor-promoting phorbol esters stimulate C3b and C3b' receptor-mediated phagocytosis in cultured human monocytes. *J Exp Med*, *156*(4), 1149-1164. https://doi.org/10.1084/jem.156.4.1149

Xia, T., Li, N., & Nel, A. E. (2009). Potential health impact of nanoparticles. *Annu Rev Public Health*, *30*, 137-150. https://doi.org/10.1146/annurev.publhealth.031308.100155

Xiao, D., Qi, H., Teng, Y., Pierre, D., Kutoka, P. T., & Liu, D. (2021). Advances and Challenges of Fluorescent Nanomaterials for Synthesis and Biomedical Applications. *Nanoscale Research Letters*, *16*(1), 167. https://doi.org/10.1186/s11671-021-03613-z

Yada, A., Ebihara, S., Matsumura, K., Endo, S., Maeda, T., Nakamura, A., Akiyama, K., Aiba, S., & Takai, T. (2003). Accelerated antigen presentation and elicitation of humoral response in vivo by FcgammaRIIB- and FcgammaRI/III-mediated immune complex uptake. *Cell Immunol*, *225*(1), 21-32. https://doi.org/10.1016/j.cellimm.2003.09.008

Yang, L., Feuchtinger, A., Möller, W., Ding, Y., Kutschke, D., Möller, G., Schittny, J. C., Burgstaller, G., Hofmann, W., Stoeger, T., Daniel, R., Walch, A., & Schmid, O. (2019). Three-Dimensional Quantitative Co-Mapping of Pulmonary Morphology and Nanoparticle Distribution with Cellular Resolution in Nondissected Murine Lungs. *ACS Nano*, *13*(2), 1029-1041. https://doi.org/10.1021/acsnano.8b07524

Yang, W., Wang, L., Mettenbrink, E. M., DeAngelis, P. L., & Wilhelm, S. (2021). Nanoparticle Toxicology. *Annu Rev Pharmacol Toxicol*, *61*, 269-289. https://doi.org/10.1146/annurev-pharmtox-032320-110338

Yipp, B. G., Kim, J. H., Lima, R., Zbytnuik, L. D., Petri, B., Swanlund, N., Ho, M., Szeto, V. G., Tak, T., Koenderman, L., Pickkers, P., Tool, A. T. J., Kuijpers, T. W., van den Berg, T. K., Looney, M. R., Krummel, M. F., & Kubes, P. (2017). The Lung is a Host Defense Niche for Immediate Neutrophil-Mediated Vascular Protection. *Sci Immunol*, *2*(10). https://doi.org/10.1126/sciimmunol.aam8929

Yohan, D., & Chithrani, B. D. (2014). Applications of nanoparticles in nanomedicine. *J Biomed Nanotechnol*, *10*(9), 2371-2392. https://doi.org/10.1166/jbn.2014.2015

Yona, S., Kim, K. W., Wolf, Y., Mildner, A., Varol, D., Breker, M., Strauss-Ayali, D., Viukov, S., Guilliams, M., Misharin, A., Hume, D. A., Perlman, H., Malissen, B., Zelzer, E., & Jung, S. (2013). Fate mapping reveals origins and dynamics of monocytes and tissue macrophages under homeostasis. *Immunity*, *38*(1), 79-91. https://doi.org/10.1016/j.immuni.2012.12.001

Żelechowska, P., Brzezińska-Błaszczyk, E., Różalska, S., Agier, J., & Kozłowska, E. (2021). Native and IgE-primed rat peritoneal mast cells exert pro-inflammatory activity and migrate in response to yeast zymosan upon Dectin-1 engagement. *Immunol Res*, *69*(2), 176-188. https://doi.org/10.1007/s12026-021-09183-7

Zeng, Z., Surewaard, B. G., Wong, C. H., Geoghegan, J. A., Jenne, C. N., & Kubes, P. (2016). CRIg Functions as a Macrophage Pattern Recognition Receptor to Directly Bind and Capture Blood-Borne Gram-Positive Bacteria. *Cell Host Microbe*, *20*(1), 99-106. https://doi.org/10.1016/j.chom.2016.06.002

Zhang, L. W., Bäumer, W., & Monteiro-Riviere, N. A. (2011). Cellular uptake mechanisms and toxicity of quantum dots in dendritic cells. *Nanomedicine (Lond)*, *6*(5), 777-791. https://doi.org/10.2217/nnm.11.73

Zhang, L. W., & Monteiro-Riviere, N. A. (2009). Mechanisms of quantum dot nanoparticle cellular uptake. *Toxicol Sci*, *110*(1), 138-155. https://doi.org/10.1093/toxsci/kfp087

Zhang, T., Hu, Y., Tang, M., Kong, L., Ying, J., Wu, T., Xue, Y., & Pu, Y. (2015). Liver Toxicity of Cadmium Telluride Quantum Dots (CdTe QDs) Due to Oxidative Stress in Vitro and in Vivo. *Int J Mol Sci*, *16*(10), 23279-23299. https://doi.org/10.3390/ijms161023279

Zhao, C., Wang, X., Wu, L., Wu, W., Zheng, Y., Lin, L., Weng, S., & Lin, X. (2019). Nitrogen-doped carbon quantum dots as an antimicrobial agent against Staphylococcus for the treatment of infected wounds. *Colloids Surf B Biointerfaces*, *179*, 17-27. https://doi.org/10.1016/j.colsurfb.2019.03.042

Zhao, X., & Liu, R. (2012). Recent progress and perspectives on the toxicity of carbon nanotubes at organism, organ, cell, and biomacromolecule levels. *Environ Int*, *40*, 244-255. https://doi.org/10.1016/j.envint.2011.12.003

Zhong, H., Lin, H., Pang, Q., Zhuang, J., Liu, X., Li, X., Liu, J., & Tang, J. (2021). Macrophage ICAM-1 functions as a regulator of phagocytosis in LPS induced endotoxemia. *Inflamm Res*, *70*(2), 193-203. https://doi.org/10.1007/s00011-021-01437-2

Zhu, F., Nair, R. R., Fisher, E. M. C., & Cunningham, T. J. (2019). Humanising the mouse genome piece by piece. *Nat Commun*, *10*(1), 1845. https://doi.org/10.1038/s41467-019-09716-7

7. Appendix

7.1 Laboratory equipment and consumables

7.1.1 Laboratory equipment.

Table 4: The list of laboratory equipment.

Equipment	Type	Manufacturer
Cell culture bench	Thermo Scientific™ Herasafe™ KS	Fisher Scientific GmbH Schwerte, Germany
Centrifuge	3K15	Sigma Laborzentrifugen Osterode am Harz, Germany
Centrifuge	MICRO centrifuge Model SD 220VAC	Carl Roth GmbH + Co. KG Karlsruhe, Germany
CO2 Incubator	CB 150 #01-28940	Binder GmbH Tuttlingen, Germany
Combitips	Advanced®, 5ml	Eppendorf AG Hamburg, Germany
Freezer	Liebherr Mediline	Liebherr GmbH Ochsenhausen, Germany
Fridge	Liebherr Comfort	Liebherr GmbH Ochsenhausen, Germany
Fridge	Liebherr Profiline	Liebherr GmbH Ochsenhausen, Germany
Fridge	Siemens KU18R04	SEG Hausgeräte GmbH München, Germany
Multi-channel pipet	Research plus® 300 µl	Eppendorf AG Hamburg, Germany
Pipettes	10 µl, 20 µl, 100 µl, 200 µl, 1000 µl	STARLAB International GmbH Hamburg, Germany
Pipetting aid	pipetus®-akku	Hirschmann Laborgeräte Eberstadt, Germany
Plate reader	TECAN Infinite® M200 PRO	TECAN Group Ltd. Männedorf, Switzerland
FACS cytometer	BD FACSCanto II flow cytometer	BD Biosciences, State of New Jersey, United States
Ultrasonic homogenisers	SonoPlus HD70	Bachofer， Berlin， Germany

Table 5: Microscope equipment and consumables

Equipment	Type	Manufacturer

Water dipping objective lens	20×, NA 1.0	Carl Zeiss, Oberkochen, Germany
long distance air objective lens	20×, NA 0.4	Olympus, Hamburg, German
water immersion objective	63×, NA 1.0,	Carl Zeiss, Oberkochen, Germany
Beam splitter	T 580 lpxxr	Chroma Technology, Bellows Falls, VT, United States
Microscope	TCS SP5 SMD	Leica, Wetzlar, Germany
EMCCD cameras	Rolera EM-C2 cameras	Qimaging, Surrey, Canada
Imaging software	VisiScope A1 imaging system	Visitron Systems, Puchheim, Germany
Camera	AxioCam MRm	Carl Zeiss, Oberkochen, Germany
Fluorescence Excitation Source	CoolLED pE-4000	CoolLED Ltd, Andover, Great Britain
Gas Incubation System for CO2 and O2	Ibidi Gas Mixer	ibidi GmbH, Gräfelfing, Germany
Heating System	Universal Fit for 1 Chamber	ibidi GmbH, Gräfelfing, Germany
Microscope	Observer.Z1 Inverted Phase Contrast Fluorescence Microscope	Carl Zeiss, Oberkochen, Germany
Microscope	Axiovert 135	Carl Zeiss, Oberkochen, Germany
Microscope	Laser Scanning Confocal Microscope (LSM710)	Carl Zeiss, Oberkochen, Germany
LSFM	Ultramicroscope II	LaVision BioTec GmbH, Bielefeld, Germany
camera	sCMOS	Andor Neo, Abingdon, Oxfordshire
objective lens	MVPLAPO 2×/0.5 NA	Olympus, Tokyo, Japan
zoom body	MVX-10	Olympus, Tokyo, Japan
LED light source	pE-100	CooLED, Andover, United Kingdom
in vivo imaging system	Lumina II	Caliper/Perkin Elmer, Hopkinton, Massachusetts, United States
Electron microscope	FEI-Tecnai 12	FEI Company, Eindhoven, The Netherlands

camera	CCD camera	Megaview, Olympus-SIS, Muenster, Germany
Glass coverslips	25 x 25 mm	VWR, Radnor, USA
Micro Slide	VWR Superfrost Micro Slide	VWR, Radnor, USA

Table 6: List of consumables

Subject	Type	Manufacturer
µ-Slide 8-well	ibiTreat	ibidi GmbH, Gräfelfing, Germany
6-, 12-, 24-, 96-well Cell culture Plate, sterile	CELLSTAR® Cell culture plate	Greiner Bio-One GmbH, Frickenhausen, Germany
96-well ELISA plate	Nunc MaxiSorp™ flat-bottom	Invitrogen by Thermo Fisher Scientific Carlsbad, USA
Cell Counting Chamber	BLAUBRAND® Neubauer Improved, bright-line	Brand GmbH + Co. KG, Werthein, Germany
Cell culture dish	TC Dish 100 mm, standard	SARSTEDT AG & Co. Nümbrecht, Germany
Cell culture dish	TC Dish 100 mm, standard	SARSTEDT AG & Co. Nürmbrecht, Germany
Cell culture flask	cellstar® T25, T75	Greiner Bio-One GmbH Frickenhausen, Germany
Cellulos swabs	Askina® Brauncel	B.Braun Melsungen AG, Melsungen, Germany
Reaction Tubes	0.5 ml, 1.5 ml, 2.0 ml	Eppendorf, Hamburg, Germany
Falcon Tube	15 ml, 50 ml	Corning Incorporated New York, USA
Insulin Syringes	MicroFine™+	BD Biosciences, State of New Jersey, United States
Lab gloves	Nitril® NextGen®	Meditrade GmbH Kiefersfelden, Germany
Parafilm	PARAFILM® M	Bemis Company, Inc. Neenah, USA
Pasteur pipette	Disposable Glass Pasteur Pipettes 230mm	Poulten & Graf GmbH Wertheim, Germany
Pipette tips	10 µl, 200 µl, 1000 µl	Starlab International GmbH Hamburg, Germany
Serological pipettes	5 ml, 10 ml, 25 ml, 50 ml	Greiner Bio-One GmbH Frickenhausen, Germany
Syringe	1ml, 2 ml, 5ml, 10ml and 50ml	B.Braun Melsungen AG Melsungen, Germany

Table 7: List of chemicals

Chemicals	Type	Manufacturer
Cromolyn sodium salt	assay ≥95%	SigmaAldrich, Taufkirchen, Germany
Ketamine	10 %	Serumwerk Bernburg
TNF-α	recombinant mouse TNF-α	R&D Systems, Inc. Steinheim, Deutschland
Triton-X 100	TritonTM -X	SIGMA-ALDRICH GmbH
Trypsin-EDTA (1X)	0.25%	Life Technologies Limited, Paisley, UK
Tween®20	Viscous liquid	SIGMA-ALDRICH GmbH Steinheim, Deutschland
Ultra-pure water	500 ml	Life Technologies Limited, Paisley, UK
Tetrahydrofuran (THF)	assay ⩾99.9%	SigmaAldrich, Taufkirchen, Germany
Dichloromethane (DCM)	assay ⩾99.8%	SigmaAldrich, Taufkirchen, Germany
dibenzyl ether (DBE)	assay ≥98.0%	SigmaAldrich, Taufkirchen, Germany
Saponin Quillaja sp.	Sapogenin content, 20-35%	SigmaAldrich, Taufkirchen, Germany
Methanol	assay ⩾99.9%	SigmaAldrich, Taufkirchen, Germany
Thimerosal	assay ⩾97%	SigmaAldrich, Taufkirchen, Germany
O.C.T. Compound	Tissue-Plus™	Fisher Scientific GmbH Schwerte, Germany
Gelatin	500g, Powder	VWR, Radnor, USA

Table 8: List of NPs

Subject	Manufacturer
Qdot™ 655 ITK™ carboxyl quantum dots	Invitrogen by Thermo Fisher Scientific, Carlsbad, USA
Qdot™ 655 ITK™ amino (PEG) quantum dots	Invitrogen by Thermo Fisher Scientific, Carlsbad, USA
QtrackerTM 655 vascular labels (PEG-QDs)	Invitrogen by Thermo Fisher Scientific, Carlsbad, USA
Melamine resin particles, 940 µ m, Ex/Em 636 nm/686	microParticles GmbH, Berlin, Germany
Printex 90 caibon NPs	Spark discharge from graphite electrodes[1]

Table 9: List of cell lines

Cell line name	Manufacturer/ origin
Ana-1 cells	HMGU, Munich, Germany
LA4 cells (CCL-196TM)	ATCC, Manassas, Virginia, USA
MH-S cells (CRL-2019TM)	ATCC, Manassas, Virginia, USA
MLE-12 cells (CCL-2110TM)	ATCC, Manassas, Virginia, USA

Table 10: List of mice strains

mice strain name	Manufacturer/ origin
C57BL/6J mt/mG mice	Experimental animal facility, Helmholtz Zentrum München
B6.Cg-Tg(Csf1r-EGFP)1Hume/J- C57BL/6 mice	Jackson Laboratory, Bar Harbor, ME, USA
Lyz2-cre mt/mG C57BL/6J mice	Jackson Laboratory, Bar Harbor, ME, USA
C57BL/6 (WT) mice	Charles River, Sulzfeld, Germany

Table 11: List of cell culture consumables

Subject	Manufacturer
Ham's F12	BIOWEST SAS Nuaillé, France
RPMI Medium 1640 (1X)	Thermo Fisher Scientific, Bonn, Germany
Dulbecco´s modified eagle medium	Thermo Fisher Scientific, Bonn, Germany
UltraPureTM distilled Water	Thermo Fisher Scientific, Bonn, Germany
Trypsin-EDTA (0.5 %)	Thermo Fisher Scientific, Bonn, Germany
2-Mercaptoethanol (50 mM)	Life Technologies Limited Paisley, UK
MEM Non-Essential Amino Acids Solution (NEAA)	Thermo Fisher Scientific, Bonn, Germany
HEPES Buffer Solution	Thermo Fisher Scientific, Bonn, Germany
L-Glutamine	Life Technologies Limited Paisley, UK
Bovine Serum Albumin	SIGMA-ALDRICH GmbH Steinheim, Deutschland

Table 12: List of antibodies

Primary or secondary antibody	Clone	Manufacturer
Anti-CD11c-FITC	REA754	Miltenyi biotec GMBH, Bergisch Gladbach, Germany
Anti-Siglec-F-FITC	REA798	Miltenyi biotec GMBH, Bergisch Gladbach, Germany
Anti-CD326 (EpCAM)- VioBlue	REA977	Miltenyi biotec GMBH, Bergisch Gladbach, Germany
Anti-CD326 (EpCAM)-PE	REA977	Miltenyi biotec GMBH, Bergisch Gladbach, Germany
Alexa Fluor® 488 anti-mouse Ly-6G Antibody	1A8	BioLegend, Fell, Germany
Alexa Fluor® 488 anti-mouse CD115 (CSF-1R) Antibody	AFS98	BioLegend, Fell, Germany
In Vivo mAbs anti-mouse/human CD44	IM7	Bio X Cell, Lebanon, USA
Ultra-LEAF™ Purified anti-mouse CD88 (C5aR) mAbs	20/70	BioLegend, Fell, Germany
Ultra-LEAF™ Purified anti-mouse CD64 (FcγRI) mAbs	W18349F	BioLegend, Fell, Germany
	M17/4	Bio X Cell, Lebanon, USA
Purified anti-mouse CD54 (ICAM-1) Antibody	YN1/1.7.4	ATCC, Manasses, USA
In Vivo mAbs rat IgG2a isotype control	2A3	Bio X Cell, Lebanon, USA
Ultra-LEAF™ Purified Rat IgG2b, κ Isotype Ctrl Antibody	RTK4530	BioLegend, Fell, Germany
Alexa Fluor® 647 anti-mouse Ly-6G/Ly-6C (Gr-1) Antibody	RB6-8C5	BioLegend, Fell, Germany
Antibodies for In Vivo Mouse Platelet Labeling (X649)	anti - GPIbbeta derivative	Emfret Analytics GmbH & Co. KG, Würzburg, Germany
Mouse Podoplanin Antibody	AF3244	Bio-Techne GmbH, Wiesbaden, Germany

Table 13: List of Fluorescent dyes

Fluorescent dye	Manufacturer

pHrodo™ Green Dextran, 10,000 MW	Thermo Fisher Scientific, Bonn, Germany
pHrodo™ Green E. coli BioParticles™ Conjugate	Thermo Fisher Scientific, Bonn, Germany
PKH26 Red Fluorescent Cell Linker Kit for Phagocytic Cell Labeling	SigmaAldrich, Taufkirchen, Germany

7.2 Abbreviations

%	percent
°C	grad Celsius
µ	micro
µg	microgram
µl	microliter
µm	micrometer
2D	two-dimensional
3D	three-dimensional
AM	alveolar macrophage
aPEG-QDs	aminated PEG Quantum Dots
ATCC	American Type Culture Collection
ATP	adenosine triphosphate
BAL	bronchoalveolar lavage
BSA	Bovine serum albumin
CdSe	cadmium selenide
CdTe	cadmium telluride
cm	centimeter
C5aR1	Complement C5a Receptor 1
CD	Cluster of differentiation
CO2	Carbon dioxide
CR	Complement receptor
Csfr1	Colony stimulating factor 1 receptor
Ctrl	Control
cQD	carboxyl Quantum Dot
CXCL1	Chemokine (C-X-C motif) ligand 1
DBE	Dibenzyl ether
DCM	Dichloromethane
DNA	deoxyribonucleic Acid
ECs	Endothelial cells
EDTA	Ethylenediaminetetraacetic acid
e.g.	*exempli gratia*
ELISA	enzyme-linked immunosorbent assay
EpCAM	Epithelial Cell Adhesion Molecule
et al.	et alii
FACS	fluorescence-activated cell sorting
FBS	fetal bovine serum
Fc	Fragment crystallizable region
Fig.	figure
g	gram
h	hour
H2O	water

hrs	hours
i.e.	id est
ICAM-1	intercellular adhesion molecule 1
IFN	interferon
L	liter
LFA-1	Lymphocyte function-associated antigen 1
L-IVM	Lung intravital microscope
Lyz2	lysozyme 2
IL	interleukin
IL1r1	Interleukin 1 receptor, type I
i.v.	intravenous
IVIS	in vivo imaging system
kDa	Kilo Dalton
LPS	Lipopolysaccharide
m	milli
MeOH	Methanol
mg	milligram
min	minutes
MIP	maximum intensity projection
ml	Milliliter
mM	Millimolar per liter
mRNA	messenger RNA
NEAA	Non-Essential Amino Acids
NF-kB	Nuclear factor 'kappa-light-chain-enhancer' of activated B-cells
NP	NP
nm	Nanometer
NAC	N-Acetyl-L-Cystein
NO	nitric oxide
NP	NP
O_2	oxygen
O.C.T compound	Optimal cutting temperature compound
P/S	penicillin/streptomycin
PBS	Phosphate buffered saline
PCLs	precision cut Lung slices
PEG-QDs	PEGylated Quantum Dots
pH	potential of hydrogen
QDs	Quantum Dots
RNA	ribonucleic acid
ROS	reactive oxygen species
rpm	revolutions per minute
PFA	Paraformaldehyde
RT	room temperature
TEM	Transmission electron microscopy

THF	Tetrahydrofuran
WST-1	Water soluble tetrazolium salt 1
USA	United States of America
ZnS	zinc sulfide

7.3 Publications and presentations

7.3.1 Publications

Real time in vivo investigation of NP dynamics and immune response during ventilator-assisted NP inhalation

Qiongliang Liu, Lin Yang, Chenxi Li, Otmar Schmid, Tobias Stoeger and Markus Rehberg

In preparation

Multimodality imaging and deep learning unveil acinar migration of tissue-resident, NP-laden macrophages in the lung

Lin Yang, **Qiongliang Liu**, Pramod Kumar, Arunima Sengupta, Ali Farnoud, Ruolin Shen, Darya Trofimova, David Kutschke, Marie Piraud, Fabian Isensee, Gerald Burgstaller, Markus Rehberg, Tobias Stoeger, Otmar Schmid

In preparation

Course of lung inflammation and injury caused by NP inhalation depends on material specific cellular perturbation patterns

Carola Voss*, Meshal Ansari*, Maximilian Strunz, Ilias Angelidis, Verena Häfner, Christoph Mayr, Carol Ballester-Lopez, **Qiongliang Liu**, Lianyong Han, Tom Conlon, Markus Rehberg, Herbert B. Schiller, Tobias Stöger

In preparation

7.3.2 Oral presentations

Real time in vivo investigation of particle dynamics and innate immune responses during ventilator-assisted NP inhalation

Qiongliang Liu, Otmar Schmid, Tobias Stoeger and Markus Rehberg

Nanotox 2021 – 10th International Conference on Nanotoxicology, 20th – 22nd April 2021, Virtual.

Real time in vivo investigation of particle dynamics and innate immune responses during ventilator-assisted NP inhalation

Qiongliang Liu, Otmar Schmid, Tobias Stoeger and Markus Rehberg

7th Nano Today Conference, 16th -18th November 2021, Virtual.

7.3.3 Poster presentations

Elucidating particle and leukocyte dynamics during the course of particle triggered pulmonary inflammation by in vivo imaging

Qiongliang Liu, Lin Yang, Otmar Schmid, Tobias Stoeger and Markus Rehberg

11th interact conference, 27th - 28th February 2020, Munich, Germany

Real time in vivo investigation of particle and innate immune cell dynamics during ventilator-assisted NP inhalation

Qiongliang Liu, Otmar Schmid, Tobias Stoeger and Markus Rehberg

20th ERS Lung Science Conference, 10th -13th March 2022, Estoril, Portugal

Real time in vivo investigation of the innate immune response during ventilator-assisted NP inhalation

Qiongliang Liu, Otmar Schmid, Tobias Stoeger and Markus Rehberg

20th Fraunhofer Seminar “Models of Lung Disease” and satellite workshop “Alternatives to Animal Testing”, 22nd -24th June 2022, Hannover, Germany

Real time in vivo investigation of particle dynamics and innate immune responses during ventilator-assisted NP inhalation

Qiongliang Liu, Yang Lin, Chenxi Li, Otmar Schmid, Tobias Stoeger and Markus Rehberg

10th DZL Annual Meeting, 6th -7th July 2022, Hannover, Germany

8. Acknowledgments

I address my most sincere gratitude to all the people who contributed in some way to the work described in this thesis. First and foremost, I would like to express my deepest appreciation to my first supervisor, Prof. Dr. Markus Rehberg (LHI/CPC), for continuously guidance and support for my project. During the past four years of working together, what I have learned from him are not only subtle experimental designs, experimental knowledges, especially as it relates to imaging, but also the rigorous attitude to scientific research and the unending enthusiasm. In November 2018, Prof. Rehberg introduced the L-IVM technology platform from the UK together, and since then, Markus and I have faced various difficulties and challenges from this new platform. A stable and mature L-IVM platform is now formed, which is inseparable from the patient guidance and continuous support of Prof. Rehberg. Hope we will have a great harvest this year. Words cannot express how thankful I am for you, Markus! This academic thesis is just a summary of the first phase of our enjoyable academic journey, and I indeed look forward to having more interactions with you in the future.

Additionally, I want to express the depth of my gratitude to Dr. Tobias Stoeger (LHI/CPC), who supplied me the opportunity to conduct doctoral research in his group. During my PhD student career, he contributed to a rewarding graduate school experience by sharing a wealth of nanotoxicology and immunology

knowledge and advice, offering me an academic environment based on full trust and freedom and supporting my attendance at various conferences, seminars and courses. With his selfless and countless support, I have enjoyed the research works in his group for nearly four years.

Furthermore, I would like to thank my committee member Prof. Dr. med. Markus Sperandio (Walter-Brendel-Centre, LMU), close collaborators Prof. Dr. Otmar Schmid (LHI/CPC, Helmholtz Zentrum München), Dr. Leo Carlin (The Beatson Institute for Cancer Research, UK) and Dr. Dagmar Zeuschner (Max Planck Institute for Molecular Biomedicine) for their constant support, insightful discussion, and constructive advice.

Every result described in this thesis was accomplished with the help and support of fellow colleagues and collaborators. Special thanks to Dr. Lin Yang for selfless sharing of ideas and imaging experiences, perceptive discussion and prompt feedback. Many thanks to my colleagues Chenxi Li for her daily support, help and high-quality discussions.

I also appreciate a lot to my collaborators Dr. Judith Secklehner (The Beatson Institute for Cancer Research, UK) for the help of L-IVM platform, Dr. rer. nat. Benjamin Tast and M.Sc. Pardis Khosravani (Core Facility Flow cytometry, BMC Munich) for the support of flow cytometry and data analysis. Dr. Annette Feuchtinger for providing me the guidance and support of light-sheet fluorescent microscopy and Schröppel, Andreas for the help with inhalation devices and imaging work platforms.

I would like to deeply thank to all former and current members of our group (AG Stoeger lab (LHI/CPC) and AG Schmid labs (LHI/CPC): Miriam Kastlmeier, Eva Günther, Dr. Carolina Ballester López, Mehwish Ishaque, Yasmin Shaalan, Elisabeth Folwarczny, Dr. Pramod Kumar, Anna Fuchs, especially for David Kutschke, Dr. Carola Voss, Dr. Qiaoxia Zhou, Lianyong Han, Verena Häfner, Hongyu Ren for their discussion and support.

My deep gratitude goes to an excellent CPC Research School team, specifically PD Dr. Claudia Staab-Weijnitz, Dr. Doreen Franke, Karin Agnes Herbert and Melanie Penning for their help, organization and enthusiasm during the entire graduate school program, which has greatly benefited me during my four-year PhD candidate career. In addition, I am very grateful to the secretory Kaori sumikawa and Silke Lauer for the support and help on general tasks and in personal life.

I would like to address my special acknowledgment to all my classmates, colleagues and friends of Helmholtz Zentrum München, especially Dr. Dongshen Jiang, Dr. Hengshuo Liu, Xin Zhang, Qianjiang Hu, Haifeng Ye, Ruoxuan Dai, Shaohua Zhu, Dr. Carmela Morrone, Dr. Xianming Wang, with whom we had a lot of pleasantly scientific discussion and invaluable living memories.

I would like to thank China Scholarship Council (CSC) for providing me with a scholarship to ensure my daily expenses while studying in Germany, allowing me to focus on my research.

Most importantly, I feel extremely fortunate to have the tremendous support and endless love from Dr. Rui Zhuo (Shanghai Normal University), the girl I wish I could spend the rest of my life with. Will you marry me?

I will end with saying thanks to two people who first showed me how to speak. Thanks mom and dad, Min Zhang and Jianguo Liu, for everything I can imagine.